Task 10. Cobalt Catalyst Mechanism Study

The objective of this task is to determine the impact of secondary reactions on the relationship of cobalt Fischer-Tropsch catalysts under conditions appropriate to slurry bubble column reactors.

A. The Formation of Branched Hydrocarbons in the Fe and Co Catalyzed FT Reactions

Introduction

To fully understand the mechanism for the FT reactions, it is important to understand how branched alkanes and alkenes being formed. If they are the products of the secondary reactions, the question to be answered is how and under what conditions that they are produced. On the other hand, if they are the primary products of the FT reactions, then it is necessary for any mechanistic scheme proposed for FT reactions to include the formation of branched alkenes and alkanes. In this study, we want to know how much branched hydrocarbon is formed under different conditions and different catalysts and try to understand which factor or factors plays the more important role in the formation of the branched products.

In order to understand how branched alkenes and alkanes being formed, it is necessary to quantitatively measure each isomers of each carbon number. Since some GC peaks of branched alkanes were buried in the branched alkene peaks and the vise versa, it is necessary to use indirect means to measure the amount of each isomer. In this study, the FT products were hydrogenated or brominated and an accurate amount of each branched alkane was obtained.

Experimental

1. Hydrogenation of FT Products

Six grams of FT products (oil and wax) and 0.5 g of Pt/C were placed in a jar. The reaction mixture was reduced under hydrogen pressure (30 psig) at room temperature with

excellent stirring until no alkenes were found in the reaction mixture. Then the reaction mixture was filtered prior to GC and GC/MS analysis. The FT products hydrogenated are the following: for Fe catalyzed FT products: Bao20, Bao22, Bao26, Bao28 and Bao29; for Co catalyzed FT products: L366, L367 and L368 (Table 1).

2. Bromination of FT Products

To the FT oil (for some samples, oil and wax), 22.3% bromine in acetic acid was added drop by drop with vigorously stirring until the solution gave a permanent yellow to orange color. The oils brominated are: for Fe catalyzed FT products: Bao20, Bao22, Bao26, Bao28 and Bao29; for Co catalyzed FT products: L366, L367 and L368.

3. Analysis of FT Products

The FT oil and the samples after hydrogenation and bromination were analyzed by GC and GC/MS. The branched alkanes in each carbon number were identified by GC/MS, and quantitatively determined by GC/FID.

Results and Discussion

Five oil samples from Fe catalyzed FT reactions and 3 oil samples from Co catalyzed FT reactions were hydrogenated and brominated. The FT reaction conditions and the catalyst compositions were given in Tables 1 and 2.

All of the FT products in the runs reported in this report contain 1-alkene, alkane, 2-alkenes, alcohols as well as branched hydrocarbons. After hydrogenation, the alkenes were converted to corresponding alkanes; after bromination, the alkenes were converted to corresponding dibromides.

Figure 1 is a partial chromatogram of the sample from Fe catalyzed FT reaction (Bao20). The top curve in this figure is for the FT products; the bottom figure is the sample after bromination and the middle chromatogram is for the sample after hydrogenation.

Figures 2 through 6 are the chromatograms of carbon 7, 8, 9, 10 and 11 of run Bao20, respectively. Again, the top in each figure is the FT products; the middle, after hydrogenation; and the bottom, after bromination (for the other 4 Fe catalyzed FT samples, the figures are similar and are not reproted). After hydrogenation, the branched alkenes were converted to the corresponding branched alkanes and normal alkenes were converted to normal the alkane. The mole percent of branched alkanes of each carbon number is defined as:

$$\%\ branched = \frac{branched\ alkanes}{branched\ alkanes + normal\ alkane}\ X\ 100 \qquad \textbf{(1)}$$

In the case of hydrogenated sample, the % branched alkanes represent the total branched hydrocarbons (branched alkenes plus branched alkanes). Since it is difficult to quantitatively measure the amount of branched alkanes in the original FT oil due to peak overlap, bromination of the FT oil is useful. The bromination of FT oil enable us to quantitatively measure the % branched alkanes from C_7 to C_{11} since the dibromide formed from these olefins elute following C_{11}. In this case, the % branched alkanes represents the total branched alkanes in the reaction product. The results are given in Tables 3-7 for Fe catalyzed FT reactions produced in runs Bao20, Bao22, Bao26, Bao28 and Bao29, respectively.

Figure 7 is the partial chromatogram of a sample from the Co catalyzed FT reaction (L366), and Figures 8 through 12 are the chromatograms of carbon numbers 7, 8, 9, 10 and 11 formed during run L366, respectively. The chromatograms of the other two Co catalyzed FT runs (L367 and L368) are similar to Figures 7 through 12. As Figures 1 through 6, the top is the FT products; the middle, after hydrogenation; bottom, after bromination. The mole percent of branched alkanes are compiled in Table 8.

As can be seen from Tables 3 and 4, Runs Bao20 and Bao22 were conducted using the same catalyst and same reaction conditions except temperature. Bao20 was run at 230^{o}C and

Bao22 was run at 270°C. As the reaction temperature was increased, the amount of branched alkanes in most of the carbon numbers increased by more than 5%.

Runs Bao22 and Bao26 (data in Table 4 and Table 5) were conducted using the same catalyst at the same temperature but at different H_2:CO ratios and WHSV. When the H2:CO ratio increased from 0.67 to 1.70 and the WHSV increased from 10 to 40, the amount of branched alkanes (Bao26) decreased by 5-10% for all of the carbon numbers, with few exceptions.

In all of the five Fe catalyzed FT runs, it appears that the catalyst composition has a more significant impact on the formation of branched hydrocarbons than the reaction conditions, such as temperature, flow rate and H_2:CO ratio. The only difference between runs Bao26 (data in Table 5) and Bao28 (data in Table 6) is that the catalyst used in the run Bao28 differs slightly from that of Bao26 (1.4% and 4% K, respectively), and yet the amount of the branched alkanes increased more than 10% for most carbon numbers for the higher potassium containing catalyst.

Run Bao29 was conducted using pure Fe catalyst (100% Fe). The amount of branched alkanes (data in Table 7) is lower than runs Bao22 and Bao28. Since this run was also conducted at a higher H_2:CO ratio, lower temperature and lower WHSV, it is difficult to tell which factor played the major role.

The major difference between Fe catalyzed FT reactions and Co catalyzed FT reactions is the production of larger amounts of branched hydrocarbons with the catalyzed FT reaction. As can be seen from Tables 3 through 8, the Fe catalyzed FT reaction produced 10 to 25% of branched hydrocarbon (data after hydrogenation), whereas the Co catalyzed FT reaction produced only 1-4% of branched hydrocarbons (Table 8).

The reaction conditions of the three Co catalyzed FT reactions are different (see Table 2) and the catalyst compositions are also slightly different. Therefore, it is hard to tell which factor

is more responsible for the formation of the branched hydrocarbons. Run L367 produced highest percentage of branched hydrocarbons (about 4%) among these three runs and this is probably due to the low WHSV.

The mole percent of branched alkanes after hydrogenation is the percentage of total branched hydrocarbons (branched alkenes and branched alkanes) in the total hydrocarbons. Designating the P_B as branched alkanes; O_B, branched alkenes; P_n, normal alkane; O_n, normal alkenes, then after hydrogenation, we have:

$$Mol\%\ (branched\ alkanes\ after\ hydrogenation) = \frac{P_B + O_B}{P_B + O_B + P_n + O_n} X\ 100 \qquad \textbf{(2)}$$

The mole percent of branched alkanes after FT reaction can be represented by the mole percent of branched alkanes after bromination as shown in eq. 3:

$$Mol\%(branched\ alkanes\ after\ bromination) = \frac{P_B}{P_B + P_n} X\ 100 \qquad \textbf{(3)}$$

If $O_n/P_n = O_B/P_B$, it can be proven that

Mol% (branched alkanes after [H]) = Mol% (branched alkanes after [Br]) **(4)**

However, if $O_n/P_n < O_B/P_B$, then

Mol% (branched alkanes after [H]) > Mol% (branched alkanes after [Br]) **(5)**

And if $O_n/P_n > O_B/P_B$, then

Mol% (branched alkanes after [H]) < Mol% (branched alkanes after [Br]) **(6)**

As seen in Figures 13 through 17 for in Fe catalyzed FT reactions, the mole percent of branched alkane after hydrogenation in all of these five runs is either higher than or close to that of the branched alkanes after bromination. This indicated that the ratio of O_n/P_n is less than or

close to the ratio of O_B/P_B. These results suggest that during the formation of these FT products, the rate of hydrogenation of n-alkenes is close to or only slightly larger than that of branched alkenes. Similar results were obtained for Co catalyzed FT reactions (Figures 18 through 20).

The relative ratio of n-alkenes/n-alkane (O_n/P_n) can be measured accurately based on the GC. Because of the GC peak overlap, it is very difficult to measure accurately the ratio of branched-alkenes/branched alkanes (O_B/P_B). However, the ratio of O_B/P_B can be calculated based on the mole percent of the branched alkanes (after hydrogenation and after bromination) and the ratio of O_n/P_n.

Let

$$(P_B + O_B)/(P_B + O_B + P_n + O_n) = \alpha \quad \textbf{(7)}$$

where α is the mole percent of branched alkanes after hydrogenation, and

$$P_B/(P_B + P_n) = \beta \quad \textbf{(8)}$$

where β is the mole percent of branched alkanes after bromination. The ratio of n-alkenes/n-alkane is represented in eq. 9:

$$O_n/P_n = \gamma \quad \textbf{(9)}$$

Solving the eq. 7, 8 and 9, we have

$$O_B/P_B = \frac{\alpha(1-\beta)(1+\gamma) - \beta(1-\alpha)}{\beta(1-\alpha)} \quad \textbf{(10)}$$

Based on eq. 10, the ratio of O_B/P_B can be calculated. Also based on the eq. 10, it can be proven that if $\alpha = \beta$, then $O_B/P_B = O_n/P_n = \gamma$; if $\alpha > \beta$, then $O_B/P_B > O_n/P_n$; if $\alpha < \beta$, then $O_B/P_B < O_n/P_n$.

The representative results were given in Table 9 (for Fe catalyzed FT reactions) and Table 10 (for Co catalyzed FT reactions).

The mole percent of branched alkanes in Fe catalyzed FT products (Figure 21) varies from run to run. However, for any run, the different carbon number compounds have about same mole percent of branched alkanes. This is also true for Co catalyzed FT reactions (Figure 22). The major difference between Fe and Co catalyzed FT reaction in term of mole percent of branched alkanes is that Co catalyzed FT reactions only produce 1-4% of branched alkanes, whereas the Fe catalyzed FT reactions can produce as high as 20% (probably more) of branched alkanes.

Table 1

The Reaction Conditions and the Catalyst in the Fe Catalyzed FT Reactions

Run ID	Bao20	Bao22	Bao26	Bao28	Bao29
Catalyst	4.6% Si, 64.6% Fe, 2.0% Cu, 1.4% K	4.6% Si, 64.6% Fe, 2.0% Cu, 1.4% K	4.6% Si, 64.6% Fe, 2.0% Cu, 1.4% K	4.6% Si, 62.2% Fe, 2.0% Cu, 5% K	100% Fe
Temp. (^{o}C)	230	270	270	270	255
H_2 : CO	0.67	0.67	1.70	1.70	1.91
WHSV	10	10	40	40	3.0

Table 2

The Reaction Conditions and the Catalyst in the Co Catalyzed FT Reactions

Run ID	L366	L367	L368
Catalyst	10% Co/0.2% Ru/ TiO_2	15% Co/ 0.5% Ru/ SiO_2	15% Co/ 0.53% Pt/ Al_2O_3
temp. (^oC)	230	220	220
Pressure (psig)	350	300	275
H_2 : CO	2	2	2
WHSV	18.29	6.73	13.40

Table 3

The Mole Percent of Branched Alkanes in Fe Catalyzed FT Products (Run ID: Bao20)

	FT Products		After Hydrogenation		After Bromination	
Carbon #	# of isomers	Mol %	# of isomers	Mol %	# of isomers	Mol %
7	-	-	2	15.12	2	11.03
8	2	26.1	3	14.50	3	14.43
9	3	18.12	3	11.51	3	11.31
10	2	12.06	6	12.59	4	11.15
11	4	12.23	4	8.93	4	9.68
12	3	4.58	5	7.16		
13	3	7.43	5	11.61		

Table 4

The Mole Percent of Branched Alkanes in Fe Catalyzed Ft Products (Run ID: Bao22)

	FT Products		After Hydrogenation		After Bromination	
Carbon #	# of isomers	Mol %	# of isomers	Mol %	# of isomers	Mol %
7	2	8.82	2	16.05	2	5.10
8	3	17.67	3	19.71	3	15.92
9	3	16.60	5	19.01	3	15.32
10	4	12.69	5	19.06	4	17.27
11	4	11.89	5	20.00	4	17.27
12	4	18.94	5	15.47		
13	5	21.71	5	20.43		

Table 5

The Mole Percent of Branched Alkanes in Fe Catalyzed FT Products (Run ID: Bao26)

	FT Products		After Hydrogenation		After Bromination	
Carbon #	# of isomers	Mol %	# of isomers	Mol %	# of isomers	Mol %
7	2	9.81	2	9.03	2	10.44
8	3	15.67	3	8.89	3	11.25
9	3	9.62	3	10.05	3	9.42
10	4	9.44	5	10.39	4	9.02
11	4	9.57	4	9.37	4	5.72
12	3	6.14	4	8.35		
13	4	5.89	5	9.15		

Table 6

The Mole percent of Branched Alkanes in Fe Catalyzed FT Products (Run ID: Bao28)

	FT Products		After Hydrogenation		After Bromination	
Carbon #	# of isomers	Mol%	# of isomers	Mol%	# of isomers	Mol%
7	-	-	2	14.82	2	19.21
8	2	19.68	2	25.74	3	18.04
9	3	18.50	7	20.73	3	18.04
10	3	20.86	7	19.99	3	16.41
11	4	24.77	6	19.42	4	11.71

Table 7

The Mole Percent of Branched Alkanes in Fe Catalyzed FT Products (Run ID: Bao29)

	FT Products		After Hydrogenation		After Bromination	
Carbon #	# of isomers	Mol%	# of isomers	Mol%	# of isomers	Mol%
7	-	-	2	10.05	2	13.48
8	2	15.18	3	14.50	3	14.58
9	3	13.86	3	10.89	3	11.90
10	3	12.88	6	12.27	4	11.55
11	4	11.83	5	10.37	5	11.43
12	-	-	-	-	-	-
13	-	-	-	-	-	-

Table 8
The Mole percent of Branched Alkanes in Co Catalyzed FT Products

		FT Products		After Hydrogenation		After Bromination	
Carbon #	Run #	# of isomers	Mol%	# of isomers	Mol%	# of isomers	Mol%
7	L366	2	1.85	2	1.99	2	1.40
	L367	2	7.52	2	6.00	2	3.71
	L368	2	2.28	2	1.55	2	1.18
8	L366	2	2.33	2	2.45	3	1.67
	L367	3	4.69	3	4.15	3	4.05
	L368	3	2.26	3	1.57	3	1.35
9	L366	3	2.81	3	2.17	3	2.06
	L367	3	4.80	3	3.78	3	4.10
	L368	3	1.53	3	1.62	3	1.34
10	L366	3	2.19	3	2.39	3	2.08
	L367	4	4.34	4	4.05	4	4.29
	L368	3	1.51	3	1.61	3	1.37
11	L366	4	2.62	4	2.79	4	2.00
	L367	4	4.47	4	4.26	4	4.35
	L368	4	1.69	4	1.84	4	1.84
12	L366	4	1.87	5	3.02		
	L367	5	4.31	5	4.26		
	L368	4	1.60	4	1.73		
13	L366	5	3.10	5	3.34		
	L367	5	4.70	5	4.59		
	L368	5	1.84	5	1.96		
14	L366	5	3.45	5	3.72		
	L367	5	4.88	5	4.86		
	L368	-	-	-	-		

Table 9

The Relative Ratio of the Products in Fe Catalyzed FT reactions (Run ID: Bao22)

Carbon Number	branched- hydrocarbons/ total- hydrocarbons	branched-alkanes/ total alkanes	n-alkenes/ n-alkane	branched-alkenes/ branched alkanes
7	0.1605	0.051	2.3329	1.8574
8	0.1971	0.1592	2.0029	1.9647
9	0.1901	0.1532	1.6416	1.6063
10	0.1906	0.1727	1.4831	1.4688
11	0.2000	0.1727	1.2705	1.2516

Table 10

The Relative Ratio of the Products in Co Catalyzed FT reactions (Run ID: L367)

Carbon Number	branched- hydrocarbons/ total- hydrocarbons	branched-alkanes/ total alkanes	n-alkenes/ n-alkane	branched-alkenes/ branched alkanes
7	0.0600	0.0371	0.371	0.2018
8	0.0415	0.0405	0.2973	0.2871
9	0.0378	0.041	0.2390	0.2738
10	0.0405	0.0429	0.1973	0.2193
11	0.0426	0.0435	0.1645	0.1719

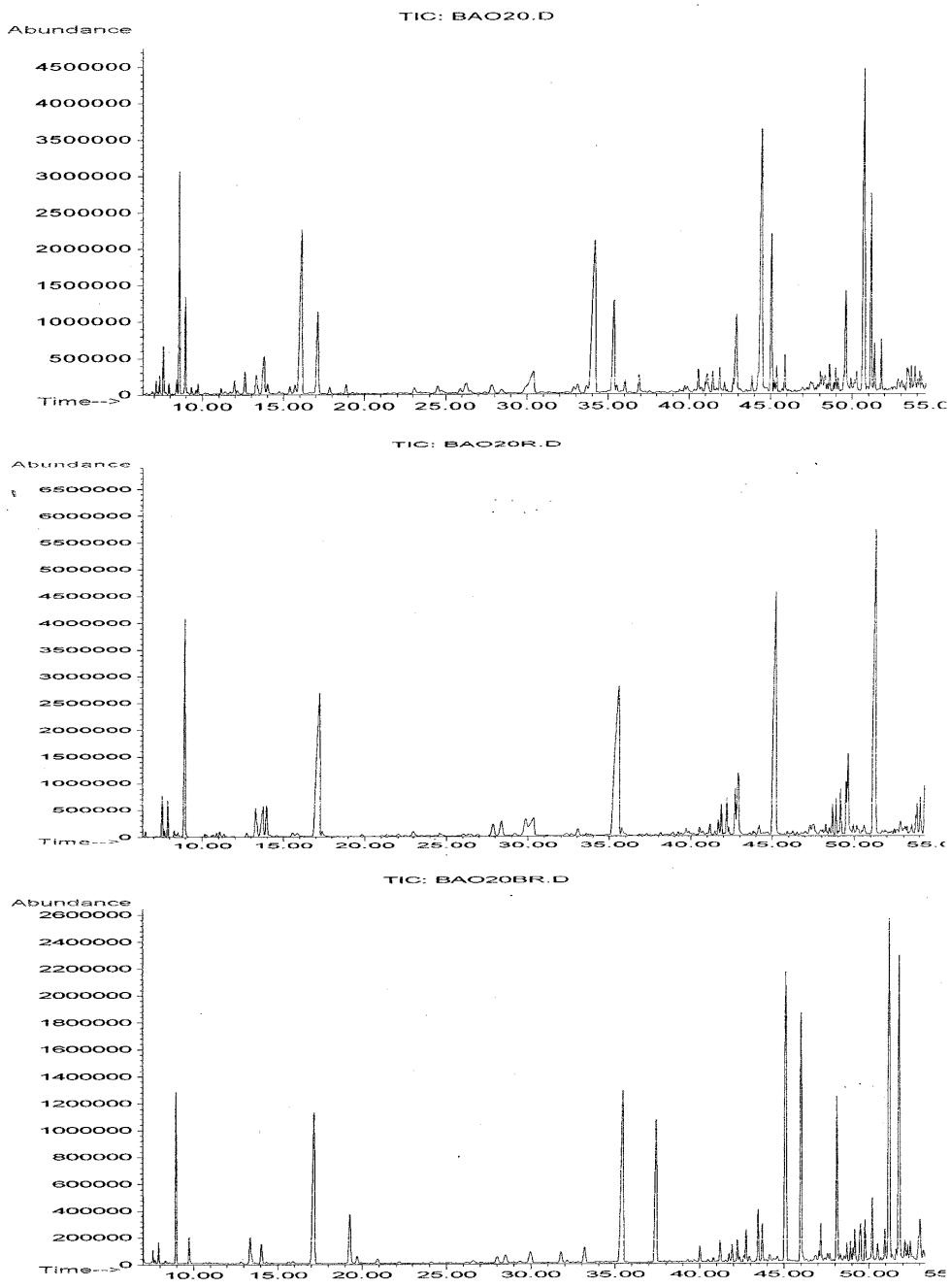

Figure 1. The Partial Chromatogram of the Oil Sample from Fe Catalyzed FT reaction (Run ID: Bao20) (Top: FT products; Middle: after hydrogenation; Bottom: after bromination).

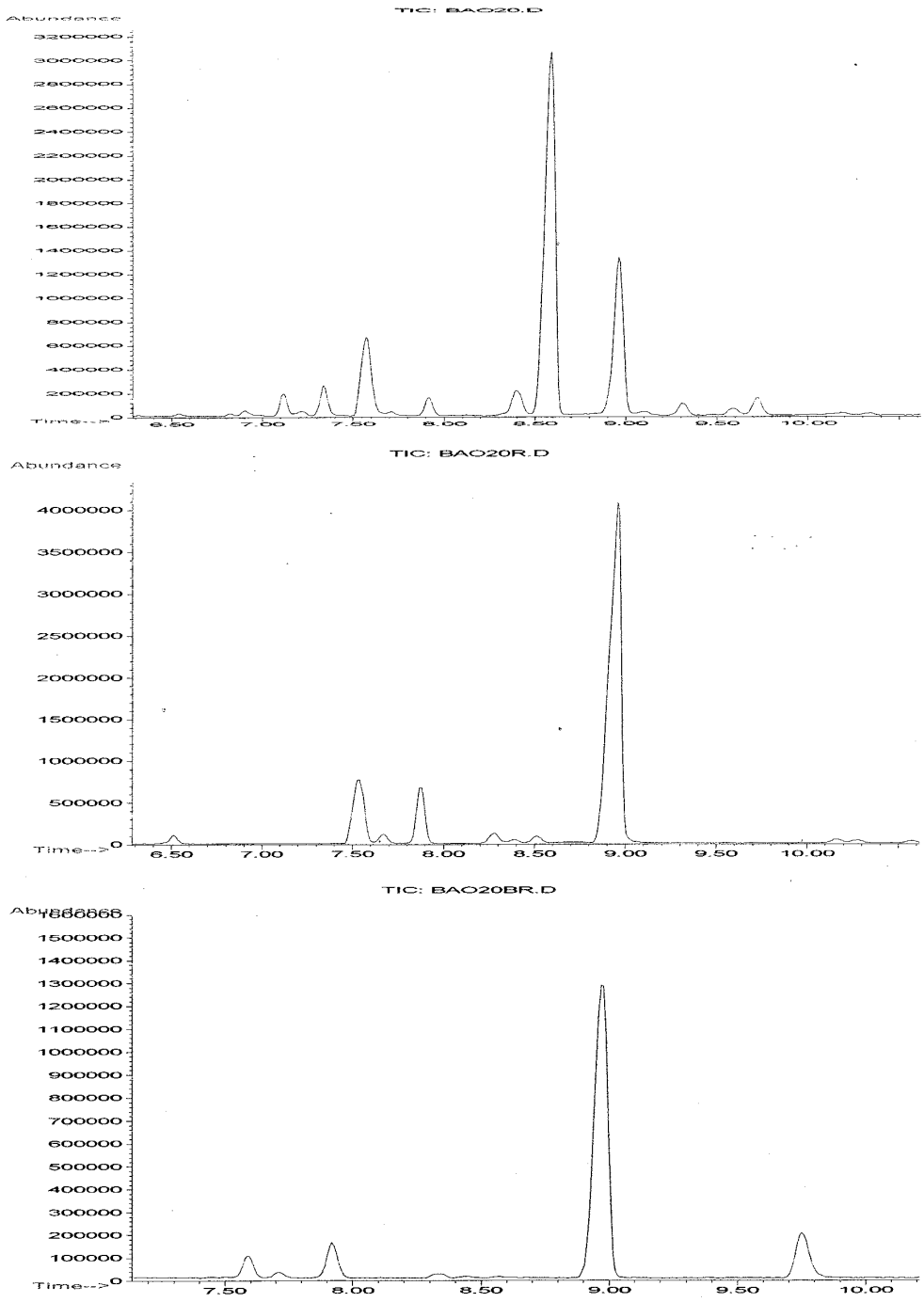

Figure 2. The Chromatogram of the Carbon-7 of the Run Bao20 (Top: FT products; Middle: after hydrogenation; Bottom: after bromination).

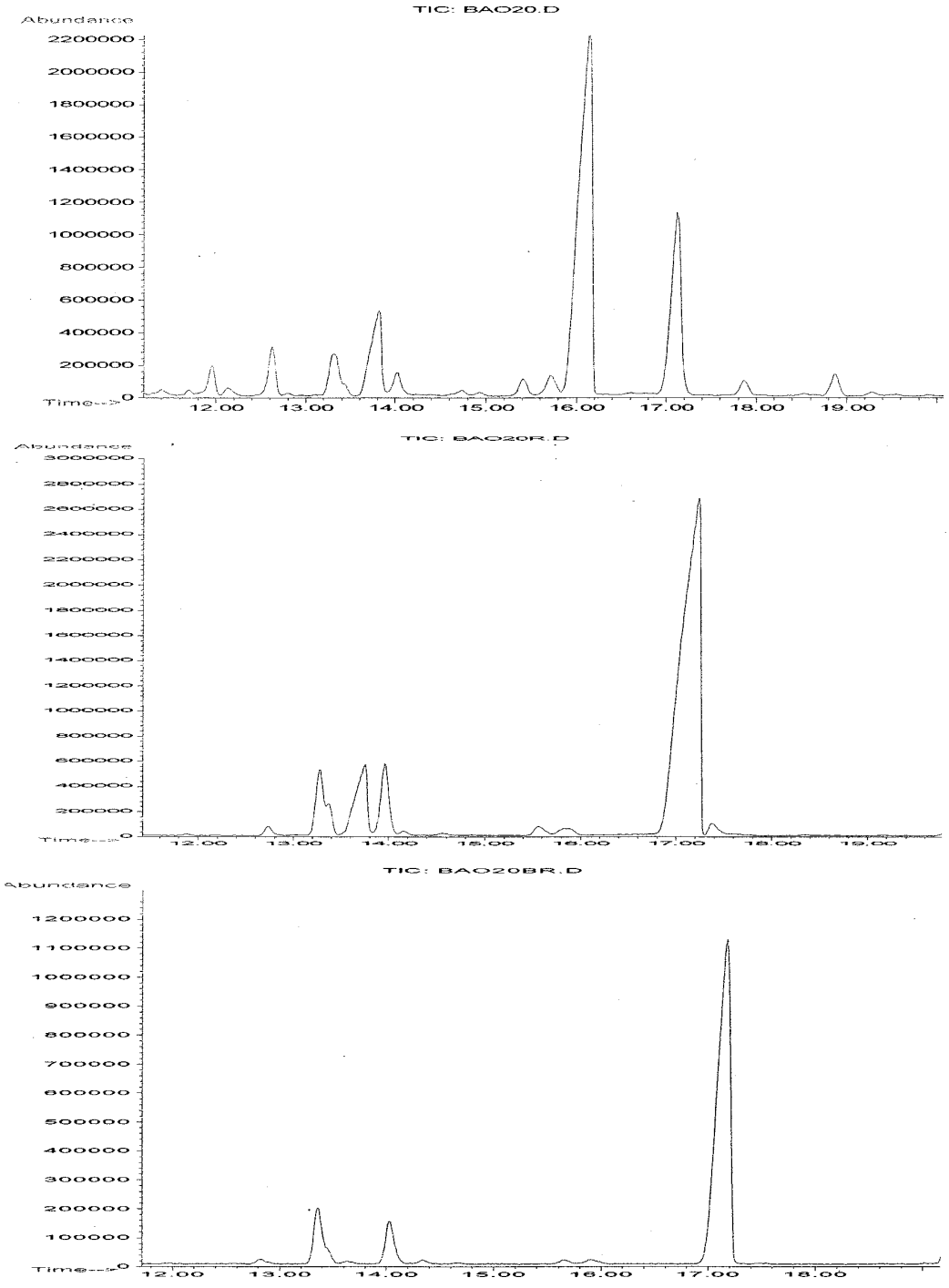

Figure 3. The Chromatogram of the Carbon-8 of the Run Bao20 (Top: FT products; Middle: after hydrogenation; Bottom: after bromination).

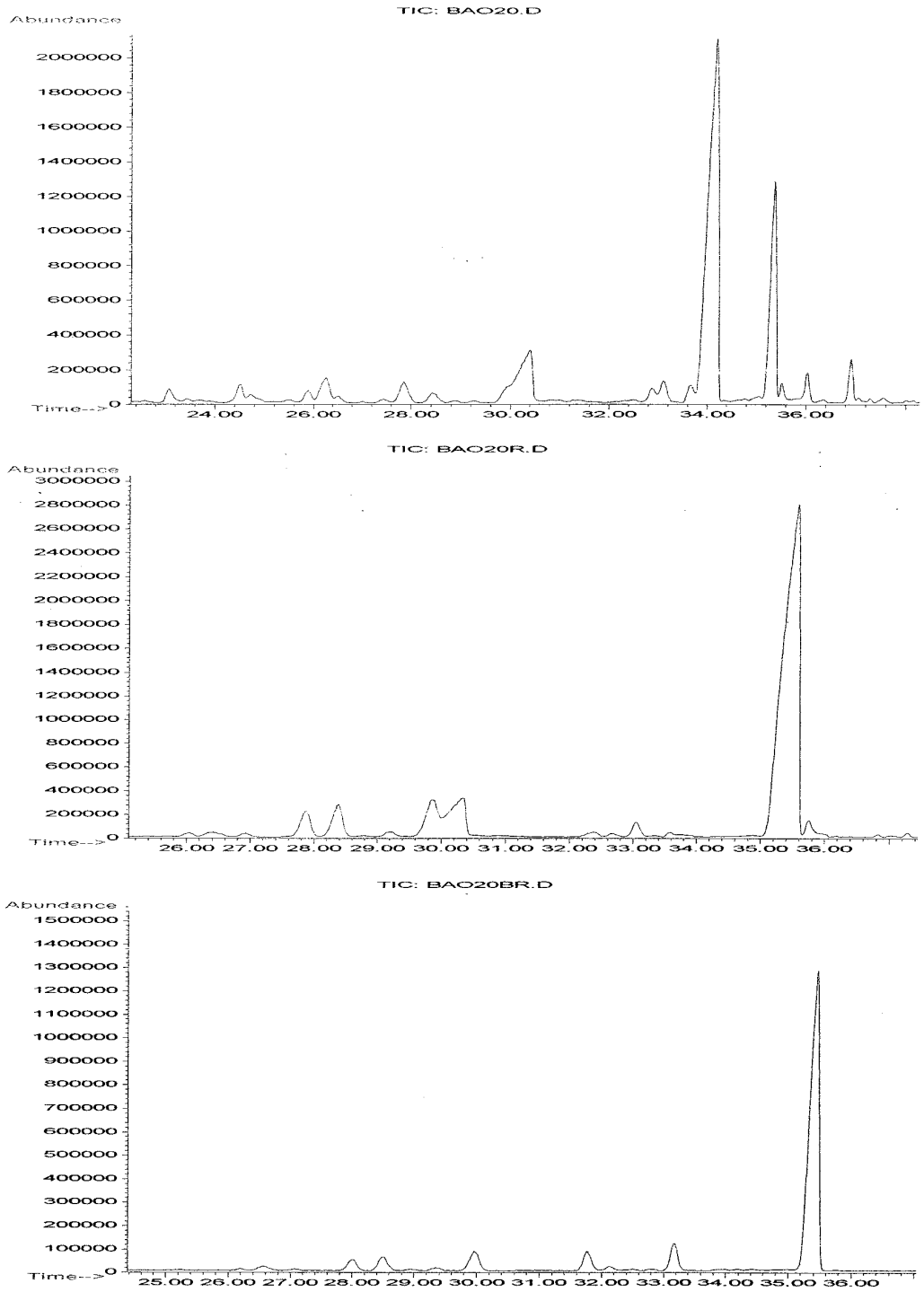

Figure 4. The Chromatogram of the Carbon-9 of the Run Bao20 (Top: FT products; Middle: after hydrogenation; Bottom: after bromination).

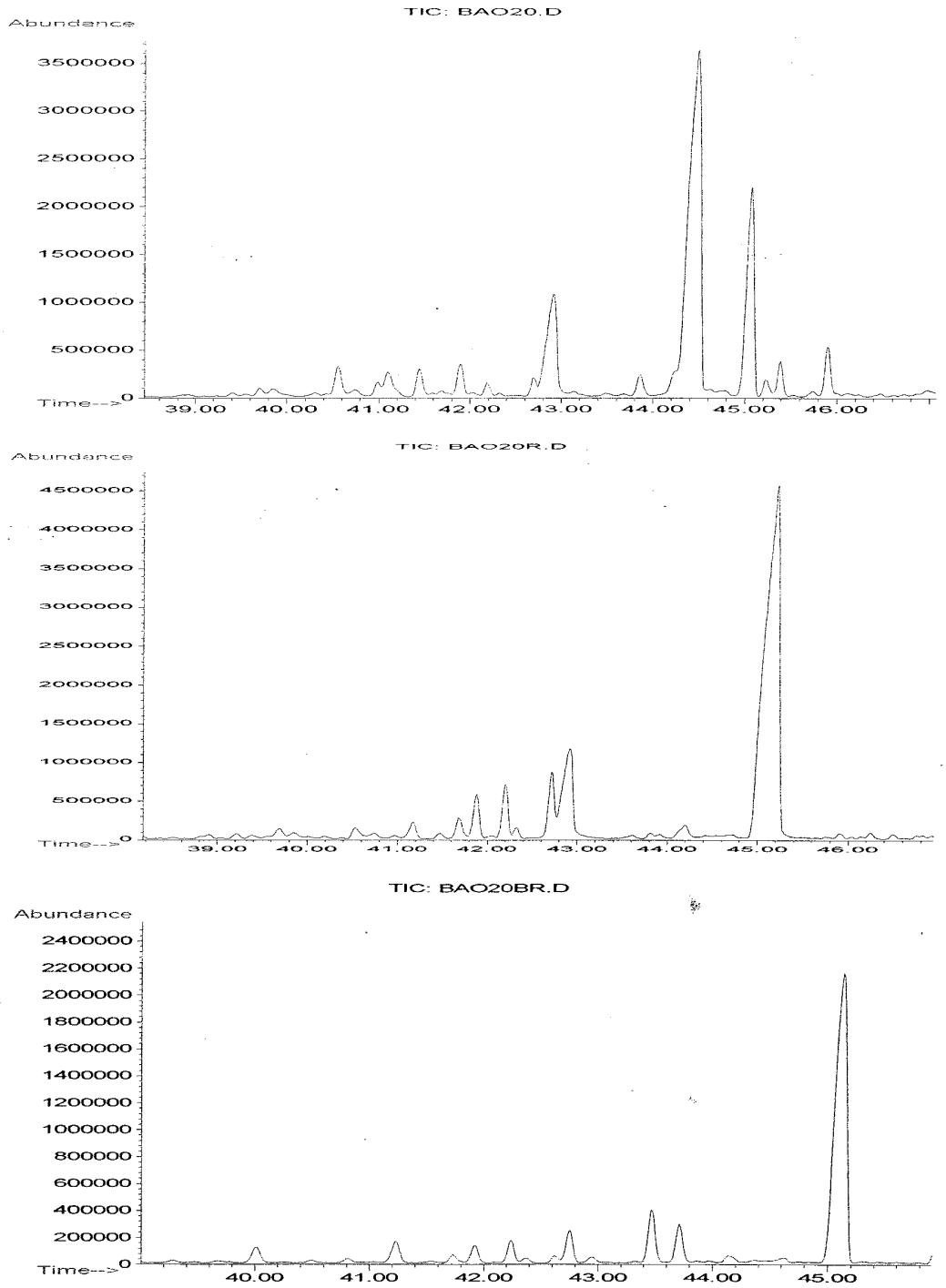

Figure 5. The Chromatogram of the Carbon-10 of the Run Bao20 (Top: FT products; Middle: after hydrogenation; Bottom: after bromination).

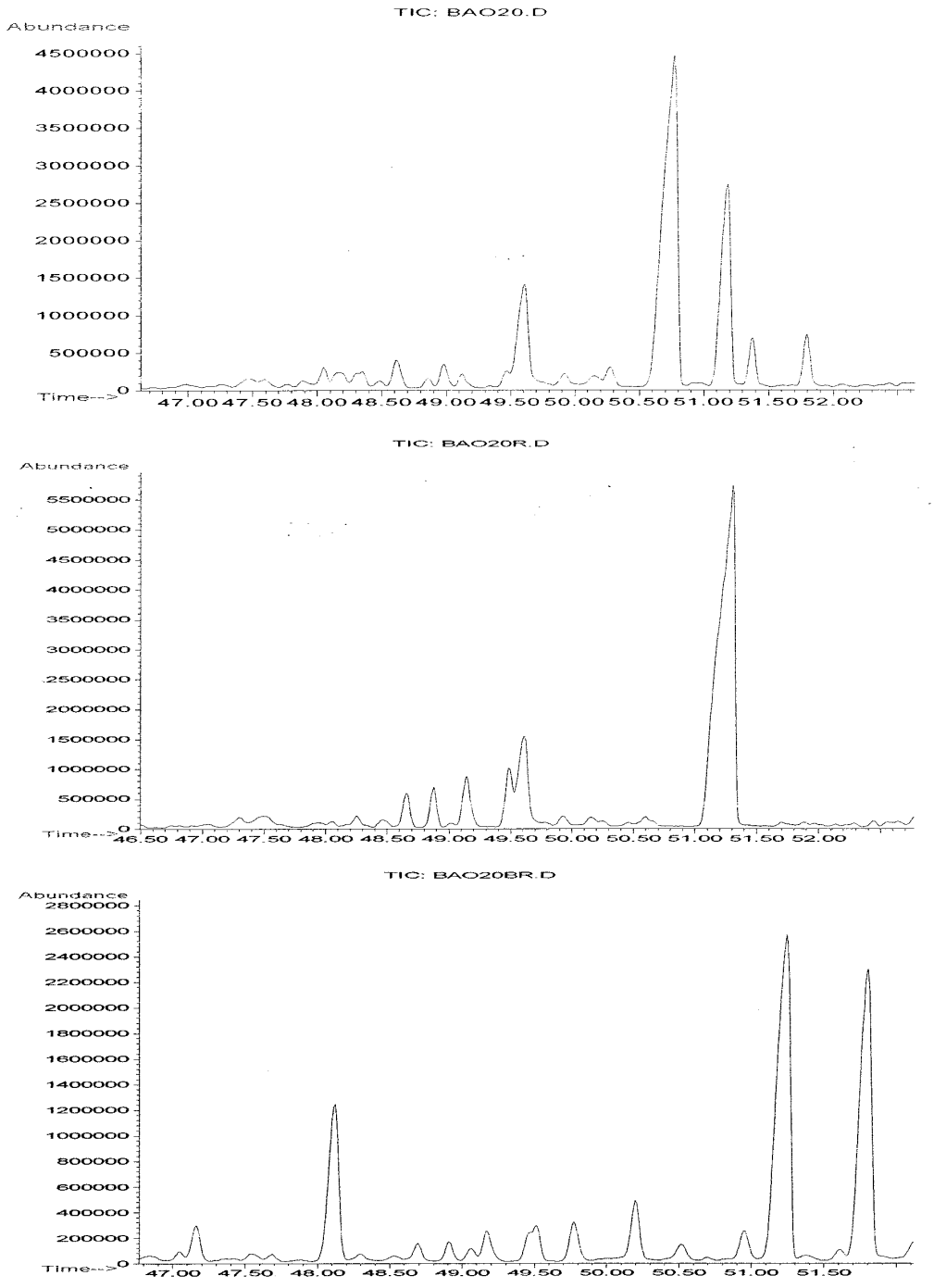

Figure 6. The Chromatogram of the Carbon-11 of the Run Bao20 (Top: FT products; Middle: after hydrogenation; Bottom: after bromination).

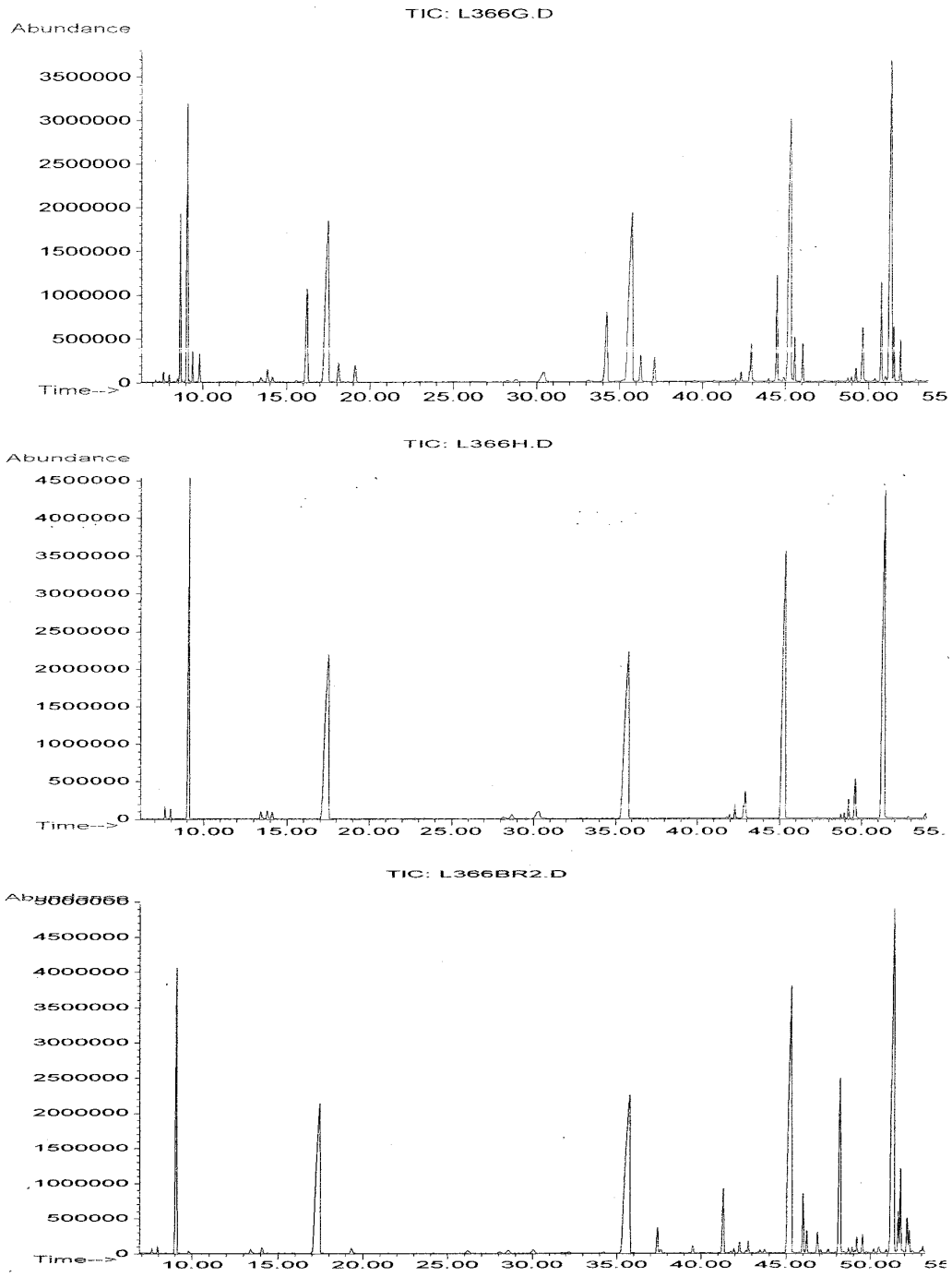

Figure 7. The Partial Chromatogram of the Oil Sample from Co Catalyzed FT reaction (Run ID: L366) (Top: FT products; Middle: after hydrogenation; Bottom: after bromination).

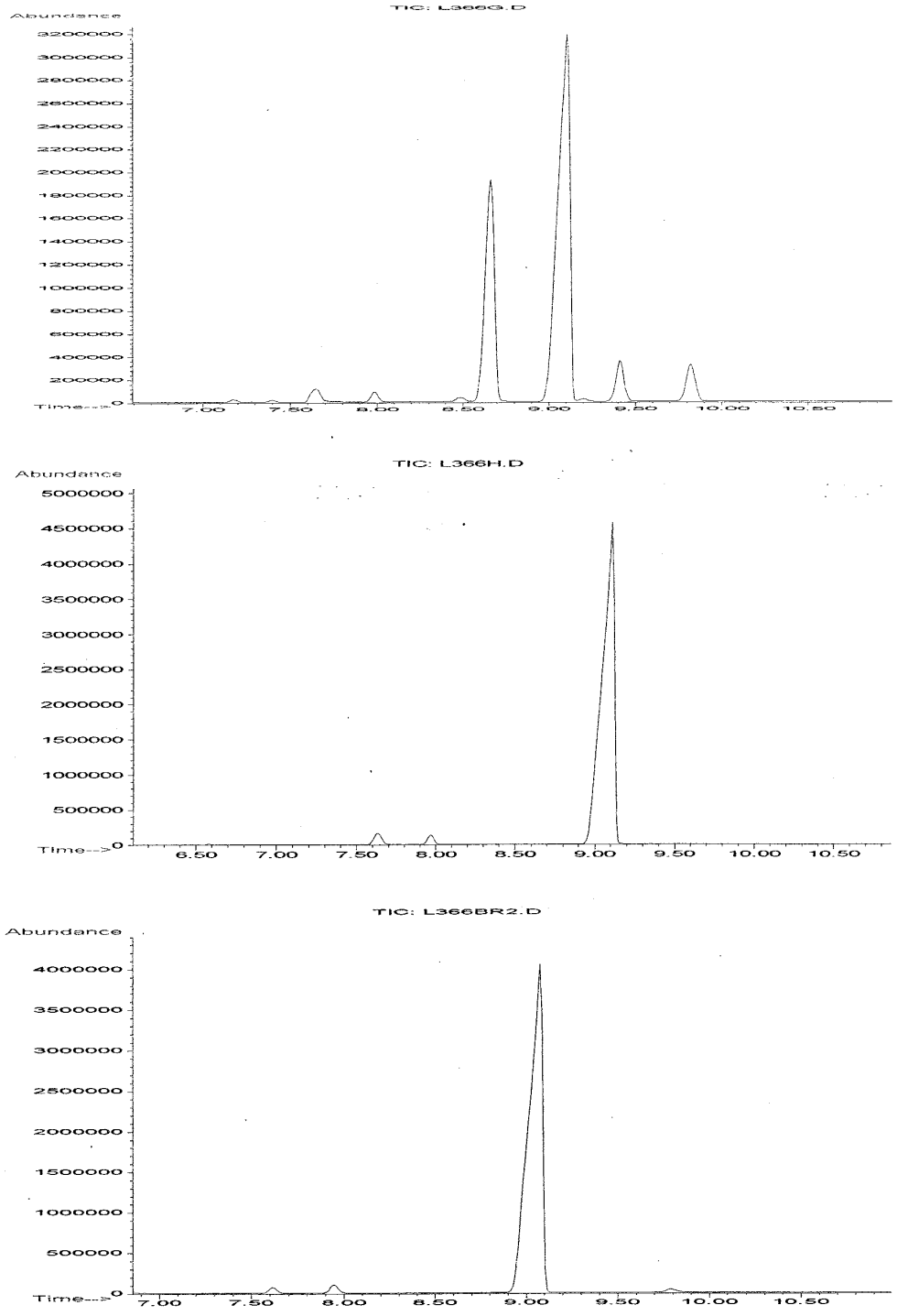

Figure 8. The Chromatogram of the Carbon-7 of the Run Bao20 (Top: FT products; Middle: after hydrogenation; Bottom: after bromination).

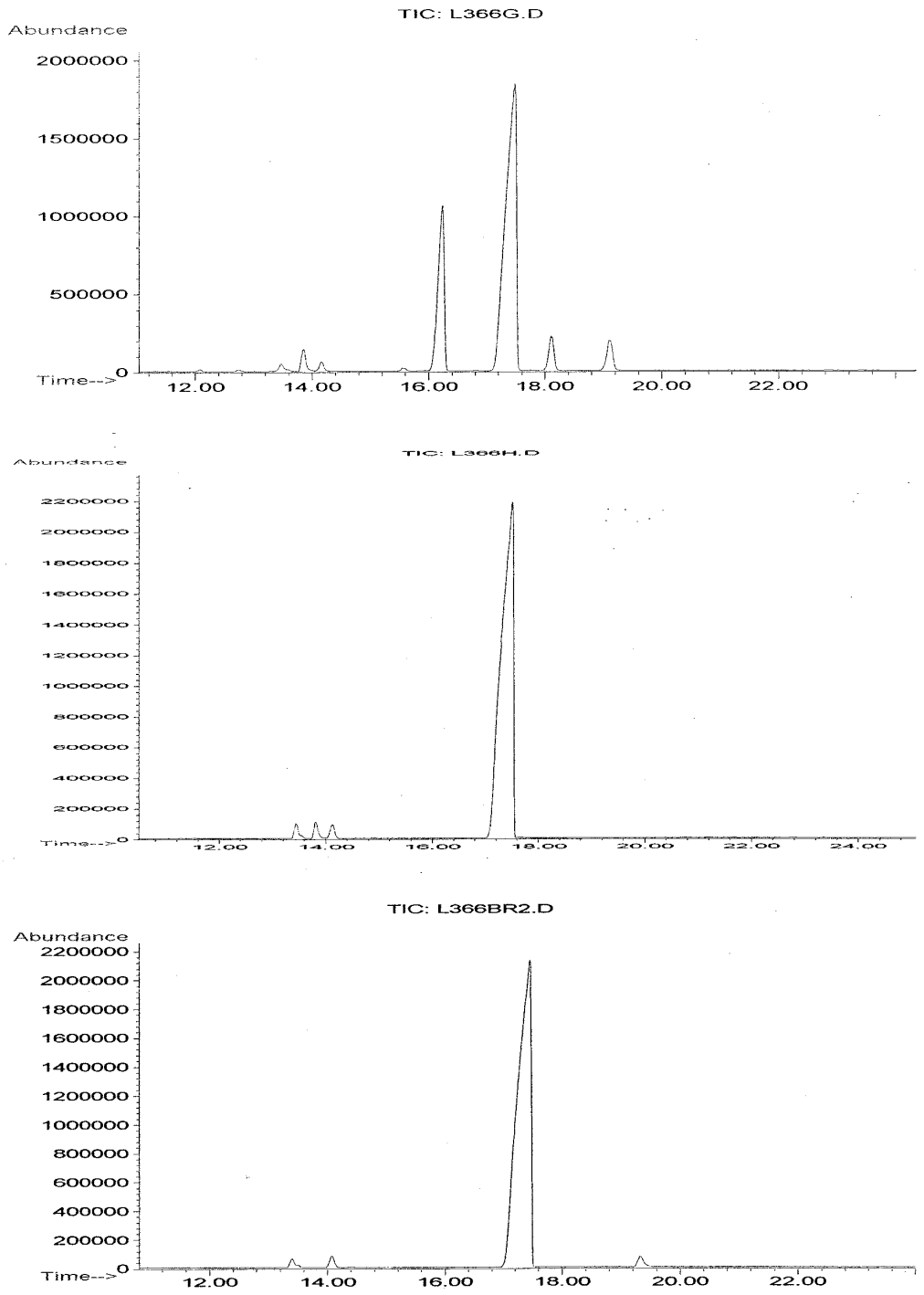

Figure 9. The Chromatogram of the Carbon-8 of the Run Bao20 (Top: FT products; Middle: after hydrogenation; Bottom: after bromination).

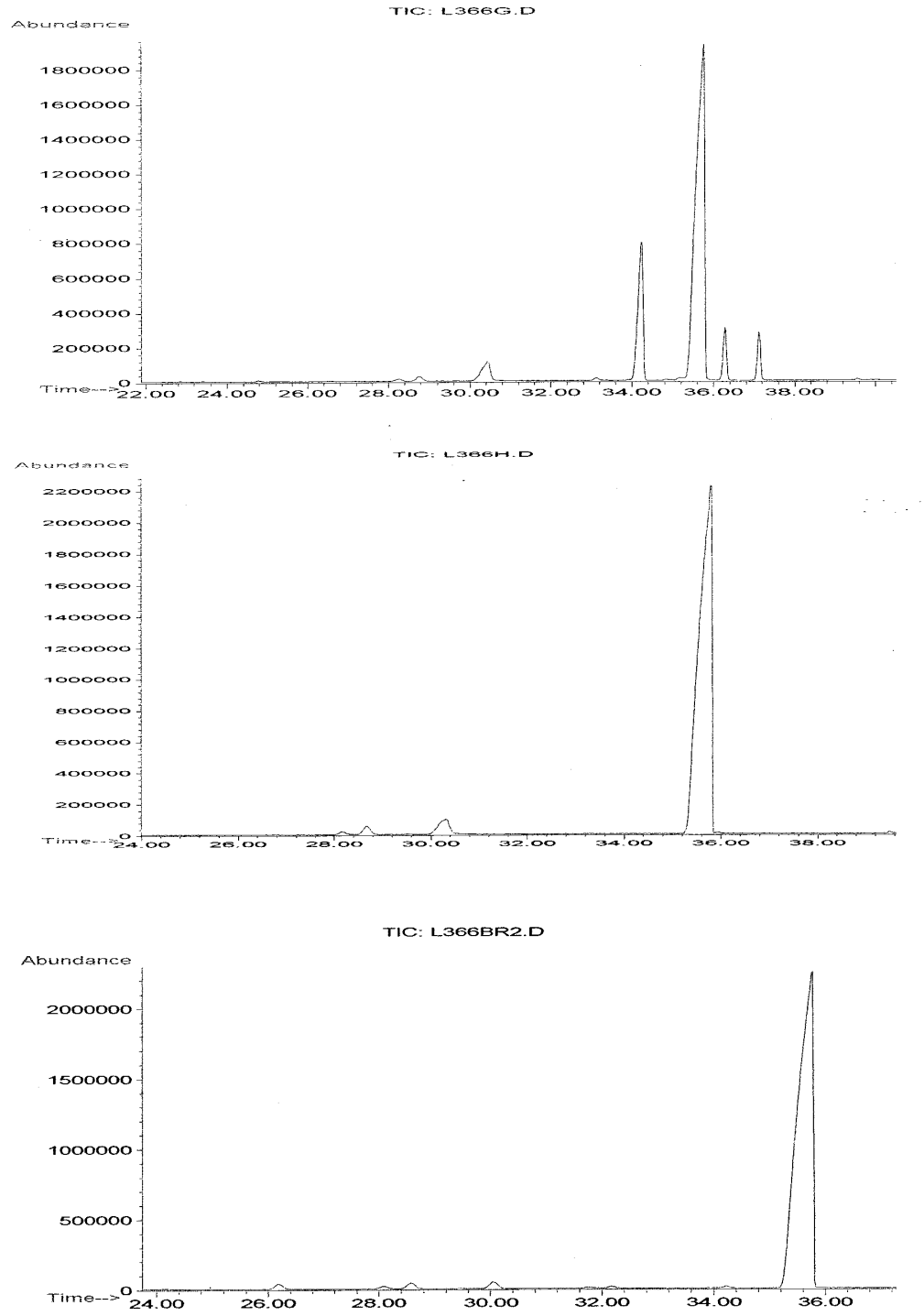

Figure 10. The Chromatogram of the Carbon-9 of the Run Bao20 (Top: FT products; Middle: after hydrogenation; Bottom: after bromination).

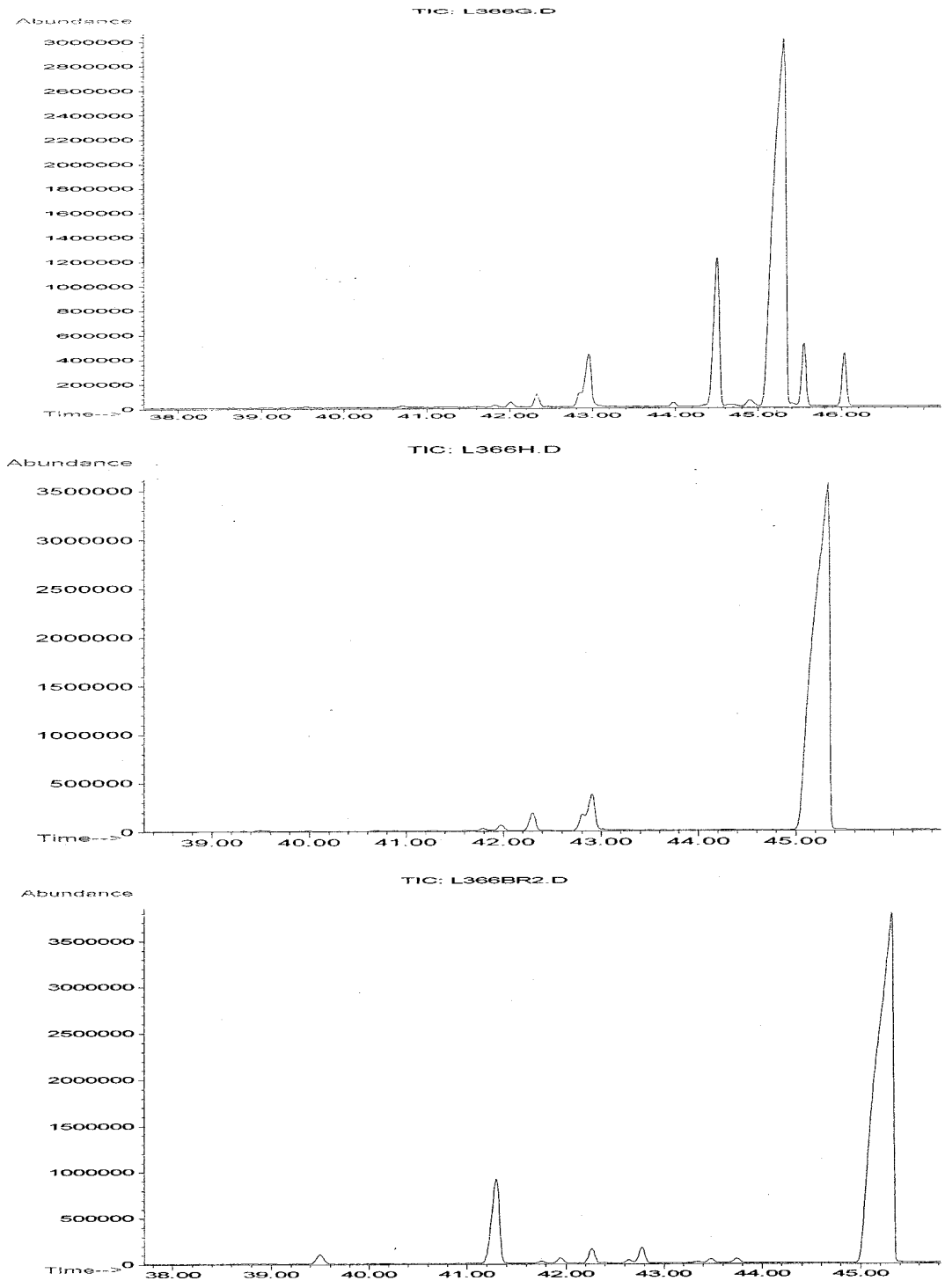

Figure 11. The Chromatogram of the Carbon-10 of the Run Bao20 (Top: FT products; Middle: after hydrogenation; Bottom: after bromination).

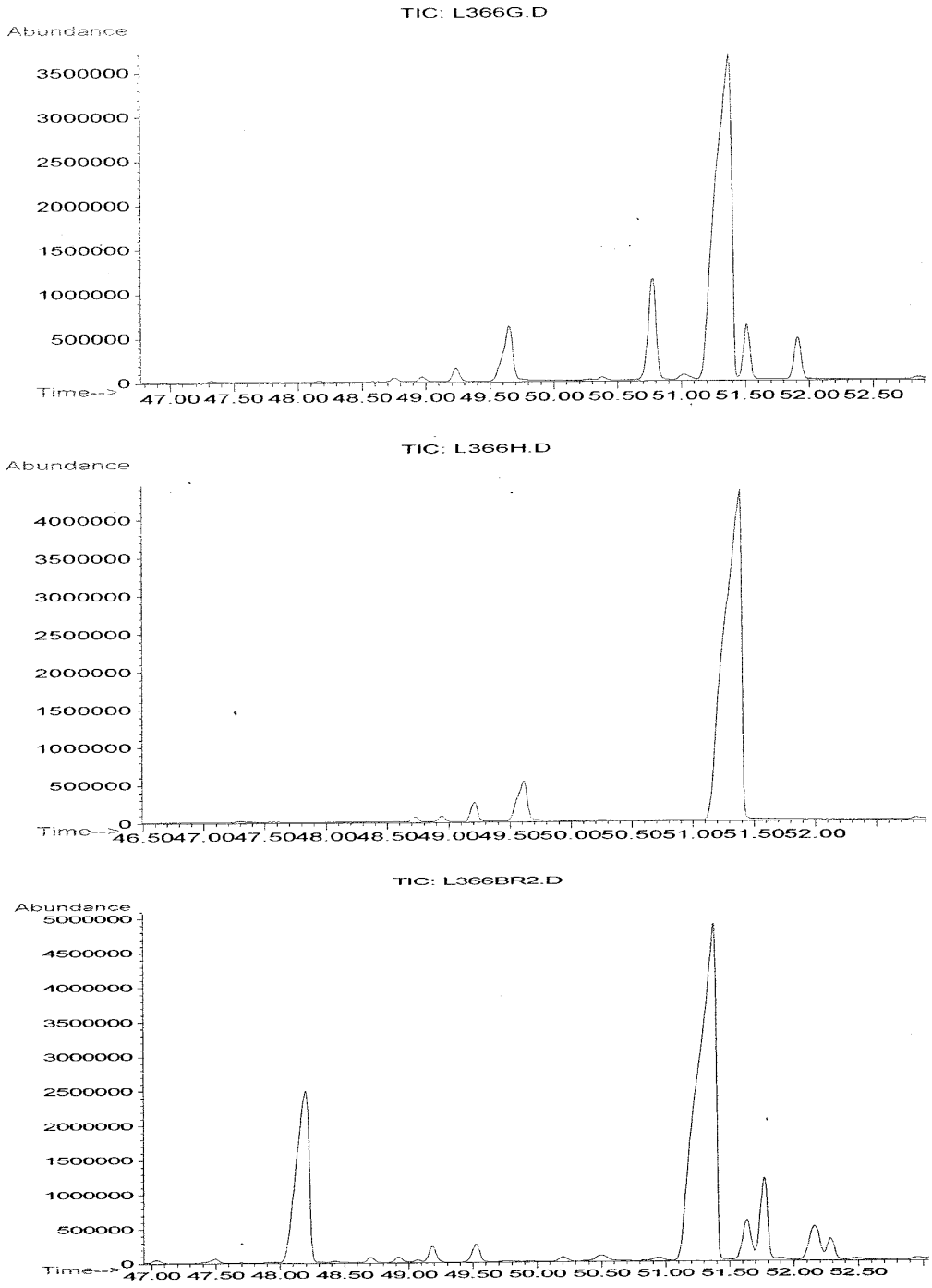

Figure 12. The Chromatogram of the Carbon-11 of the Run Bao20 (Top: FT products; Middle: after hydrogenation; Bottom: after bromination).

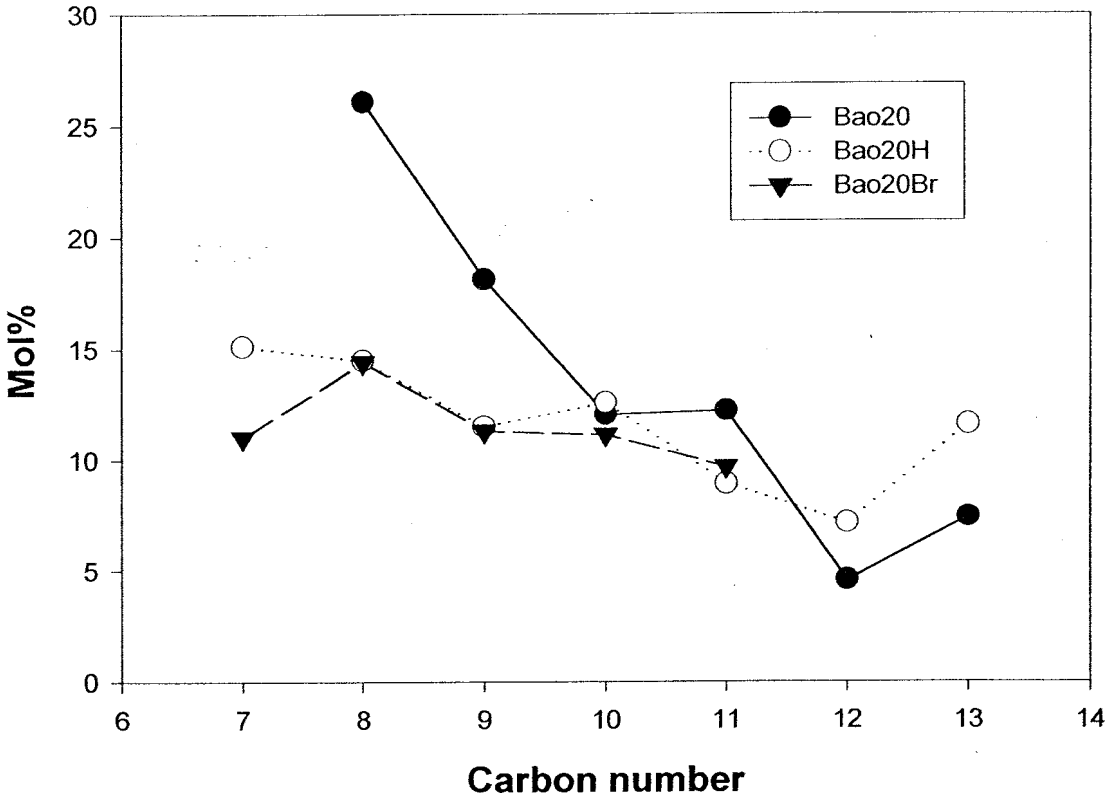

Figure 13. The Mole Percent of Branched Alkanes in Fe Catalyzed FT Products (Run ID: Bao20).

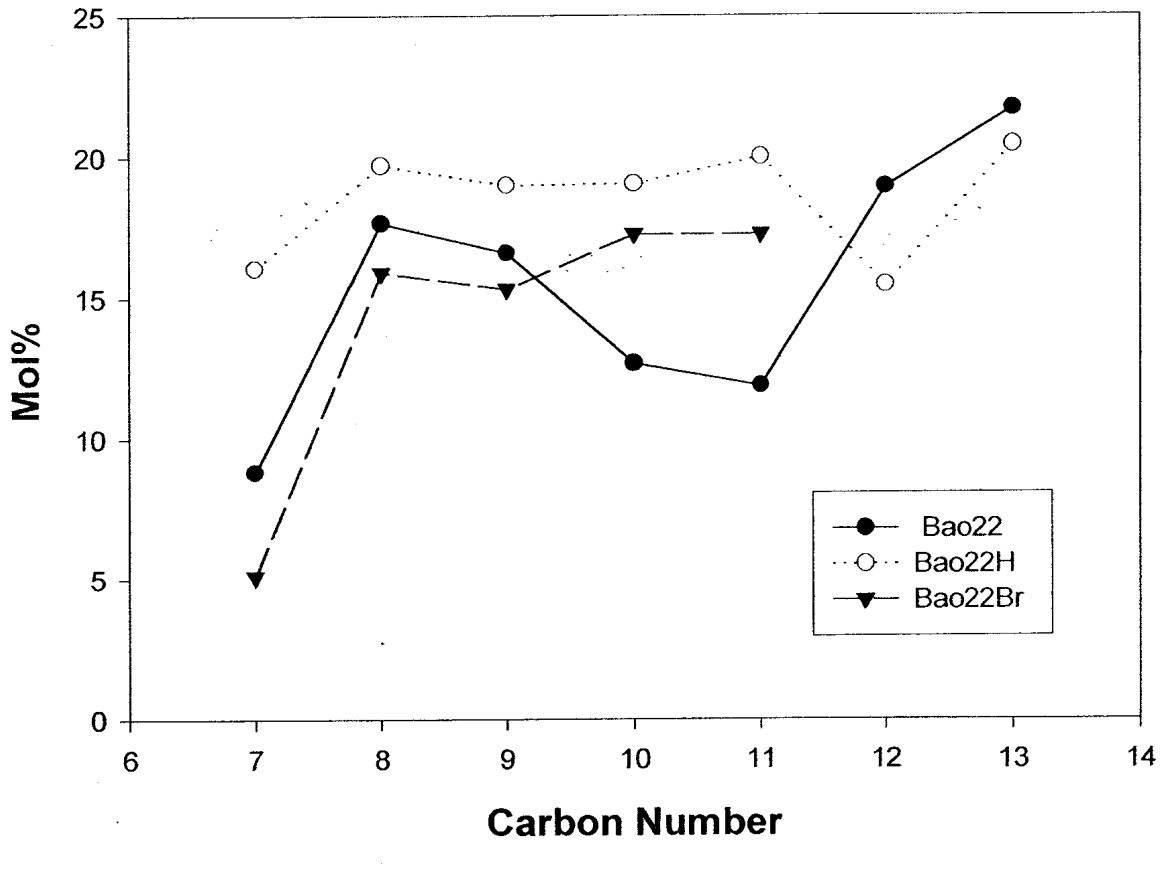

Figure 14. The Mole Percent of Branched Alkanes in Fe Catalyzed FT Products (Run ID: Bao22).

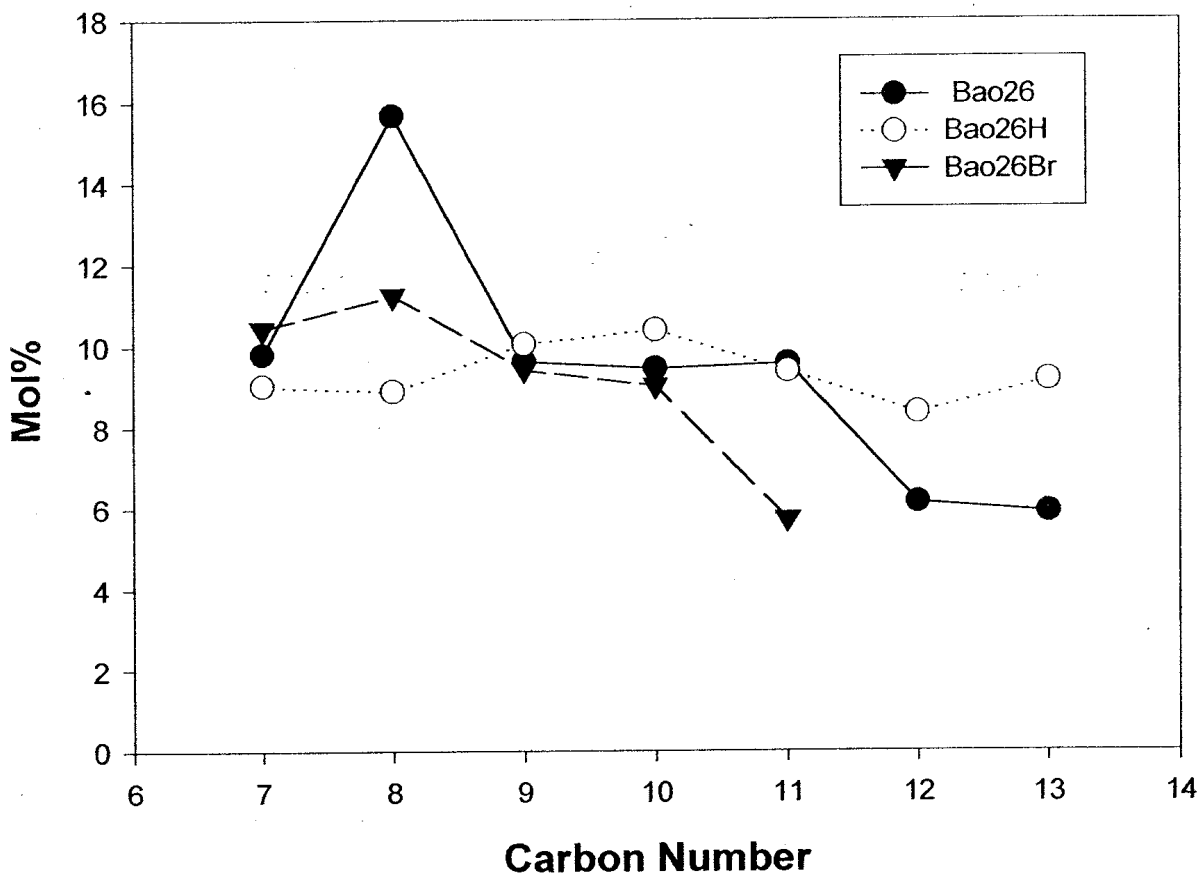

Figure 15. The Mole Percent of Branched Alkanes in Fe Catalyzed FT Products (Run ID: Bao26).

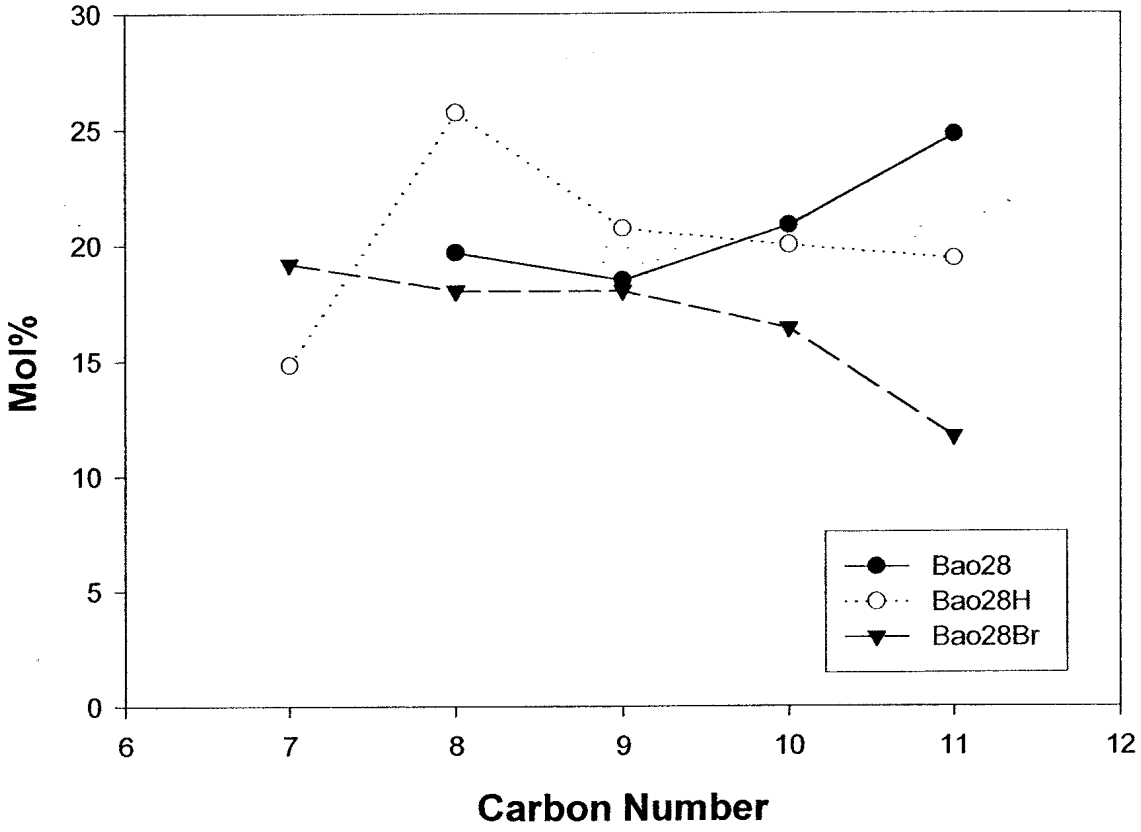

Figure 16. The Mole Percent of Branched Alkanes in Fe Catalyzed FT Products (Run ID: Bao28).

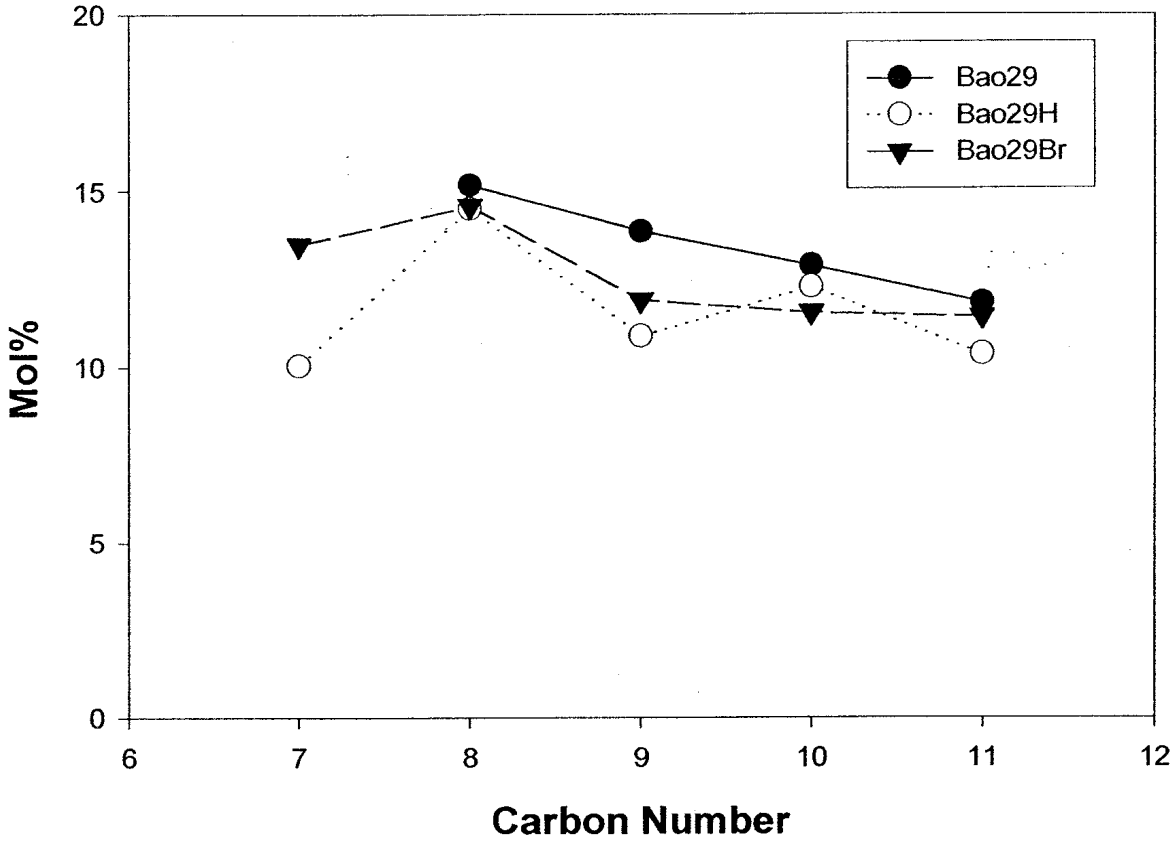

Figure 17. The Mole Percent of Branched Alkanes in Fe Catalyzed FT Products (Run ID: Bao29).

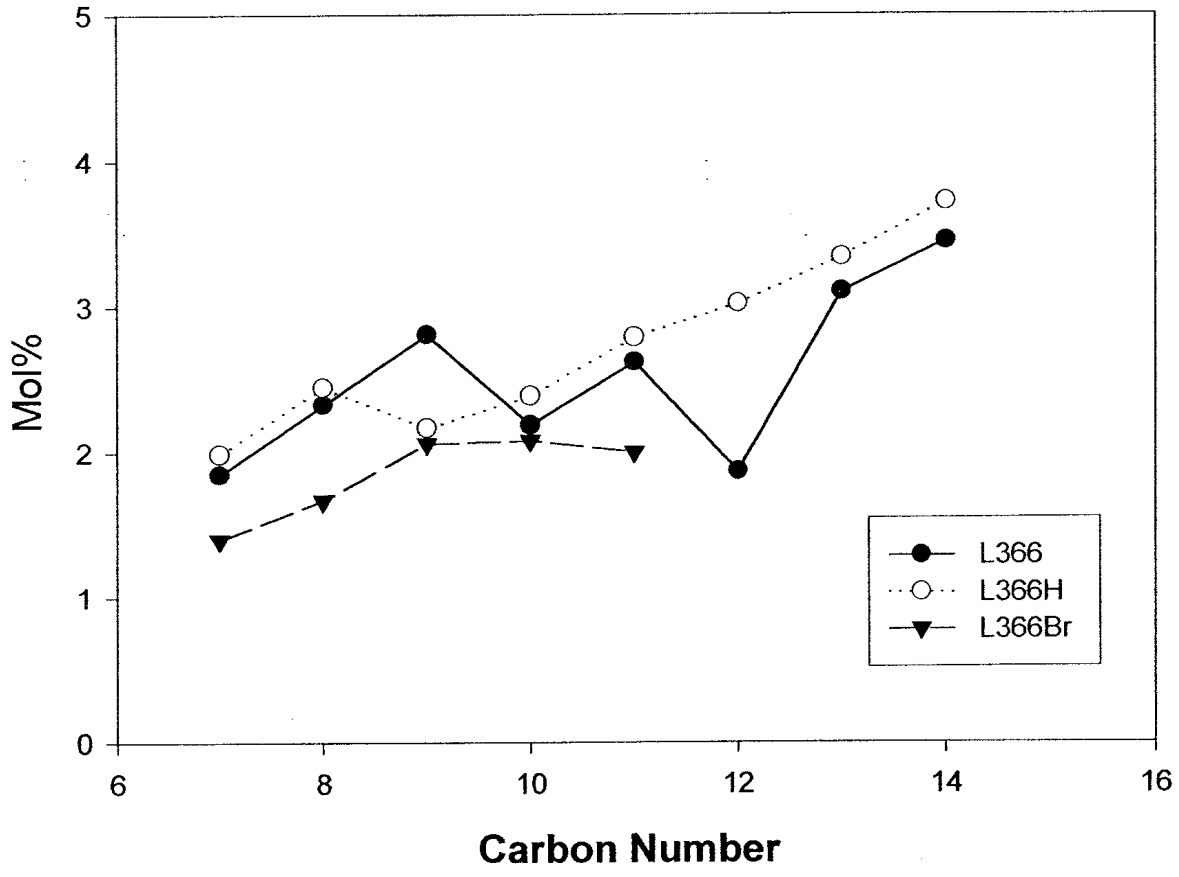

Figure 18. The Mole Percent of Branched Alkanes in Co Catalyzed FT Products (Run ID: L366).

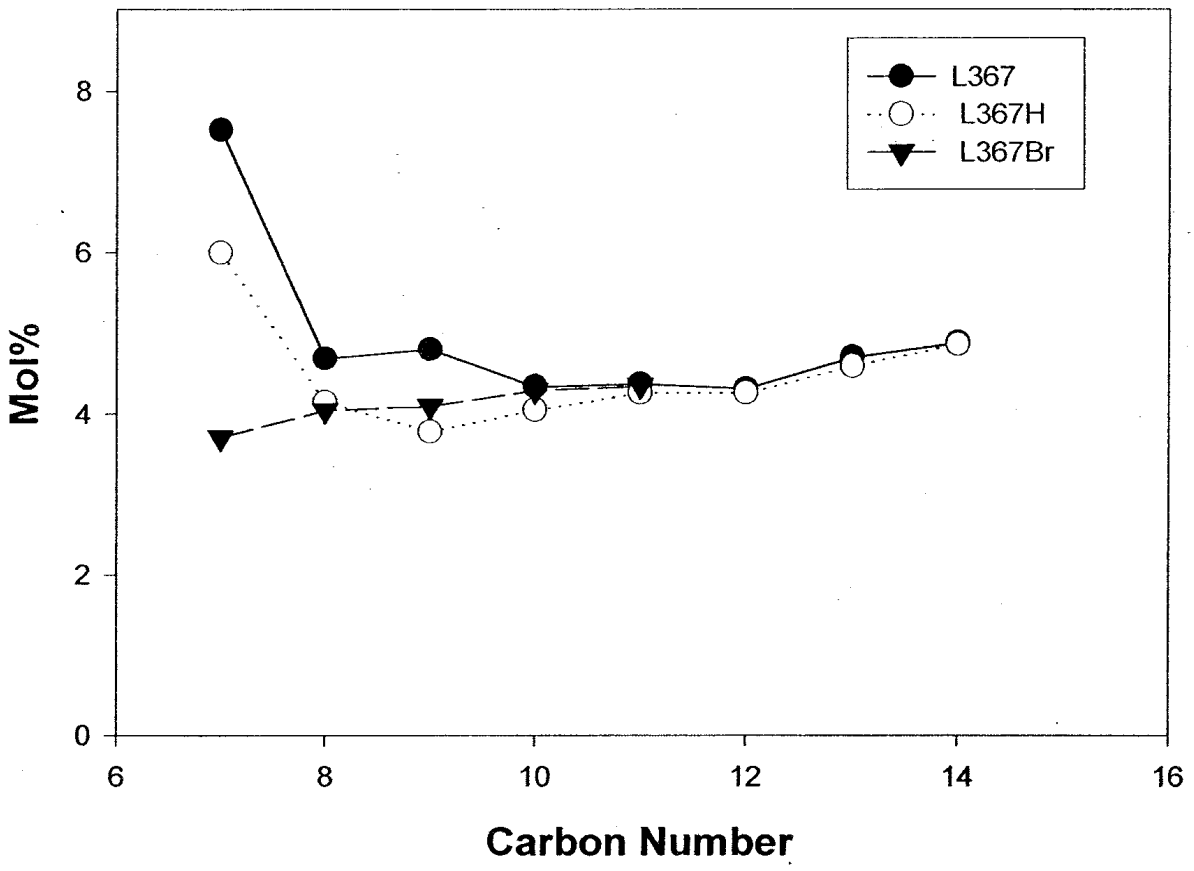

Figure 19. The Mole Percent of Branched Alkanes in Co Catalyzed FT Products (Run ID: L367).

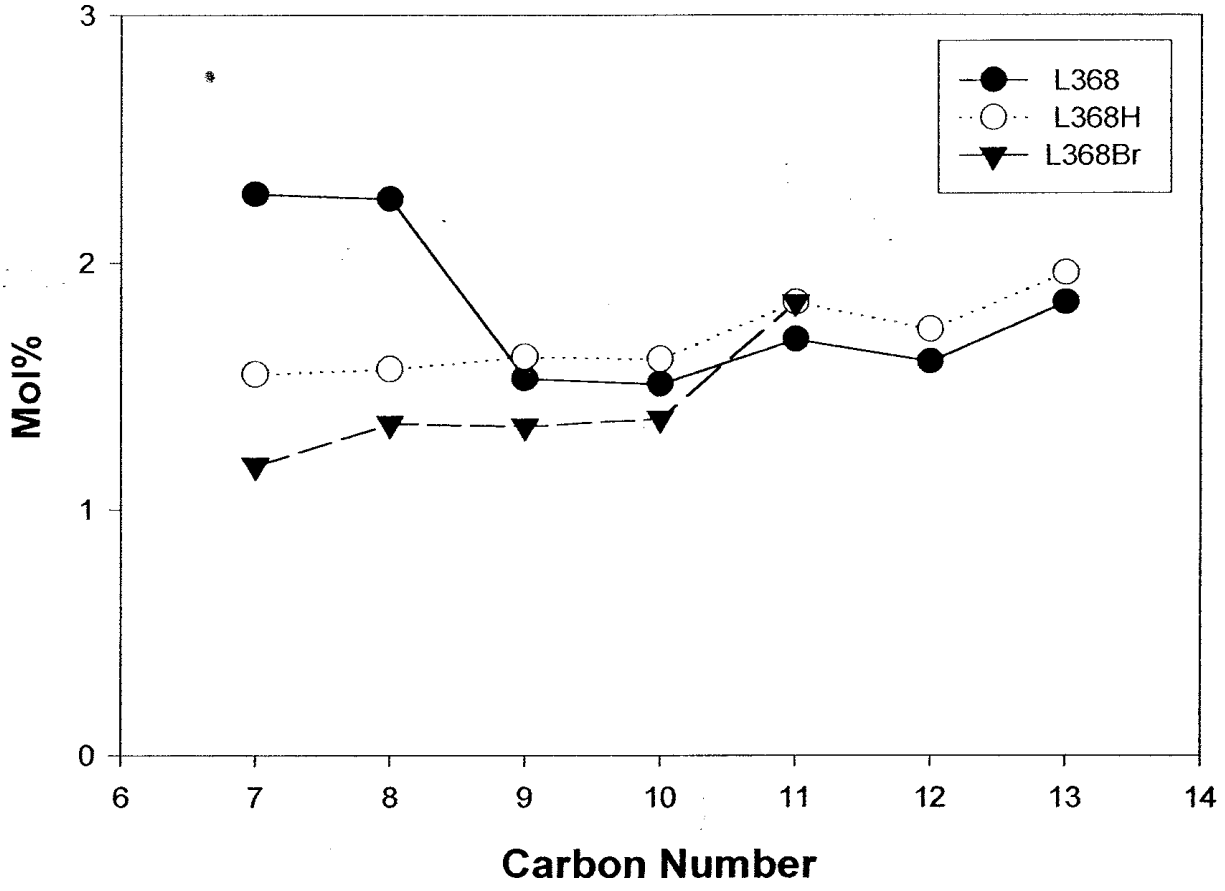

Figure 20. The Mole Percent of Branched Alkanes in Co Catalyzed FT Products (Run ID: L368).

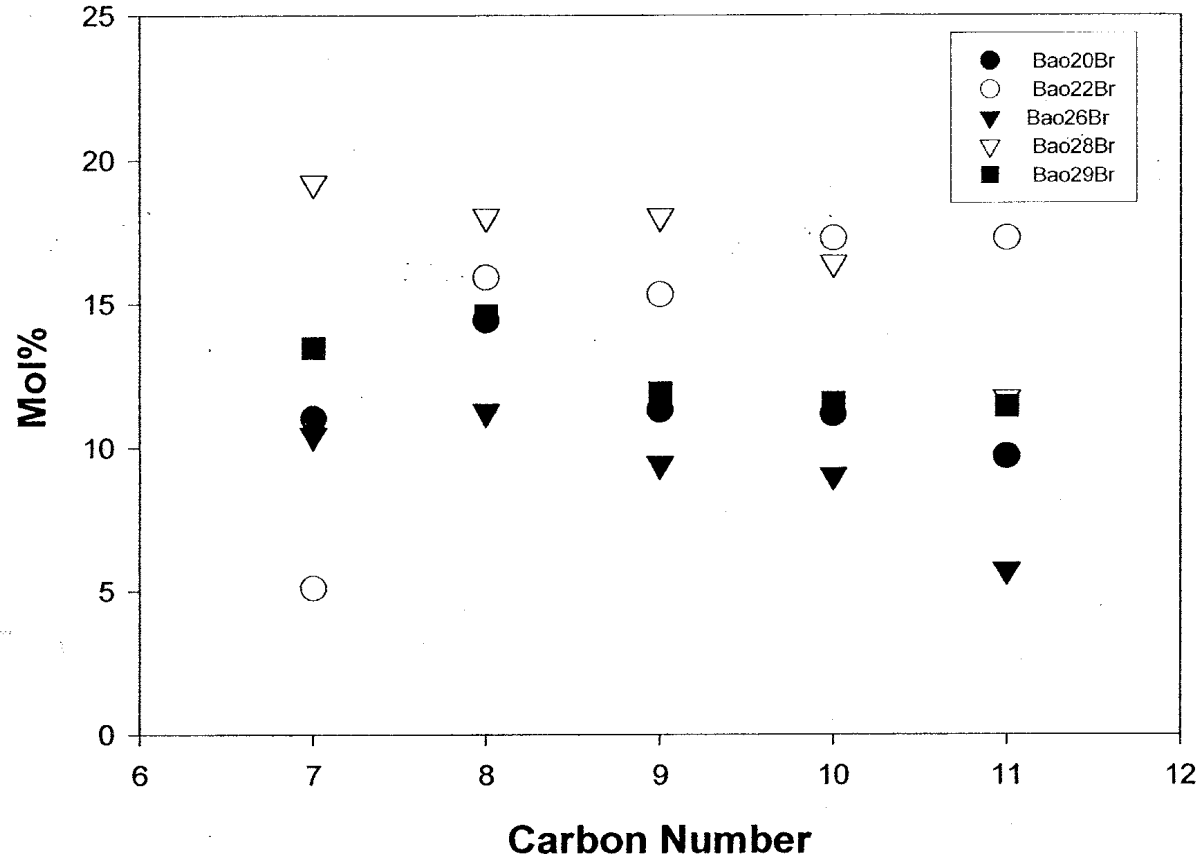

Figure 21. The Mole Percent of Branched Alkanes in Fe Catalyzed FT Products (after bromination).

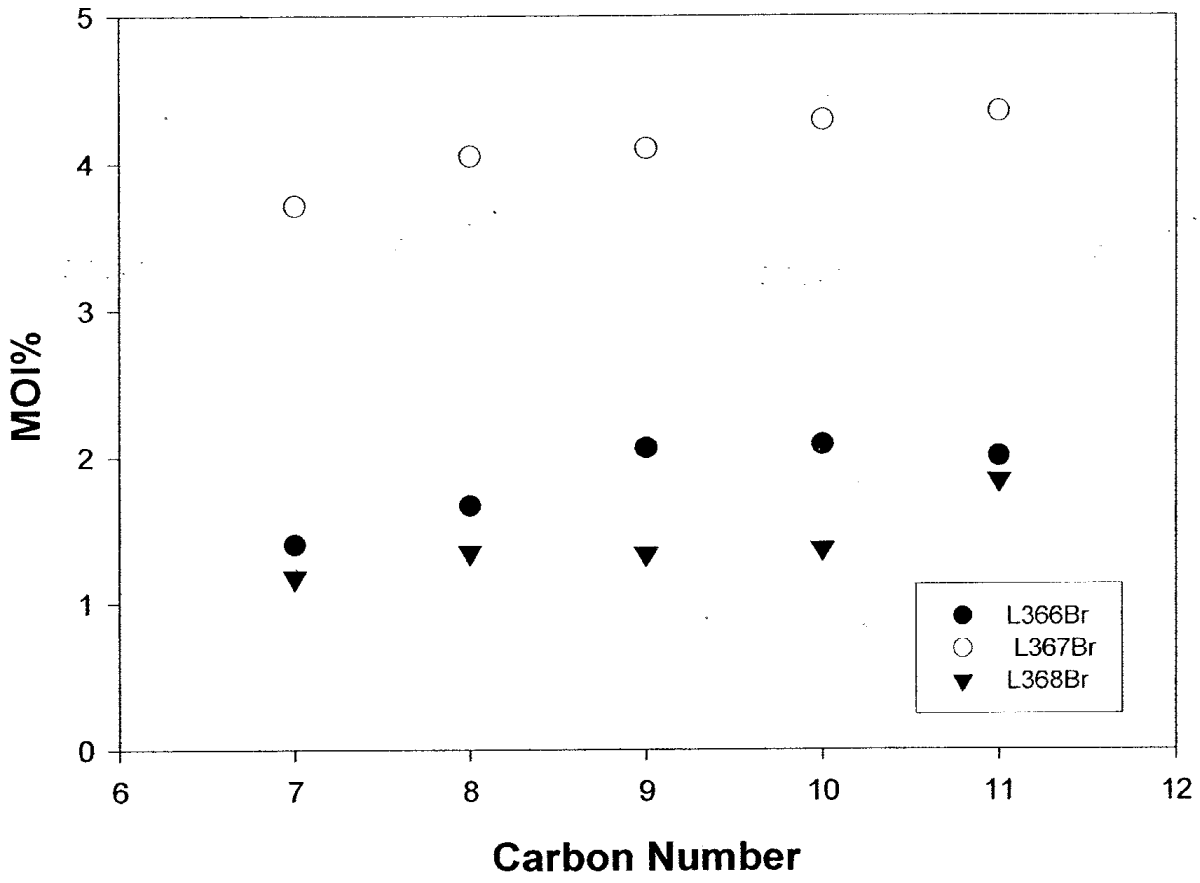

Figure 22. The Mole Percent of Branched Alkanes in Co Catalyzed FT Products (after bromination).

B. D_2O Tracer Studies in Co Catalyzed Fischer-Tropsch Reaction

Abstract

The data show that the deuterium added in water together with synthesis gas provides hydrogen for the Fischer-Tropsch synthesis. In fact, the deuterium initially present in water nearly equilibrates with the hydrogen present in synthesis gas. Thus, water, once formed, is not inert but adsorbs competitively on the cobalt-titania catalyst to activate hydrogen. The data do not permit a definition of whether the exchange occurs on cobalt or the alumina support. The H/D ratio in the paraffin products is 4.4 and is very close to the H/D ratio in the feed of D_2O/H_2 (4.1).

Keywords: Cobalt-alumina; isotopic tracer; Fischer-Tropsch Synthesis; deuterium, deuterium oxide; water, deuterated.

Introduction

The Fischer-Tropsch (FT) reaction can be summarized by Equation 1.

$$nCO + (2n + 1)H_2 \text{ ---> } C_nH_{2n+2} + nH_2O \quad (1)$$

Under FT reaction conditions, with some catalysts and/or reaction conditions, the water-gas shift (WGS) reaction also can occur as a side reaction (eq. 2).

$$H_2O + CO \rightleftharpoons CO_2 + H_2 \quad (2)$$

The amount of water converted to hydrogen by the WGS reaction depends on the reaction conditions and the catalyst used. It has been reported that water can affect the FT reaction rate and the selectivity [1].

According to eq. 2, water can be converted to hydrogen, which can be used by FT reaction to produce hydrocarbons. The question how effective a hydrogen source the H_2O can be in the FT synthesis with a cobalt catalyst is still not answered. In this study, D_2O was used as a probe to study the deuterium distribution of FT products. The H/D ratio of the products give

some clue about H/D ratio of the surface H-D pool and quantitative measure of the effectiveness of H_2O as the hydrogen source.

Experimental

The FT reaction (LGX372) was carried out in a 1-L continuously stirred autoclave reactor (CSTR) as described previously [2]. Fourteen grams of catalyst (Co (10 wt.%)/ Ru (0.2 wt.%)/TiO_2) was activated using H_2 at 300°C in a plug flow reactor and transferred to the CSTR without exposure to air. Synthesis was conducted at 2.40 MPa (350 psig) and 230°C using 300 g of PW 3000 as the startup oil (a polyethylene fraction with average MW = 3000). Three traps follow the reactor and are held at 200°, 130° and 0°C. For the D_2O tracer run, D_2O was co-fed with syngas (D_2O, 4.19 SLPH; H_2, 17.09 SLPH; CO, 8.50 SLPH) for 7 hours. Immediately prior to addition of the tracer, the three product traps were emptied. At the end of the addition of D_2O, the product traps were again drained and the contents were analyzed using the normal GC procedures as well as GC/MS analysis. During the tracer run, a gas sample was taken every 1.5 hours for analysis.

The relative amounts of the isotopomers of the hydrocarbons were determined by GC/MS. The data were corrected for the ^{13}C content of the products. Because of the inverse isotope effect of the deuterated compounds with gas chromatography, the relative amount of the total area of the molecular ion of each isotopomer was used to calculate the molar ratio [3].

The relative amount of H_2, HD and D_2 were measured by GC using a 90-meter molecular sieve column and He carrier. H_2, HD and D_2 were separated at 80°C. The thermal conductivity differences of hydrogen and the carrier causes a negative peak to be obtained for H_2.

The relative amount of H_2O, HDO and D_2O was analyzed using GC/MS. The ratio of H/D obtained using this method has a standard deviation of $\pm$ 0.12.

Results and Discussion

Table 1 contains the deuterium distribution of alkane products collected following the 7-hour D_2O tracer run of a Co catalyzed FT reaction. The relative amounts of the isotopomers of each carbon number from C_5 to C_{16} were determined the using the GC/MS method. As can be seen from the data in Table 1, the relative amount of d_0 isomer of each carbon number is unusual higher than expected if we assume a binomial distribution of H and D atoms in a compound. Also, the relative amount of the d_0 isotopomer of alkanes increases as the carbon number increases. These results indicate the presence of accumulated products (Δ) [4,5].

Products accumulation (Δ) is a phenomena that must always be considered for an isotope tracer study in FT reactions. In most tracer studies of the FT synthesis, the unlabeled syngas conversion is conducted until the catalytic activity has stabilized and then the labeled compound is added for some time period. Usually the products are collected during the period of labeled compound addition. The products thus collected will consist of three fractions: (1) the products derived from the labeled compounds, which will contain at least one labeled atom; (2) the products from the normal FT synthesis that are derived from the unlabeled syngas, and (3) any products formed from unlabeled synthesis gas during the period of activity stabilization, that is, the period before the labeled compound is added.

It has been reported [6] that the relative value of Δ of a carbon number increases as the carbon number increases. It also has been reported that product accumulation (Δ) can affect the data interpretation of all of isotope tracer studies in FT reaction run at both small flow and large CSTR reactors [4]. Failing to include this factor in the data analysis could led to conclusions that are consistent with the data but are not representative of the reaction mechanism [4,7,8].

Since the presence of product accumulation is the nature of the isotope tracer experiment in FT reaction, this factor cannot be eliminated completely. However, the effect of the

accumulated products can be minimized by applying some experimental techniques. For example, by collecting the gas sample of a tracer experiment after the experiment has run for a period of time (3 hours under the present conditions, for instance) and using the data derived from only the gas sample, the accumulation factor can be minimized. In ^{13}C and deuterium labeled tracer experiments, this factor can be removed by utilizing only the products that contain ^{13}C or deuterium for all carbon numbers. This method has been used to reinterpret ^{13}C labeled tracer data [4]. In this study, this method is used to interpret the data that has been obtained for the D_2O tracer experimental data shown in Table 1.

The d_0 isomers of each carbon number in Table 1 come from two sources: the product accumulation (Δ) and the products from normal FT synthesis that are derived from the unlabeled syngas. In the D_2O tracer experiment, the amount of d_0 isomer of each carbon number from normal FT synthesis during the tracer experiment is determined by the H/D ratio of the surface pool as well as the carbon number. As can be seen from the data in Table 2, by assuming the H/D ratio of 4, based upon the total H and D in the feed, as the surface H-D pool, the amount of d_0 isotopomer of C_7 alkane that could be produced during the tracer experiment is 2.8%. As the carbon number increases, the amount of d_0 isotopomer decreases, with the amount of d_0 isomer of C_{16} alkane decreasing to 0.05%. These values are smaller than the experimental error of GC/MS analysis [3]. Therefor, if we eliminate the d_0 isomers in considering the data in Table 1 and recalculate the deuterium distribution of the remaining isotopomers of each alkane, the products present in the reactor before the tracer experiment are eliminated from consideration since all of the Δs are d_0 isomers. Also, based on the above analysis and the data in Table 2, removing all of the d_0 isomer in each carbon number introduces very small errors.

Table 3 lists the deuterium distribution of the isotopomers of each carbon number calculated after eliminating the d_0 isotopomers. As can be seen from the data in this table, the

deuterium distribution of each compounds is close to a binomial distribution with a H/D ratio of about 4.4. For example, a plot is shown in Figure 1 for the deuterium distribution of octane (d_0 isomer was eliminated) that was obtained experimentally and one that is calculated for the binomial distribution and the agreement of the two is excellent. Based on the mol% of each isotopomer, the H/D ratio of octane (Table 3) was calculated to be 4.4. Assuming a binomial distribution of the deuterium with a H/D ratio of 4.4 in the surface H-D pool, the calculated mol% of each isotopomer fit the experimental value nicely.

Figure 2 shows the H/D ratio of alkanes measured for carbon numbers C_5 to C_{16}. When the d_0 isomer is included for each carbon number, the H/D ratio increases as the carbon number increases, consistent with the impact of accumulated products. When the d_0 isomers are not included for each carbon number, the H/D ratio is essentially constant (in this case, 4.4), indicating that all of the deuterium and hydrogen in the compounds comes from a common H-D source: the surface H-D pool with a ratio of 4.4.

Table 4 is the summary of the samples analyzed. The ratio of H/D in the feed is based on accurately measured rates of addition of D_2O, H_2 and CO. The H/D ratio of the hydrocarbons was obtained from GC/MS data as described above. The H/D ratio of water was measured using GC/MS. Known mixtures of H_2O and D_2O were prepared by accurate weight and the calibration curve was nearly linear (Figure 3). The H_2, HD and D_2 were separated by GC as shown in Figure 4 with H_2 as a negative peak. The r^2 for the standard calibration data for H_2, HD and D_2 are 0.994, 0.997 and 0.999, respectively.

There is an inverse kinetic isotope effect (kie) for the hydrogenation of carbon monoxide (9). Thus, it is not unusual for the D/H ratio in the hydrocarbons to be higher than was present in the feed if the syngas contained an equimolar mixture of H_2 and D_2. Introducing the isotopes as H_2 and D_2O complicates the situation so that the inverse kie cannot be used to predict the results.

Based upon the average H/D in the hydrocarbons, the kie is not as great as when H_2 or D_2 are used alone.

References

1. E. Iglesia, Appl. Catal. A: General 161 (1997) 59.

2. B. Shi, R. J. O'Brien, S. Bao and B. H. Davis, J. Catal. 199 (2001) 202.

3. B. Shi and B. H. Davis, unpublished results.

4. B. Shi and B. H. Davis, Catalyst Today, 58 (2000) 255.

5. B. Shi and B. H. Davis, Catalyst Today, 65, 95 (2001).

6. B. Shi and B. H. Davis, The results were reported on 217th ACS national meeting, Anaheih, CA, March 21-28, (1999).

7. M. L. Turner, H. C. Long, A. Shenton, P. K. Byer and P. M. Maitlis, Chem. Euro. J., 1 (1995) 549.

8. L. M. Tau, H. A. Dabbagh and B. H. Davis, Energy & Fuels 5 (1991) 174.

9. A. Raje and B. H. Davis, in "Fischer-Tropsch Synthesis, Mechanism Studies Using Isotope, Catalysis" (J. J. Spring, Ed), Vol. 12, p. 52, The Royal Chem. Soc., Cambridge, 1996.

Table 1

The Deuterium Distribution of the Alkane Products of the FT Reaction (while adding D_2O)

# of C[a]	C_5[c]	C_6	C_7	C_8	C_9	C_{10}	C_{11}	C_{12}	C_{13}	C_{14}	C_{15}	C_{16}
# of D[b]												
0	41.7	45.9	49.4	61.0	70.2	73.5	78.0	80.7	84.2	87.7	91.0	94.1
1	16.1	9.8	7.3	6.2	4.4	4.1	3.4	2.9	2.5	1.9	1.6	0.7
2	17.6	12.7	10.6	7.4	4.9	3.3	2.3	2.0	1.4	1.2	0.8	0.5
3	13.9	13.1	12.3	8.4	5.8	4.3	3.1	2.4	1.8	1.2	0.8	0.5
4	7.5	9.8	9.9	7.7	5.9	4.9	3.9	3.0	2.2	1.6	0.9	0.7
5	2.4	5.5	6.1	5.1	4.4	4.3	3.6	3.2	2.5	1.7	1.2	0.8
6	0.8	2.3	3.0	2.8	2.7	3.0	2.7	2.6	2.2	1.7	1.3	0.8
7	0.12	0.8	1.0	1.1	1.2	1.6	1.7	1.7	1.6	1.4	1.0	0.8
8		0.2	0.3	0.4	0.5	0.7	0.9	1.0	1.1	0.9	0.8	0.7
9				0.1	0.1	0.3	0.4	0.5	0.6	0.6	0.5	0.4
10							0.1	0.2	0.2	0.2	0.3	0.3
11									0.1	0.2	0.1	
H/D	7.6	7.7	8.8	12.8	17.8	20.5	25.5	29.9	37.3	49.5	69.2	104

a. Carbon number.
b. Number of deuterium.
c. The values for all isotopomers of all the alkanes are mol%.

Table 2

The Mol% of d_0 Isomers Calculated for C_5-C_{16} Hydrocarbons that are Produced for a Binomial Distribution from a Syngas with a H/D Ratio of 4

Carbon Number	d_0 isomer (mol%)
C5	6.9
C6	4.4
C7	2.8
C8	1.8
C9	1.2
C10	0.7
C11	0.5
C12	0.3
C13	0.2
C14	0.1
C15	0.08
C16	0.05

Table 3

The Deuterium Distribution of the Alkane Products of the FT Reaction (Tracer: D_2O; after eliminated d_0 isomers of each carbon number of the data in Table 1

# of C[a]	C_5[c]	C_6	C_7	C_8	C_9	C_{10}	C_{11}	C_{12}	C_{13}	C_{14}	C_{15}	C_{16}
# of D[b]												
1	27.5	18.1	14.5	15.9	15.0	16.0	16.2	16.5	17.5	18.0	20.5	15.1
2	30.2	23.5	21.1	19.2	16.6	13.0	11.1	11.1	10.0	11.3	10.7	9.9
3	23.8	24.3	24.5	21.9	19.9	17.0	15.2	13.7	12.5	10.9	10.7	11.2
4	12.9	18.2	19.8	19.9	20.2	19.3	18.8	17.0	15.8	14.8	12.0	13.4
5	4.1	10.2	12.1	13.2	14.9	16.7	17.4	17.8	17.5	16.0	16.1	16.8
6	1.3	4.3	6.1	7.2	9.3	11.9	13.0	14.6	15.7	15.8	16.9	16.2
7	0.2	1.4	2.0	2.9	4.2	6.2	8.4	9.4	11.2	13.3	13.2	17.5
8		0.3	0.6	0.9	1.7	2.9	4.2	5.9	7.6	8.3	10.6	14.0
9			0.1	0.1	0.3	1.1	2.1	2.9	4.1	6.0	6.6	8.3
10						0.2	0.4	0.9	1.7	2.1	3.2	5.6
11								0.2	0.5	1.4	1.8	0.8
H/D	4.0	3.7	3.9	4.4	4.6	4.7	4.8	5.0	5.2	5.4	5.6	5.5

a. Carbon number.
b. Number of deuterium.
c. The values in all the alkanes are mol%.

Table 4

The H/D Ratio of Starting Reagents, Products and Unreacted Gas

Category	Compounds Analyzed	H/D
Starting Reagents	D_2O; H_2	4.1
Products	Alkanes	4.4
Products	H_2O; HDO; D_2O	2.5
Unconverted Gas	H_2; HD; D_2	5.8

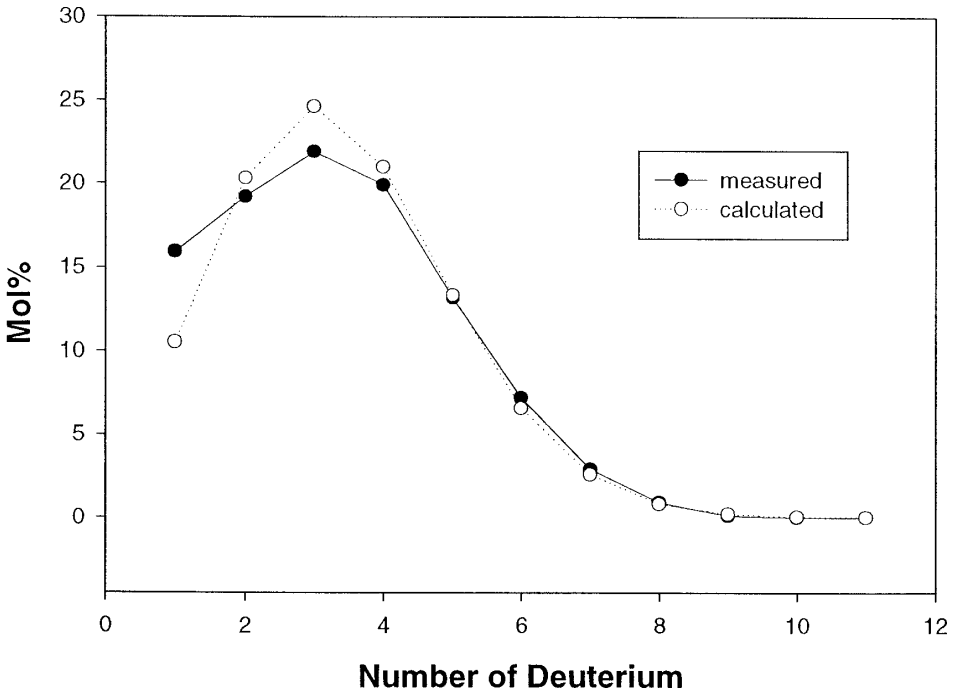

Figure 1. The deuterium distribution of the isotopomers of octane.

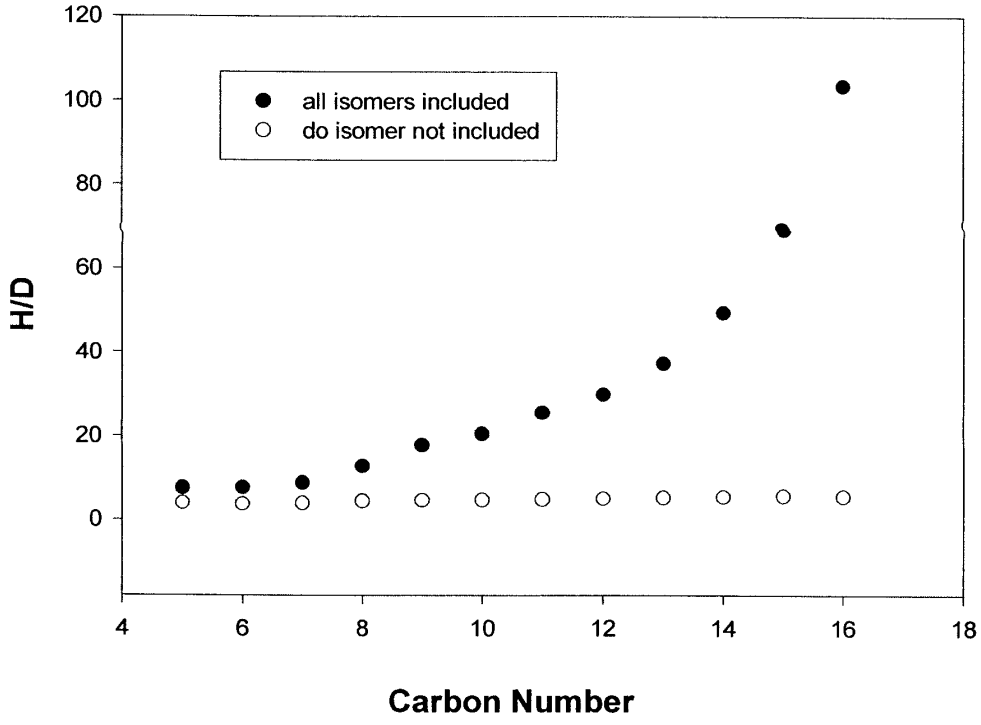

Figure 2. The ratio of H/D of alkanes in Co catalyzed FT reactions (Tracer: D_2O (H_2:D_2O = 4:1).

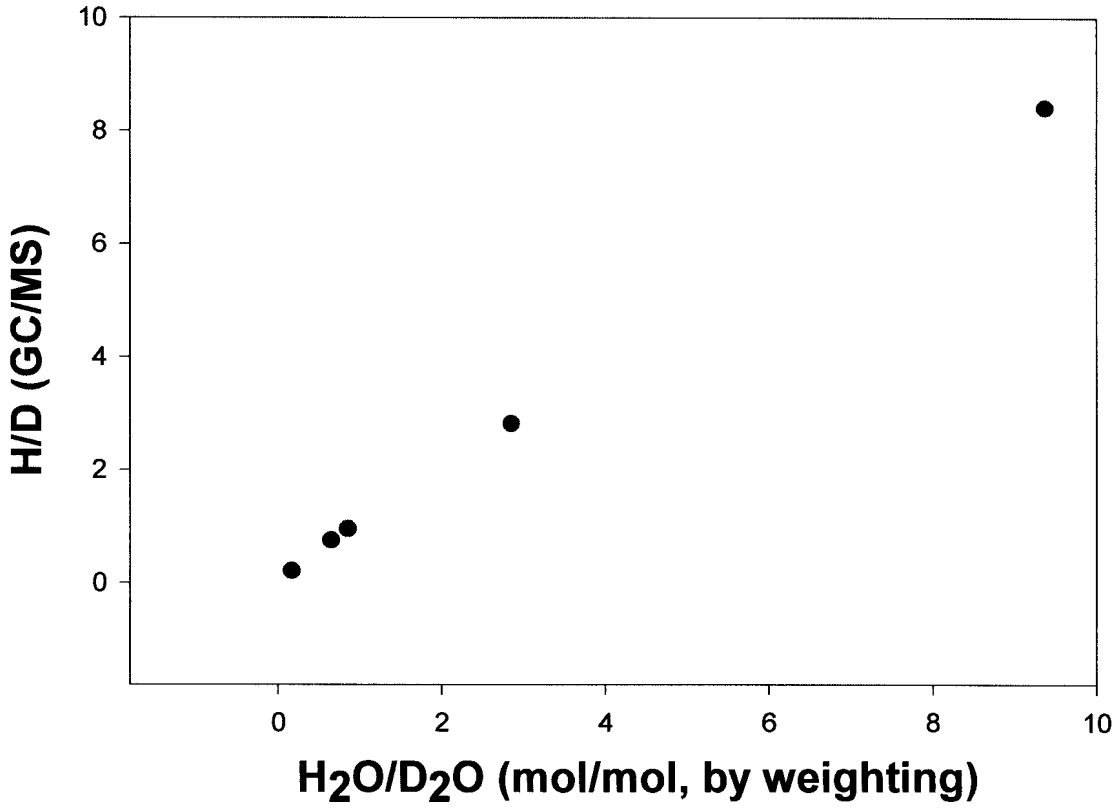

Figure 3. Plot of H/D ratio in standard H_2O/D_2O samples prepared by weight versus the H/D ratio from GC water peak.

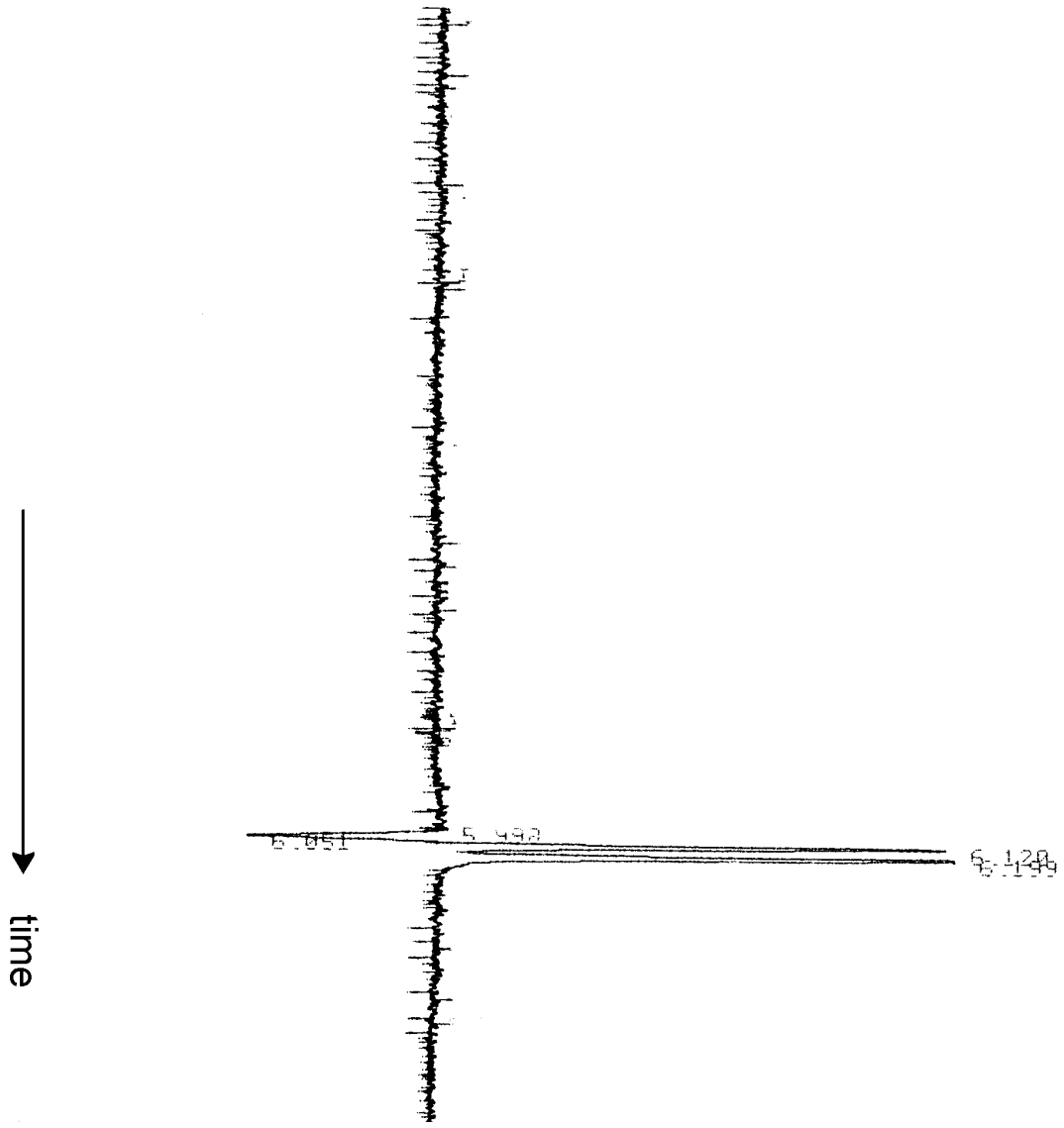

Figure 4. GC trace of signal from thermal conductivity cell (First peak H_2; middle peak, HD and last peak D_2).

C. Fischer-Tropsch Synthesis: Supercritical Conversion Using a Co/Al_2O_3 Catalyst in a Fixed Bed Reactor

Abstract

A cobalt catalyst ($25\%Co/\gamma\text{-}Al_2O_3$) was used in a fixed bed reactor under a pressure/density tuned supercritical fluid mixture of n-pentane/n-hexane. By using inert gas as a balancing gas to maintain a constant pressure, the density of the supercritical fluid could be tuned near the supercritical point while maintaining constant space velocity within the reactor. The benefits of the mixture allowed for optimization of transport and solubility properties at an optimum reaction temperature for Fischer Tropsch synthesis with a cobalt catalyst. There was an important increase in conversion due to greater accessibility to active sites after extraction of heavy wax from the catalyst, and additional benefits included decreased methane and carbon dioxide selectivities. Decreased paraffin/(olefin + paraffin) selectivities with increasing carbon number were also observed, in line with extraction of the hydrocarbon from the pore. Faster diffusion rates of wax products resulted in lower residence times in the catalyst pores, and therefore, decreased probability for readsorption and reaction to the hydrogenated product. Even so, there was not an increase in the alpha value over that obtained with just the inert gas.

1. INTRODUCTION

In the near future, increasing dependence on stranded natural gas reserves for fuel production is expected. This combined with increasing political pressure on oil companies to limit flaring of gas has renewed focus on Gas-to-Liquids (GTL) technology. Most GTL plants considered for commercialization consist of three process steps: (1) synthesis gas production from natural gas; (2) Fischer-Tropsch synthesis (FTS) to convert syngas to a crude hydrocarbon mixture (syncrude); and (3) hydroprocessing of syncrude to transportation fuels. Due to the

perception of high activity and stability, the catalyst of choice for FTS is typically a supported cobalt catalyst.

There are positive features as well as drawbacks to conducting Fischer-Tropsch by the traditional gas phase route or even by the more advanced liquid phase methods. For example, gas phase FTS, which is typically carried out in a fixed or fluid bed reactor, produces high product yields, due to the superior catalyst concentration per reactor volume. However, these higher initial rates, coupled with the potential for poor heat removal capacities of fixed-bed gas phase processing, typically lead to localized overheating of the catalyst, due to the exothermicity of the reaction, resulting in sintering of cobalt clusters, as well as the deposition of heavy waxes within catalyst pores, both contributing adversely to catalyst deactivation.

Better heat control throughout the reactor can be gained by conducting FTS in the liquid phase, due to the better heat removal capacities of the liquid. Liquid phase FTS is typically conducted in the laboratory in a continuously stirred tank reactor (CSTR) or commercially in the slurry bubble column reactor (SBCR). Deactivation rates are lower because the liquid media facilitates dissolving wax products, both internal and external to the catalyst pores. However, the liquid itself provides a resistance to the diffusional transport of gas phase reactants to active sites, resulting in a possible decrease of the reaction rate in comparison to gas phase FTS. Also, separation of the attrited catalyst fines from the waxy product remains a demanding task for liquid phase FTS in comparison to the typical fixed bed gas phase reactor, whereby the wax products typically trickle down the catalyst bed.

By conducting FT in a supercritical media [1], where the supercritical fluid is usually a relatively low molecular weight solvent, one may take advantage of both the gas-like transport properties as well as the liquid-like heat capacity and solubility characteristics of a liquid, and utilize the fixed bed reactor. Implementing a fixed bed supercritical reactor process may achieve

two important goals of improving the economics of GTL operations: (1) catalyst lifetimes can be extended by suppressing deactivation by pore plugging via heavy molecular weight wax products and (2) the requirement of filtration to effect the removal of the wax product, as is needed for CSTR and SBCR operations, is avoided.

A 25%Co/γ-Al_2O_3 catalyst, prepared using a slurry phase impregnation method, was found to exhibit high activity and stability in a CSTR (H_2/CO = 2, T = 220°C, P= 1.9 MPa). Considerable effort was made to stabilize the catalyst against deactivation by reoxidation and other instabilities, which occur when the cluster size of cobalt is below about 10 nm [2,3].

Choice of supercritical fluid, in our case a mixture, was based on, with some modification, the following criteria set forth by Fujimoto et al. [4]:

A. The critical temperature and pressure should be slightly lower than the typical reaction temperature and pressure. In this case, reaction temperature was similar to normal FTS, but the reactor total pressure (8.24 MPa) was considerably higher than used for either a gas-phase or liquid phase FTS reactor (approximately 2.00 MPa). Although much less sensitive to total pressure than temperature, FTS is reported to shift to produce heavier products with an increase in the total pressure of syngas [5]. This pressure dependence is more pronounced for cobalt than for an iron catalyst [6].

B. The solvent should be one which does not poison the catalyst and should be stable under the reaction conditions. The low molecular weight paraffins chosen for this study are unreactive and stable. Also, the paraffins are not coke precursors under the mild temperatures of FTS.

C. The solvent should have a high affinity for aliphatic hydrocarbons to extract the wax from the catalyst surface and reactor.

Because the upper optimum temperature for FTS for cobalt catalysts is approximately 220°C, the critical temperature of the solvent was selected to be below this temperature. In a previous study [7] by our group, and reproduced here in Figures 1 and 2, it was determined using the Hysys 2.1 process simulator that a 55% hexane/45% pentane mixture should give favorable liquid-like densities, while still maintaining gas-like transport properties at a pressure of approximately 8.24 MPa. Using these conditions with the 25%Co/Al_2O_3 catalyst, supercritical studies were conducted by varying the partial pressure of the supercritical fluid, maintaining constant space velocity by using argon as a balancing gas, to determine if the increased solubility of the wax products in the supercritical fluid improved the activity and deactivation profile during reaction testing.

2. EXPERIMENTAL

2.1 Catalyst Preparation

Condea Vista Catalox (high purity γ-alumina, 100-200 mesh, 175 m^2/g) was used as the support material for the cobalt FTS catalyst. The catalyst was prepared by a slurry impregnation method, and cobalt nitrate was used as the precursor. In this method, which follows a Sasol patent [8], the ratio of the volume of solution used to the weight of alumina was 1:1, such that approximately 2.5 times the pore volume of solution was used to prepare the cobalt solution. Two impregnation steps were used, each to load 12.5% of Co by weight. Between each step the catalyst was dried at 333 K under vacuum in a rotary evaporator and the temperature was slowly increased to 373 K. After the second impregnation/drying step, the catalyst was calcined under an air flow at 673K.

2.2 BET Measurements

The surface areas of the support and catalyst were measured by BET using a Micromeritics Tri-Star system. Prior to the measurement, the sample was slowly ramped to 433 K and evacuated for 4 hrs to approximately 6.7 Pa. Results of physisorption measurements are shown in Table 1.

2.3 Hydrogen Chemisorption with Pulse Reoxidation

Hydrogen chemisorption measurements were performed using a Zeton Altamira AMI-200 unit, which incorporates a thermal conductivity detector (TCD). The sample weight was 0.220 g. The catalyst was activated at 623 K for 10 hrs using a flow of pure hydrogen at atmospheric pressure and then cooled under flowing hydrogen to 373 K. The sample was held at 373 K under flowing Ar to prevent physisorption of weakly bound species prior to increasing the temperature slowly to 623 K. At that temperature, the catalyst was held under flowing Ar to desorb the remaining chemisorbed hydrogen so that the TCD signal returned to the baseline. The TPD spectrum was integrated and the number of moles of desorbed hydrogen determined by comparing to the areas of calibrated hydrogen pulses. Prior to experiments, the sample loop was calibrated with pulses of N_2 in helium flow and compared against a calibration line produced from gas tight syringe injections of N_2 under helium flow.

After TPD of H_2, the sample was reoxidized at 623 K by injecting pulses of pure O_2 in helium referenced to helium gas. After oxidation of the cobalt metal clusters, the number of moles of O_2 consumed was determined, and the percent reducibility calculated assuming that the Co^0 reoxidized to Co_3O_4.

2.4 Temperature Programmed Reduction

The temperature programmed reduction (TPR) profile of the fresh catalyst was obtained using a Zeton Altamira AMI-200 unit (Figure 3). The calcined fresh sample was first heated and purged at 473 K in flowing Ar to remove traces of water. TPR was performed using 30 cc/min

10%H_2/Ar mixture referenced to Ar. The ramp was 5 K/min from 303 K to 623 K, and the sample was held at 623 K for 30 min.

2.5 X-ray Diffraction

The powder diffractogram of the calcined catalyst was recorded using a Philips X'Pert diffractometer. First, short-time scans were taken over the range from 2θ of 20° to 70° to verify the formation of Co_3O_4 after calcination. A long-time scan was then made over the intense peak at 36.8° corresponding to (311) so that estimates of Co_3O_4 cluster size could be assessed from Scherrer line broadening analysis. The scanning step was 0.01, the scan speed was 0.0025 sec^{-1}, and the scan time was 4 sec.

2.6 Reaction Testing

The plug flow reactor configuration illustrated in Figure 4 was used and operated at a total pressure of 8.24 MPa. The catalyst (3 g) was diluted in 15 g of glass beads (80-100 mesh). Temperature control was achieved using a three heating-zone furnace. Reactant feed gases (H_2 and CO; H_2:CO of 2:1), as well as argon balancing gas and nitrogen calibration gas, were introduced into the reactor by Brooks 5850 mass flow controllers, which were calibrated over a wide range of pressure for each of the gases. The solvent, a mixture of 55% hexane and 45% pentane (by volume), was introduced to the reactor using an Altex Model 110A liquid feed pump.

The configuration, with dual hot and cold traps, allowed for switching of the product stream in order to maintain the reactor under normal operation and system total pressure during sample collection. The traps were maintained at 423 K and 273 K, respectively. In addition, a dry ice/acetone trap was brought online as necessary. Since collection of the oil, liquid, and supercritical fluid caused a substantial drop in the pressure of the traps, they were repressurized

to system pressure using argon as the inert gas prior to restoring the traps online. This complicated the gas analysis, since the gas stream from the traps was diluted by the argon used to bring the traps back to operating pressure. To solve this problem and assess CO conversion, inert N_2 gas was used for calibration, as follows:

For the reactor:

$X_{CO} = (N_{CO,\,in} - N_{CO,\,out})/(N_{CO,\,in})$

$X_{CO} = [(V_{in})(y_{CO,\,in}) - (V_{out})(y_{CO,out})]/[(V_{in})(y_{CO,\,in})]$

In the calculation, $N_{CO,\,out}$ refers to the moles of CO exiting the reactor, not the traps, which contain diluted gases. Nitrogen is unreactive and, therefore, the molar flow of nitrogen will be the same entering and exiting the reactor. To correct for the argon dilution of the traps, nitrogen is used to calibrate as follows.

For the traps:

calibration factor = C_F = molar flow $_{N_2,in}$ / molar flow $_{N_2,out}$

$$C_F = [(V_{in})(y_{N_2,in})] / [(V_{out})(y_{N_2,out})]$$

$X_{CO} = [(V_{in})(y_{CO,\,in}) - (V_{out})(y_{CO,out})(C_F)]/[(V_{in})(y_{CO,\,in})]$

Note that the molar flow of nitrogen entering the trap is the same as the molar flow of nitrogen exiting the reactor, which is the same as the molar flow of nitrogen entering the reactor. Therefore, all quantities are easily measured. Trap outlet gas flows were measured using a wet test meter. This procedure was implemented to address problems encountered in our earlier work [7].

As another means to calculate the conversion, the CO:N_2 ratio was analyzed both before entering and after reaction, as follows.

$X_{CO} = 1 - (N_2/CO)_{in}/(N_2/CO)_{out}$

Organic phase condensed liquid products of Fischer-Tropsch synthesis were analyzed by gas chromatography. The analyses of C_5 - C_{30} hydrocarbons were performed on a Hewlett Packard (HP 5890) Gas Chromatograph equipped with a capillary column DB-5 (length: 60m, i.d.: 0.32 mm and film thickness: 0.25 micrometer), He as a carrier gas and FID, and operated with temperature programming from 308-598 K at 4 K/min. The analyses of reactor wax were performed on a Hewlett Packard (HP 5890) Gas Chromatograph equipped with a capillary column (length: 25 m, i.d.: 0.53 mm and film thickness: 0.15 micrometer), He as a carrier gas and FID with temperature programming from 323-663 K at 10 K/min. The product data were handled using Hewlett-Packard Chemstation data analysis software.

3. RESULTS AND DISCUSSION

3.1 Characterization

To obtain an estimate of the Co^0 cluster size by adsorption methods, it is necessary to first determine the fraction of the cobalt that is reduced during activation of the catalyst. It is not unusual to use the weight of the catalyst and the percentage of metal to determine the number of metal atoms in the sample, and place this in the denominator for the dispersion calculation. However, the TPR profile in Figure 3 indicates that not all of the cobalt is reduced during activation at 623 K; thus, a pulse reoxidation method was used to quantify the percentage reduction, a method that has been used extensively in characterizing cobalt catalysts for Fischer-Tropsch synthesis [9]. To estimate the cluster size, the following equations are used, and the results for hydrogen TPD/pulse reoxidation are shown in Table 2.

%D = (Number of Co^0 atoms on surface × 100)/(total Co^0 atoms)

%D = (Number of Co^0 atoms on surface × 100)/[(total Co atoms in sample)(fraction reduced)]

After calcination of the catalyst, the spinel phase of Co_3O_4 was detected by XRD. To provide another estimate of the cobalt cluster size, the calcined catalyst was scanned by X-ray diffraction. Scherrer line broadening analysis by determination of the full width at half the maximum (FWHM) of the peak at 36.8° was used to estimate the average size of the Co_3O_4 clusters. After reduction, the metal cluster size should be approximately 75% of this size. Therefore, as displayed in Table 2, there is very good agreement between the results based on calculations using chemisorption with reoxidation data and the results from calculations using XRD data.

3.2 Reaction Testing

There has been great interest in utilizing the unique physical and transport properties of fluids near their critical pressures and temperatures, as they can be made either more gas-like or liquid-like by pressure tuning. With pressure tuning of the supercritical fluid, solubilities can be enhanced to facilitate the dissolution and removal of wax products from the catalyst, while maintaining gas-like diffusional properties of the reactants CO and H_2 through the elimination of interphase transport limitations on the reaction rate [10]. Figure 2 reveals that the density change from gas-like to liquid-like occurs between 1 and 6 MPa. Most previous studies of Fischer-Tropsch synthesis in the literature have focused on using pure solvents as supercritical fluids [10-12]; therefore, the solvents in these studies were not at the optimum conditions for FTS. For example, n-hexane has been used [11,12], with critical properties T_C = 506.7 K and P_C = 2.97 MPa, but the temperature of the reactor must be operated at approximately 513 K, a temperature which is too high for cobalt-based FTS catalysts and favors production of light products. n-Pentane, with critical properties T_C = 469.6 K and P_C = 3.33 MPa, was also used in previous work, but the density is not high enough to attain optimum solubility properties at the FTS conditions. Propane was also used [13], with the same problem.

Among, if not the first, group to study the pressure tuning affect of the solvent pressure on the transport and solubility properties was Subramaniam [12]. In that work, the pressure of the reactor was changed, while the CO/H_2 ratio of the gas feed and supercritical liquid feeds were kept constant. The partial pressures and the residence times were altered with each change of condition and this makes it difficult to draw solid conclusions.

As an extension to this previous work, efforts were made to overcome the above problems. In this work, a constant overall reactor pressure and constant partial pressures of the feed CO and H_2 gases were maintained. [We refer to nonsupercritical conditions although the inert gases are present at supercritical conditions but at very low density conditions.] Only the partial pressure of the supercritical fluid mixture is changed to tune the transport and solubility properties, while a balancing inert gas (argon) is fed to maintain constant space velocity. Nitrogen is also fed, but it is used as a calibration gas, so that CO conversion can be accurately assessed.

The data in Figure 5 show that when no or inadequate partial pressures of supercritical fluid are present, the catalyst undergoes deactivation, probably by heavy wax buildup. However, when the partial pressure of the supercritical fluid was 5.45 MPa, a higher CO conversion was observed due to the increased solubility of wax products in the supercritical media. The amount of wax products sampled from the collection traps increased dramatically when the partial pressure of the supercritical fluid was increased to 5.45 MPa and then declined to approach the predicted value consistent with wax extraction, as shown in Figure 6.

In practice, the chain growth probability α is used to define the distribution of products, based on Anderson-Schulz-Flory (ASF) polymerization kinetics, as follows:

$$\alpha = R_p/(R_p + R_t)$$

where R_p and R_t are the rates of chain propagation and termination. Therefore, except for deviations from this ideal model, with methane showing much higher termination probabilities yielding higher than predicted values, and C_2 products giving lower than predicted values [14], these kinetics define the distribution of products based on carbon number, n. In contrast with Fe-based FTS catalysts, the distribution of components for cobalt catalysts strongly favors paraffins, although measurable quantities of olefins and traces of oxygenated products are also present, primarily in lower carbon number components. In this study, the products were lumped into the parameter m_n, representing the sum of the components for each carbon number, where:

$$m_n = (1 - \alpha)\alpha^{n-1}$$

Therefore, the slope of the natural log of the mole fraction versus the carbon number yields α as follows:

$$\alpha = \exp[\Delta \ln m_n / \Delta n]$$

Table 3 and Figure 7 show that the resulting α value was very close to the value obtained during CSTR testing, and remained constant during the course of reaction testing with or without supercritical fluid, with values ranging between 0.87 and 0.90%.

Product selectivities were determined in two ways, as commonly reported in the literature. Methane selectivity was defined on a carbon molar basis, not on a product molar basis, and CO_2 from the water-gas-shift reaction was not included. C_5+ selectivity was defined in a similar manner. In contrast, the CO_2 selectivity was based on the rate of water-gas-shift divided by the rate of water-gas-shift plus the FTS rate, again on a carbon molar basis, as follows:

$$S_{CH_4} = r_{CH_4} / r_{FTS} = r_{CH_4} / (r_{CO} - r_{CO_2})$$

$$S_{C_{5+}} = r_{C_{5+}} / r_{FTS} = r_{C_{5+}} / (r_{CO} - r_{CO_2})$$

$$S_{CO_2} = r_{CO_2} / (r_{CO_2} + r_{FTS}) = r_{CO_2} / r_{CO}$$

The C_2+ total olefin selectivity was defined on a carbon molar basis. First, the olefin selectivity for each carbon number was calculated, as follows:

$$S_{O,n} = O/(O+P)_n$$

Then, the C_2+ total olefin selectivity "$C_2^=$+" was determined by integrating over the distribution up to C_{20}.

$$C_2^= + = \sum S_{O,n} \alpha^n n \; / \; \sum \alpha^n n$$

Initially, there are not important differences between the catalyst run with or without supercritical fluid because early in the run, the catalyst is relatively free of wax products as it is in the initial stage of deactivation. However, as shown in Table 3 and Figure 8, after the deactivation period and especially under the condition of no supercritical hydrocarbon addition during days 15 - 20, the CO_2 selectivity is approximately 10% and the methane selectivity is greater than 15%. This is the most important time to observe the differences between supercritical and non-supercritical conditions, at the point where the catalyst has deactivated by wax buildup. Clearly, after switching to the supercritical fluid partial pressure of 5.45 MPa, important benefits in product selectivity occurred, with notable decreases in the selectivities of both CO_2 and methane.

CO_2 is produced by the water-gas-shift reaction: $H_2O + CO \rightleftharpoons CO_2 + H_2$. Yokota et al. [15] attributed the decrease in CO_2 production over an iron-based catalyst to the improved extraction and transport of water by the supercritical fluid. This implies that the residence time

of the H_2O relative to the reactants H_2 and CO in the reactor was shortened and this leads to a lower production rate of CO_2. Our results are consistent with this explanation.

The methane selectivity is sensitive to changes in the process parameters. Increasing temperature, decreasing the pressure, increasing the H_2:CO, and changing conversion all may result in an increase in methane fraction for cobalt catalysts [14,16,17]. In this work, we attempted to maintain constant all parameters in our control in order to make comparisons under supercritical and nonsupercritical conditions. After deactivation of the catalyst by wax buildup, during days 15-20 under nonsupercritical conditions, the methane selectivity is high (greater than 15%). However, when the 5.45 MPa of the SCF is added, the methane selectivity decreases while the conversion increases. Therefore, one could assume that the increased availability of active sites after extraction of long chain wax from the pores resulting in increased conversion could decrease the methane selectivity. Another explanation is that the observed decreased methane selectivity is the result of better heat distribution in the reactor. That is, under supercritical conditions, localized hotspots in the reactor are avoided [18] due to the better heat capacities of the SCF, resulting in lower methane selectivities. In that case, one would also expect an increase of the chain growth parameter α. However, in Table 3, very little, if any, change in α is observed with or without addition of supercritical fluid. Another explanation is that mass transfer limitations are decreased with addition of the SCF due to the improved extraction of the FTS products from the catalyst. The slow transport of heavy wax products from the catalyst contribute to the deactivation of the catalyst and may increase the mass-transfer limitations when no SCF is present. Therefore, this could also explain the increase of methane selectivity with time onstream, since it is well known that mass transport limitations can result in an increase in the hydrogen partial pressure with increasing distance into the particle and this

leads to enhanced production of the thermodynamically favored product methane [19]. When a high enough density of SCF is achieved (5.45 MPa) and solubilization of the wax occurs, resulting in its extraction, it is possible that the mass transfer barrier is decreased, resulting in the decreased methane selectivity.

That wax extraction occurred is also evident when one considers the selectivity of olefins to paraffins with increasing carbon number. These are reported in Table 4 for both conditions - with or without SCF, and with changes in the SCF partial pressure. There is currently a debate in the literature as to the cause of the decrease in olefin content with higher carbon number for FTS. One is the higher solubility of higher carbon number product α-olefins in the liquid phase, resulting in increased residence times which lead to their increased conversion to paraffins. Henry's law constants, which indicate the fugacity (in many cases, partial pressure) of a component in the gas phase divided by the concentration of the solute gas in the liquid phase, have been observed for paraffins to decrease exponentially with carbon number, indicating higher solubility with carbon number [14]. Therefore, several authors [e.g., 14] have advanced the view that the greater solubility of larger hydrocarbons result in increased residence times and therefore, higher rates of readsorption.

However, a different explanation has been offered [20-24]. The decrease in olefin content with carbon number in this view is due to the decrease in the diffusivities of longer chain hydrocarbons, which would lengthen their time in the catalyst pores. This has been coined "diffusion enhanced α-olefin readsorption."

The results presented here show that with the addition of SCF, the paraffin content is much lower with increasing carbon number than without SCF. Therefore, the diffusivities of hydrocarbons may be much higher in the presence of the supercritical fluid. This could result in

lower residence times in the pores, and therefore, decreased probability for readsorption. Certainly, this is a possible explanation for the results. However, a more likely explanation is based on a VLE study [25]. Based on a reaction scheme which took into account reversibility of both olefin hydrogenation and adsorption and derived from material balances, it was demonstrated that the residence time of each carbon number was inversely related to the saturated vapor pressure. Moreover, the olefin to paraffin ratio was inversely related to the residence time. Therefore, the results here may be explained in terms of this model. When no SCF is present, O/(O+P) decreases with carbon number due to the higher residence times of the higher carbon number intermediates resulting from their lower saturation vapor pressures. With addition of SCF, extraction results in removal of the bulk liquid filling the catalyst pores, which results in a decrease of the residence time of intermediates and an increase in O/(O+P) as a function of carbon number relative to the nonsupercritical condition, as shown in Figures 8 and 9, and Table 4.

The research may also lead to other developments. For example, reaction intermediates could potentially be added to the supercritical fluid in order to achieve incorporation into the wax products. For example, Fujimoto's group [26] has extended the idea to explore the addition of middle α-olefins to promote wax selectivities. Also, our group has added ^{14}C labeled α-olefin compounds to the supercritical fluid in order to test the merits of α-olefin reincorporation [27].

D. CONCLUSIONS

The anticipated benefits of running FTS in a supercritical fixed bed reactor are clear. In comparison with gas phase fixed bed processes, using pressure tuned supercritical media, in this case a C_5/C_6 mixture, the condensation of high molecular weight hydrocarbons leading to catalyst deactivation was avoided. In contrast to conventional slurry phase processes, which

suffer from catalyst attrition, whereby the catalyst fines eventually breakdown to the point at which they can channel through the filter, running FTS under the supercritical media avoids this problem. With the increase in conversion due to greater accessibility to active sites after wax extraction, additional benefits included decreased methane and carbon dioxide selectivities. The decreased paraffin/(olefin + paraffin) selectivities with increasing carbon number was in line with extraction of the hydrocarbon from the pore. Two possibilities are considered. Faster diffusion rates of wax products may result in lower residence times in the pores, and therefore, decreased probability for readsorption and reaction to the hydrogenated product. A more probable explanation is that the residence times of intermediate olefins, which are inversely related to their saturation vapor pressures, are decreased due to removal of the liquid phase during extraction.

Acknowledgment

This work was supported by U.S. DOE contract number DE-FC26-98FT40308 and the Commonwealth of Kentucky.

REFERENCES

1. Baiker, A., Chem. Rev. 99 (1999) 453.
2. Schanke, D., Hilmen, A.M., Bergene, E., Kinnari, K., Rytter, E., Adnanes, E., and Holmen, A., Catal. Lett. 34 (1995) 269.
3. Hilmen, A.M., Schanke, D., Hanssen, K.F., and Holmen, A., Appl. Catal A: General 186 (1999) 169.
4. Fan, L., Fujimoto, K., Appl. Catal. A: General 186 (1999) 343.
5. Dry, M.E., Catalysis-Science and Technology (J.R. Anderson and M. Boudart, eds.), Springer-Verlag, New York, 1981, Vol. 1, pp. 160-255.
6. Jager, B., Espinoza, R., Catal. Today 23 (1995) 17.
7. Zhang, Y., Sparks, D.E., Spicer, R.L., and Davis, B.H., Symposium on Advances in Fischer-Tropsch Chemistry, Div. of Petroleum Chemistry, 219th National ACS Meeting, San Francisco, CA (March, 2000).
8. Espinoza, R.L., Visagie, J.L., van Berge, P.J., Bolder, F.H., U.S. Patent 5,733,839 (1998).
9. Vada, S., Hoff, A., Adnanes, E., Schanke, D., and Holmen, A., Topics in Catal. 2 (1995) 155.
10. Savage, P.E., Gopalan, S., Mizan, T.I., Martino, C.J., and Brock, E.E., AICHE Journal 41, No. 7 (1995) 1723.
11. Fan, L. and Fujimoto, K., Appl. Catal. A: General 186 (1999) 343.
12. Subramaniam, B., Prepr. Am. Chem. Soc., Div. Pet. Chem., 45 (2000) 194.
13. Lang, X., Akgerman, A., and Bukur, D., Ind. Eng. Chem. Res., Vol. 34, No. 1 (1995) 72.
14. Van der Laan, G.P. and Beenackers, A.A.C.M., Catal. Rev.-Sci. Eng., Vol. 41 No. 3&4 (1999) 255.

15. Yokota, K., Hanakata, Y., and Fujimoto, K., Natural Gas Conversion, (A. Homen et al. eds.) (1991) 289.

16. Iglesia, E., Reyes, S.C., and Madon, R.J., J. Catal. 129 (1991) 238.

17. Bukur, D.B., Patel, S.A., and Lang, X., Appl. Catal. A 61 (1990) 329.

18. Yokota, K., Hanakata, Y., and Fujimoto, K., Fuel 68 (1989) 255.

19. Dry, M.E., J. Mol. Catal., 17 (1982) 133.

20. Iglesia, E., Reyes, S.C., and Soled, S.L.,"Computer-Aided Design of Catalysts and Reactors", (E.R. Becker and C.J. Pereira, Eds.), Marcel Dekker, Inc., 1992.

21. Iglesia, E., Reyes, S.C., Madon, R.J., and Soled, S.L., Adv. Catal. 39 (1993) 221.

22. Madon, R., Iglesia, E., Reyes, S., Selectivity in Catalysis (1993) 181.

23. Iglesia, E., Stud. Surf. Sci. Catal., 107 (1997) 153.

24. Iglesia, E., Appl. Catal. A 161 (1997) 59.

25. Zhan, X. and Davis, B. H., AIChE Meeting, April 23, 2001.

26. Fan, L., Yoshii, K., Yan, S., Zhou, J., Fujimoto, K., Catal. Today 36 (1997) 295.

27. CAER, unpublished results.

Table 1

Results of BET Surface Area Measurements

Catalyst Description	Calcination T (K)	Measured BET SA (m_2/g)	Measured Ave. Pore Rad (nm)
Condea Vista γ-Al_2O_3 Catalox SBa-150	623K	149	5.4
25%Co/γ-al_2O_3 Catalox Sba-150 Slurry	623K	89	4.8

Table 2

Results of H_2 Chemisorption by TPD of H_2 and Pulse Reoxidation for Co/Al_2O_3 Catalysts Compared with Results from XRD by Scherrer Line Broadening Analysis

H_2 TPD/Pulse Reoxidation										
Catalyst Description	BET SA m_2/g	Red T (K)	μmol H_2 Desorbed per g	Uncorr % Disp	Uncorr Diam (nm)	μmol O_2 Uptake per g	% Red	Corr % Disp	Corr Co^o Diam (nm)	Co_3O_4 Diam (nm) XRD
25%Co/Al_2O_3	89	623	77.7	3.7	28.2	1174	42	8.7	11.8	13.7

Table 3

Product Selectivities at Different Conditions

			Average Selectivities			
TOS (days)	Condition	Final CO Conv	CO_2	CH_4	C_5+	Final α
0 - 3	No SCF	45.3%	2.1%	8.3%	89.7%	0.88
3 - 5	2.34 MPa SCF	41.9%	4.1%	9.7%	89.3%	0.90
5 - 7	3.90 MPa SCF	37.9%	5.5%	11.3%	87.4%	0.90
7 - 9	5.45 MPa SCF	41.7%	4.7%	10.7%	88.4%	0.87
9 - 11	3.90 MPa SCF	35.9%	5.7%	12.1%	87.1%	0.89
11 - 12	5.45 MPa SCF	41.8%	5.8%	12.1%	86.8%	0.90
12 - 15	2.34 MPa SCF	35.9%	7.2%	13.7%	85.0%	0.88
15 - 20	No SCF	18.9%	10.3%	16.2%	78.9%	0.88
20 - 22	5.45 MPa SCF	40.6%	4.7%	10.4%	88.9%	0.86
23 - 24	5.45 MPa SCF	42.0%	4.2%	10.5%	88.8%	0.88
24 - 25	5.45 MPa SCF	40.8%	4.3%	10.4%	89.0%	0.87
26 - 27	5.45 MPa SCF	41.6%	3.7%	9.9%	89.6%	0.88
28 - 29	5.45 MPa SCF	41.2%	4.3%	10.4%	89.0%	0.87
42 - 26	No SCF	21.3%	4.8%	18.3%	76.0%	---
46 - 53	5.45 MPa SCF	27.9%	2.2%	11.9%	87.2%	—

Table 4

Olefin Selectivities as a Function of Supercritical Fluid Partial Pressure

	O/O + P								
P_{SCF} (MPa)	No SCF	2.34	3.90	5.45	3.90	5.45	2.34	No SCF	5.45
TOS (days)	0-3	3-5	5-7	7-9	9-11	11-12	12-15	15-20	20-29
Carbon No.									
2	0.20	0.20	0.16	0.14	0.18	0.13	0.20	0.20	0.11
3	0.70	0.72	0.73	0.71	0.71	0.70	0.73	0.70	0.71
4	---	0.65	0.64	0.67	0.60	0.69	0.61	0.60	0.61
5	---	---	---	---	---	---	---	---	---
6	0.54	---	---	---	---	---	---	---	---
7	0.51	0.49	0.49	0.44	0.44	0.41	0.46	0.55	0.45
8	0.46	0.55	0.59	0.58	0.58	0.58	0.55	0.53	0.58
9	0.40	0.56	0.63	0.62	0.61	0.62	0.61	0.49	0.60
10	0.40	0.47	0.55	0.55	0.60	0.56	0.50	0.44	0.55
11	0.34	0.42	0.50	0.54	0.48	0.53	0.41	0.38	0.54
12	0.29	0.36	0.46	0.52	0.44	0.51	0.36	0.32	0.52
13	0.24	0.30	0.43	0.50	0.40	0.53	0.31	0.25	0.51
14	0.20	0.25	0.38	0.48	0.35	0.56	0.26	0.20	0.48
15	0.17	0.21	0.34	0.45	0.30	0.59	0.21	0.16	0.46
16	0.14	0.16	0.28	0.43	0.26	0.41	0.17	0.13	0.43
17	0.12	0.15	0.25	0.41	0.21	0.39	0.14	0.12	0.42
18	0.10	0.08	0.23	0.37	0.18	0.36	0.13	0.10	0.39
19	0.09	0.07	0.21	0.36	0.15	0.33	0.10	0.09	0.36
20	0.07	0.05	0.16	0.31	0.12	0.32	0.06	0.08	0.35

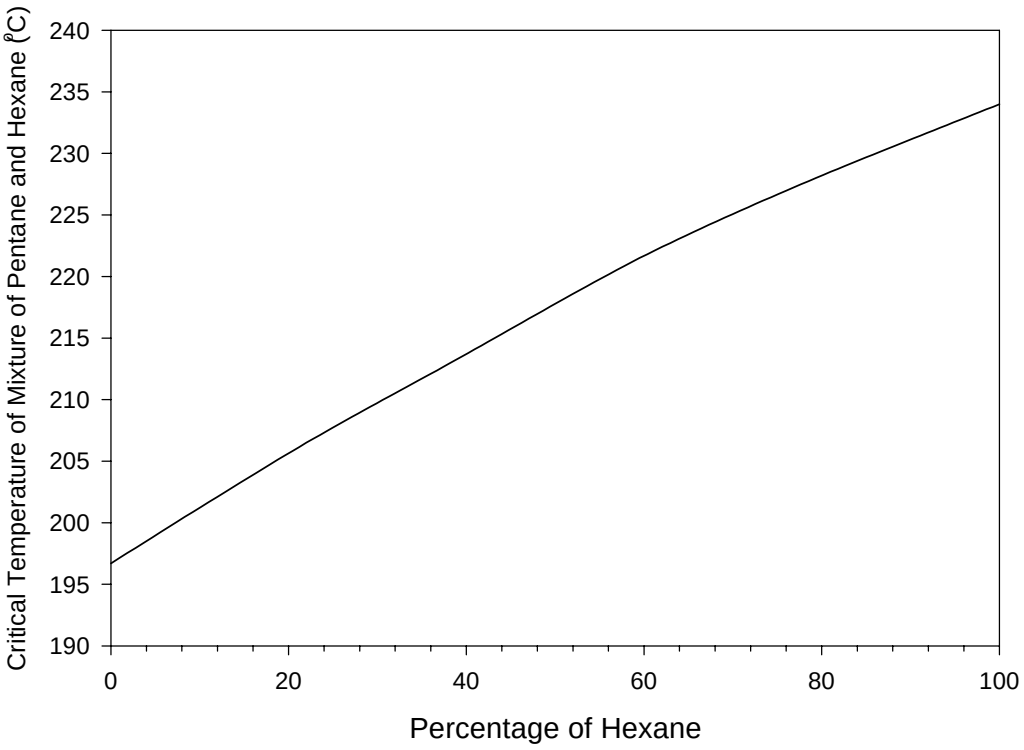

Figure 1. Critical temperature of pentane and hexane mixture with increasing hexane percentage.

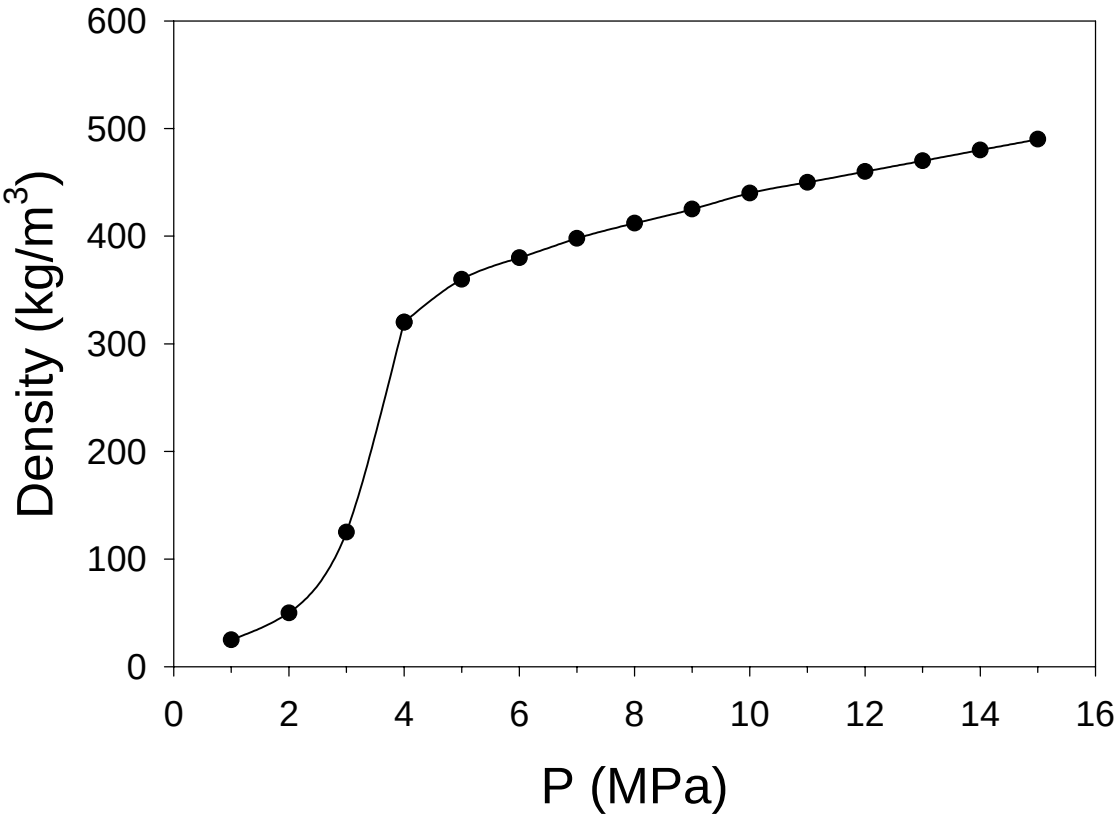

Figure 2: Density versus pressure of the mixture of 55% hexane and 45% pentane.

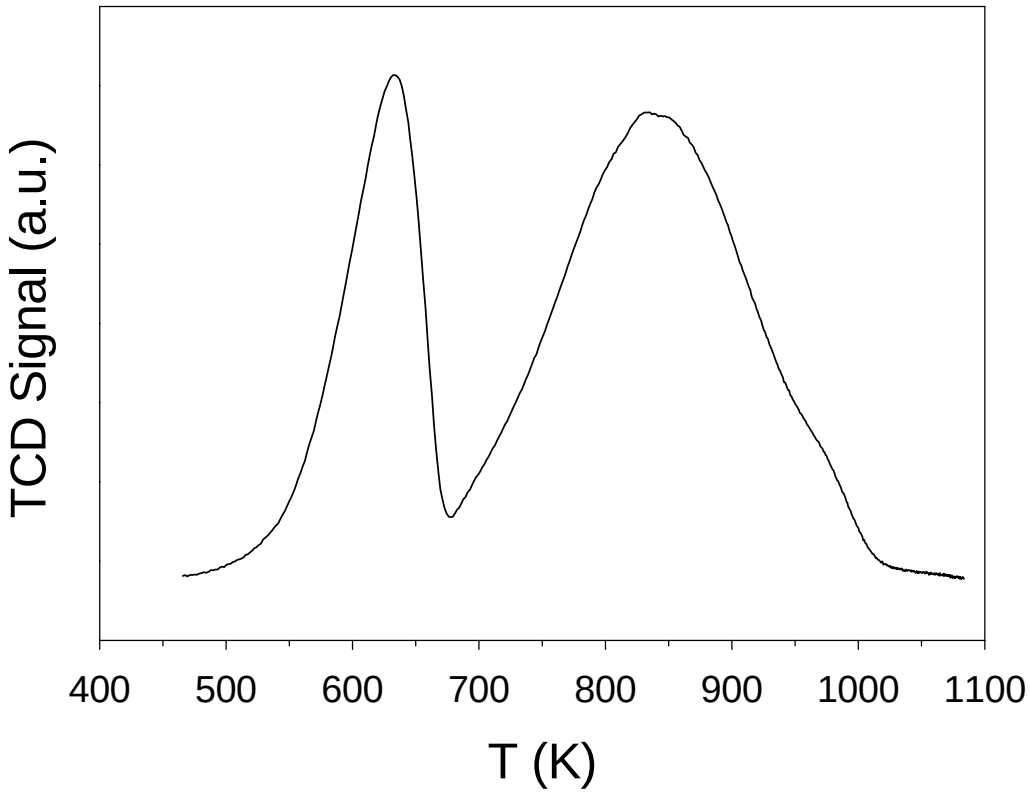

Figure 3: TPR profile of the 25%Co/Al_2O_3 catalyst prepared by the slurry phase impregnation method.

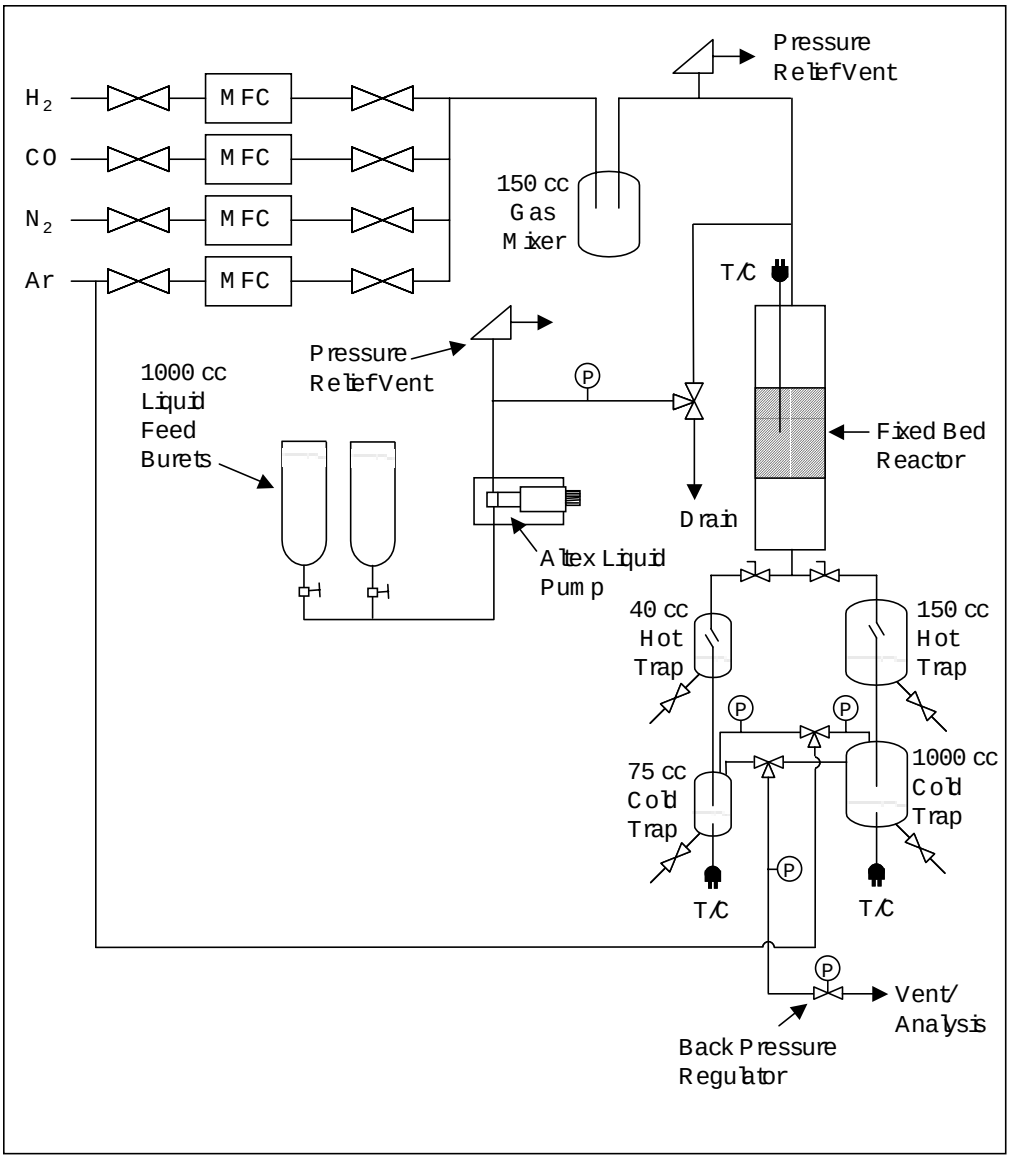

Figure 4: Flow diagram of the supercritical FT reactor system.

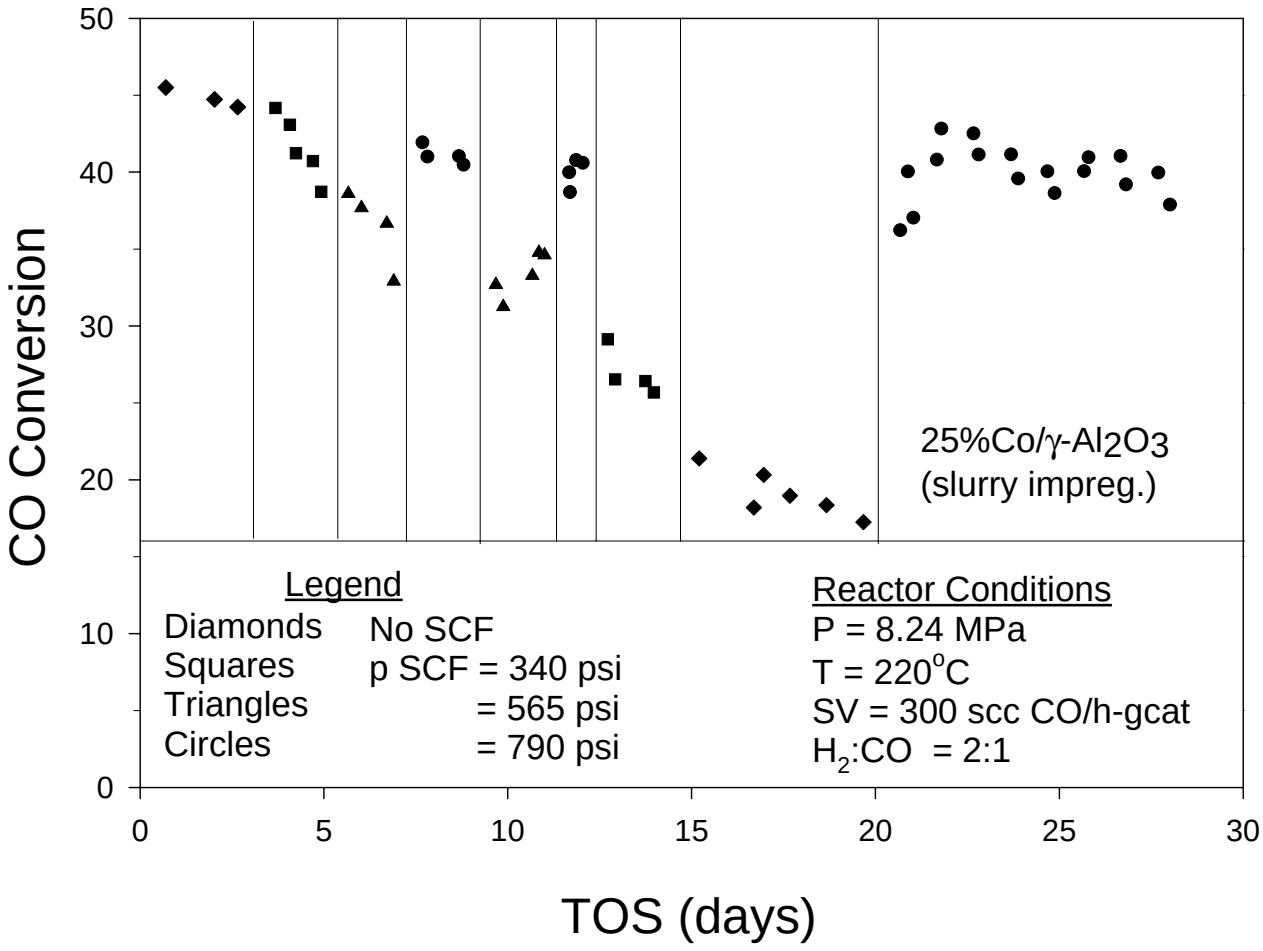

Figure 5: CO conversion vs time-on-stream on a 25%Co/γ-Al_2O_3 slurry phase impregnation catalyst in a fixed-bed reactor with varying partial pressure of SCF.

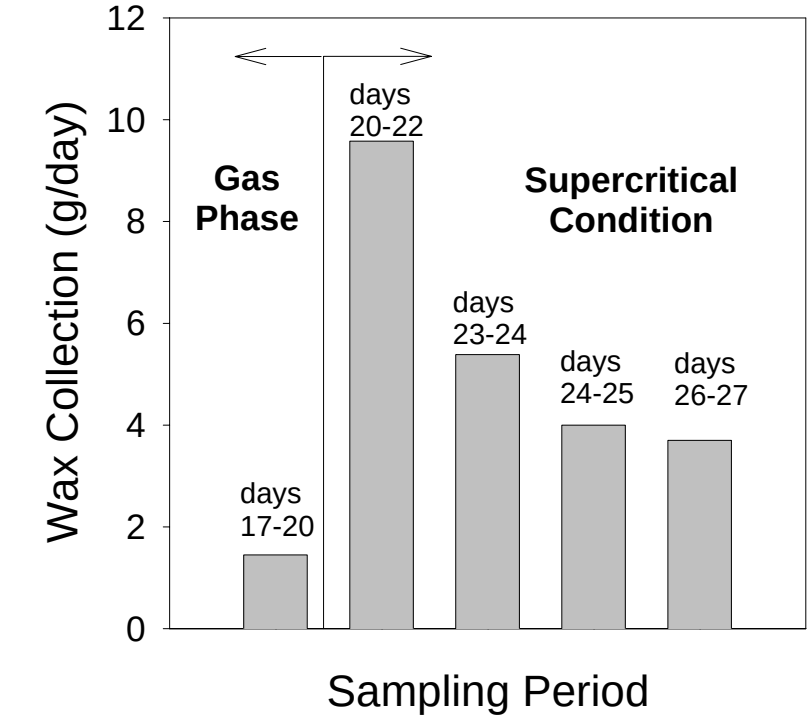

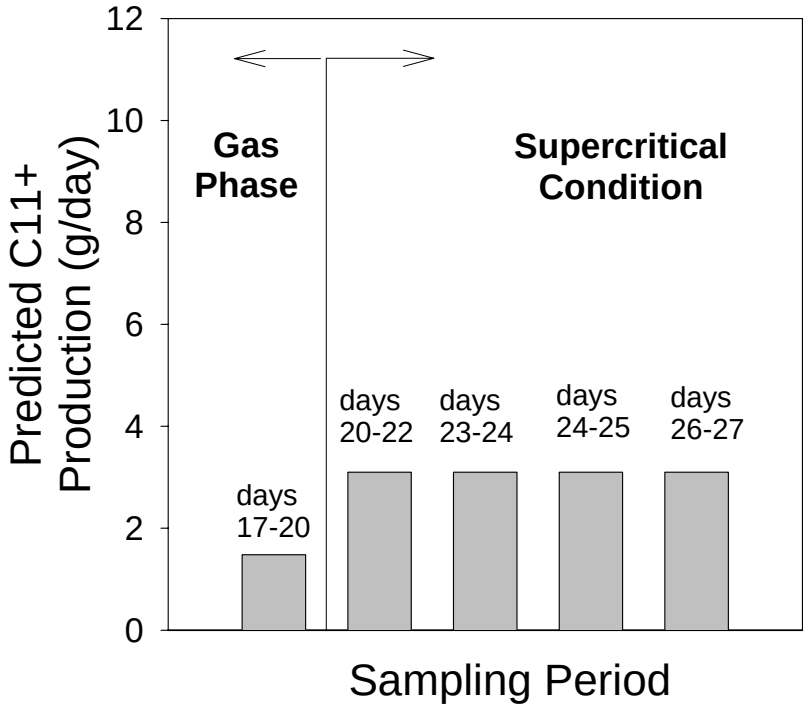

Figure 6: (top) Wax collection during each sampling period. Note that wax collected is on a wet basis and contained solvent. (bottom) Predicted C_{11}+ based on the extent of CO conversion.

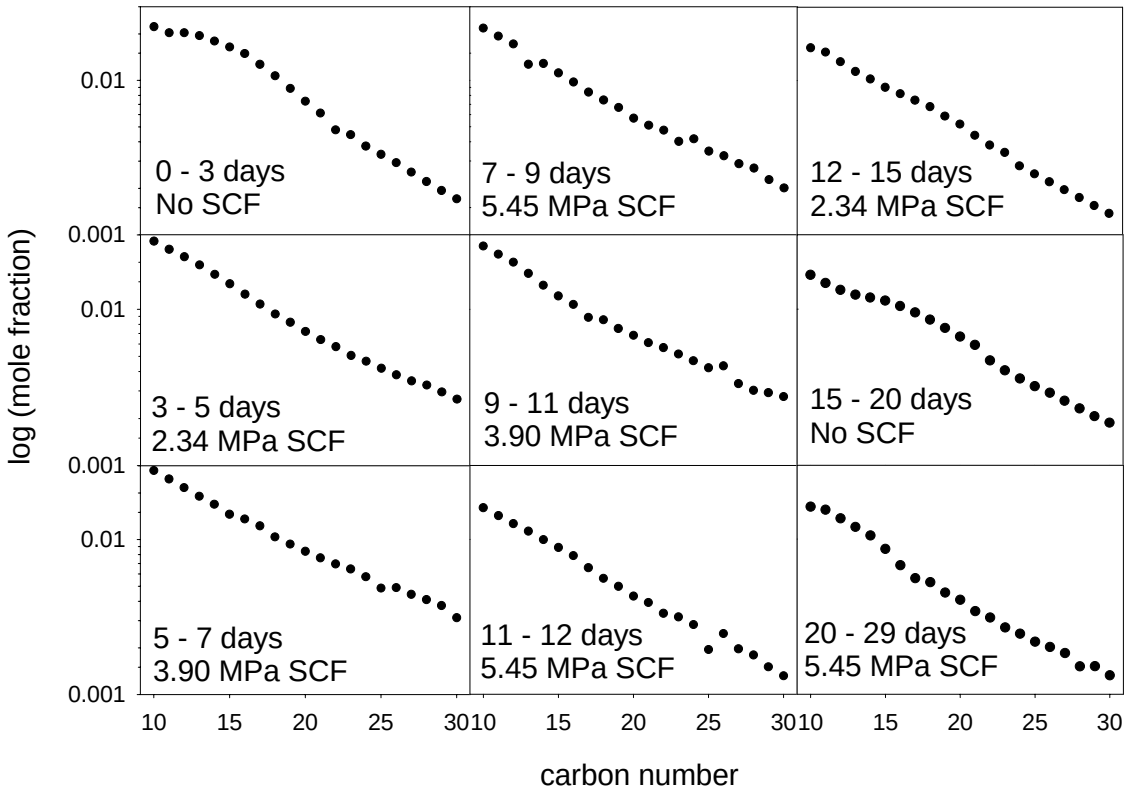

Figure 7: Wax product distribution under nonsupercritical conditions.

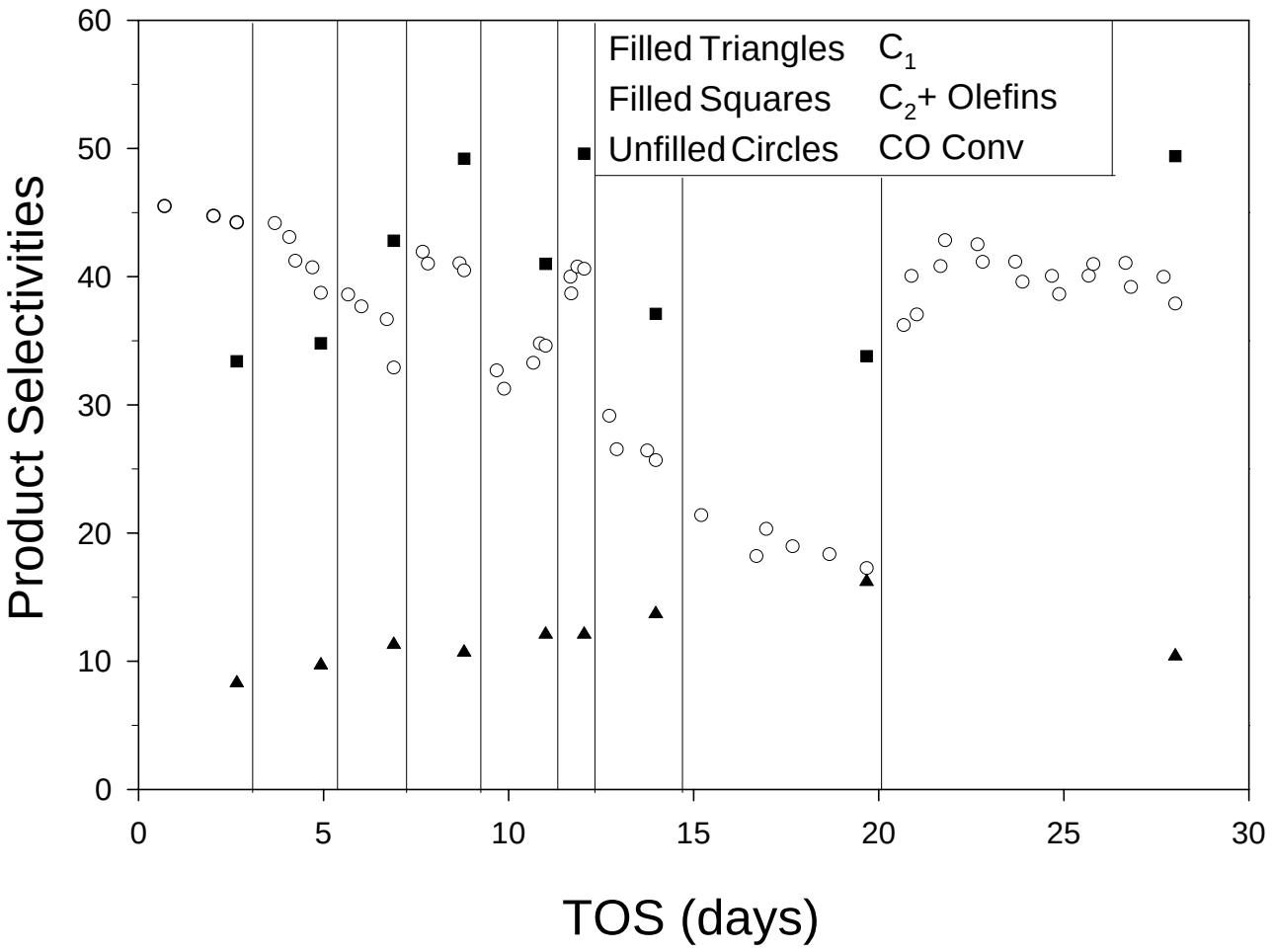

Figure 8: Product selectivities versus time-on-stream.

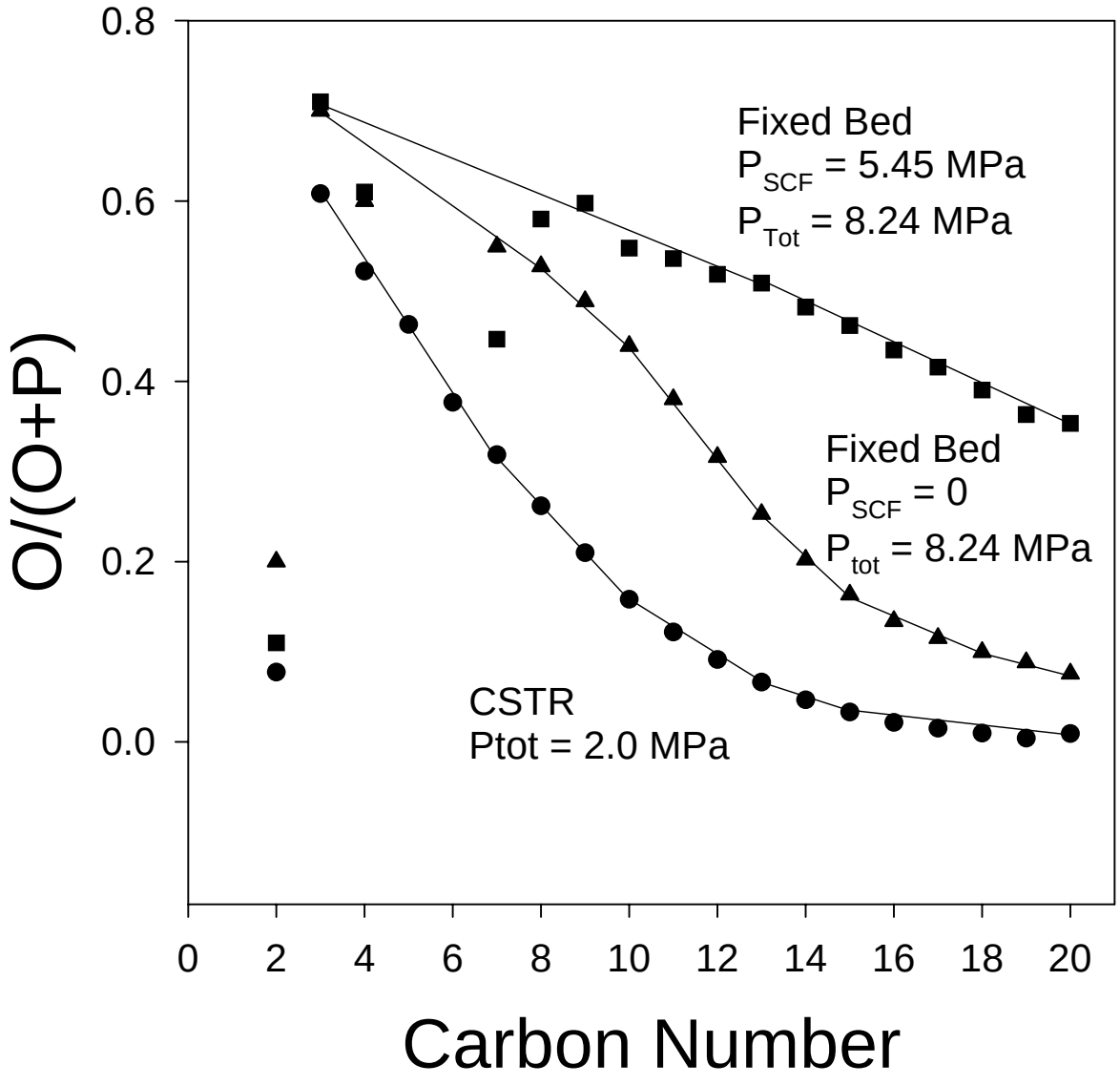

Figure 9: Olefin selectivity as a function of carbon number for supercritical and gas phase FTS.

D. Assessment of Internal Diffusion Limitation on Fischer-Tropsch Product Distribution

Abstract

A reactor is modeled for ideal vapor-liquid equilibrium conditions and is operated with a single-alpha catalyst. Under steady-state conditions, the relative concentration of hydrocarbon product in the catalyst pores decreases with increasing carbon number until about C_{20}. It is deduced that the two-alpha product distribution in Fischer-Tropsch reactions is not due to the effect of product diffusion limitations of the heavier products.

Introduction

It has been generally agreed that a simple polymerization mechanism can be used to describe the distribution of Fischer-Tropsch (FT) synthesis product. On a catalyst surface, a FT chain growth intermediate can either propagate to form another intermediate of one higher carbon number or terminate to produce an oxygenate, paraffin, or olefin of the same carbon number. The path of termination to olefin is reversible due to the well documented feature of olefin adsorption/desorption and hydrogenation/dehydrogenation (1). The propagation probability (α value) of each surface intermediate has been assumed to be a constant that is independent of carbon number (single α distribution), and this produces the so-called Anderson-Schulz-Flory distribution (ASF). The experimental observation of a two, or more, α distributions, or more precisely an α value that is an increasing function of carbon number, results in different models being proposed to explain this phenomenum. One of the prevailing ones is the diffusion enhanced olefin readsorption model which describes the effect of diffusion limited removal of olefins from catalyst pores (2-4). According to this model, since olefin termination is reversible and its diffusivity decreases rapidly with increasing carbon number, the higher olefins should have longer residence times and higher fugacities in the pores of the

catalyst pellet. As a result, accumulation of these heavy hydrocarbons in the catalyst pores leads to olefin diffusion limitation, which enhances olefin readsorption and leads to the observation of a two α product observation.

In other words, this model relies on increased hydrocarbon concentration with carbon number in catalyst pores which might result from internal diffusion limitation. The pore concentration of a hydrocarbon component relative to its surface concentration (relative concentration) must increase with carbon number to contribute to the two α distribution. It is obvious that in the presence of internal diffusion limitation of hydrocarbon products, the concentration of a hydrocarbon component in the catalyst pores must be significantly higher than that at the catalyst surface. However, the hydrocarbon concentration profile in the catalyst pores was not demonstrated and the existence of internal diffusion limitation of hydrocarbons was not verified by a theoretical approach, by simulation or by experimental data. Also, this model does not consider the existence of vapor-liquid equilibrium of hydrocarbon products in a typical low temperature Fischer-Tropsch reactor.

It is therefore of interest to examine the conditions under which product diffusion limitation might exist in catalyst pores and how reaction conditions affect this diffusion limitation. The FT reaction is simulated in a CSTR slurry reactor whose modeling and simulation has been reported previously (5).

Fischer-Tropsch Reaction

The products of the Fischer-Tropsch reaction consist primarily of a spectrum of paraffins and olefins. Paraffins and olefins of the same carbon number have essentially the same physical properties, such as vapor pressure and diffusivity. Therefore, for simplicity of discussion, it can be assumed that CO and H_2 react stoichiometrically to produce exclusively paraffins (non-reactive) and water following a single α ASF distribution. This assumption is reasonable and the

result is sufficiently informative since the objective of this work is simply to examine the possible existence of internal diffusion limitation of hydrocarbon products. Nonetheless, the olefin reactivity has also been considered and will be discussed later in this manuscript as it applies to the above assumption. Thus, for all non-reactive paraffin products, the FT reaction can be written as

$$nCO + (2n+1)H_2 \rightarrow C_nH_{2n+2} + H_2O \qquad (\bar{n} = \frac{1}{1-\alpha}) \qquad 1)$$

($\bar{n}$ is average carbon number) and the hydrogen reaction rate is assumed to follow

$$(-r_H) = k_H C_H \qquad 2)$$

Again, this simple rate expression is for ease of discussion. Adoption of a more complicated or simpler rate expressions does not change the general conclusions of this work. In addition, Equation (1) is for reactions typical of cobalt catalyst where CO_2 production is negligible. For reactions typical of iron catalysts, the water gas shift reaction should be considered and the total reaction equation has to be rewritten. The importance of addressing this difference is due to the formation of hydrogen in the latter case, whose concentration is required in this analysis for the liquid phase. However, the analysis method will be the same as described in this manuscript and we have shown that the general conclusion of this work will not change for the iron catalyst.

The only assumption that is required to develop the following equations is that the FTS products follow a single alpha distribution and that vapor-liquid equilibria is established. Since 1 mole of hydrocarbon is formed for each (2n + 1) moles of hydrogen converted, the hydrocarbon generation can be described as:

$$r_{HC} = 1 / (2n + 1)\ r_H = (1 - \alpha) / (3 - \alpha) \qquad 3)$$

Since the product hydrocarbons follow a single alpha distribution, the molar fraction of a product of carbon number i present in the product mixture is $(1 - \alpha)\ \alpha^{i-1}$. The rate, r_i, of formation of the product with carbon number i is:

$$r_i = (1-\alpha)\alpha^{i-1} r_{HC} = \frac{(1-\alpha)^2}{(3-\alpha)} \alpha^{i-1} k_H C_H = k_i C_H \qquad 4)$$

where

$$k_i = \frac{(1-\alpha)^2}{(3-\alpha)} \alpha^{i-1} k_H \qquad 5)$$

is the production rate constant of hydrocarbon component i and is a function of α.

Mass Transfer in Catalyst Pores

Assuming that the catalyst pellet is spherical, the steady state material balance of hydrogen and of a hydrocarbon component i in catalyst pores can be described by equations 6 and 7, respectively:

$$\frac{1}{r^2}\frac{d}{dr}\left(r^2 \frac{dC_H}{dr}\right) = \frac{k_H}{D_H} C_H \qquad 6)$$

$$\frac{1}{r^2}\frac{d}{dr}\left(r^2 \frac{dC_i}{dr}\right) = -\frac{k_i}{D_i} C_H \qquad 7)$$

and boundary conditions are:

$$r = R_p, \quad C_H = C_{H,s} \quad \text{and} \quad C_i = C_{i,s}$$

$$r = 0, \quad \frac{dC_H}{dr} = 0 \quad \text{and} \quad \frac{dC_i}{dr} = 0$$

where C_H, C_i : concentrations of hydrogen and hydrocarbon i in the catalyst pores, respectively; $C_{H,s}$, $C_{i,s}$: concentrations of hydrogen and hydrocarbon i at the catalyst surface, respectively; D_H, D_i : effective diffusivities of hydrogen and hydrocarbon i, respectively; k_H, k_i : rate constants of hydrogen consumption and hydrocarbon i production, respectively; and, R_p : radius of the catalyst particle.

The concentration profiles of hydrogen and a hydrocarbon component i in the catalyst pores thus can be obtained by solving the above equations analytically, as shown in Equations (8) and (9). [Note that readsorption need not be considered here since this is only a material balance equation].

$$\frac{C_H}{C_{H,s}} = \left(\frac{R_p}{r}\right)\frac{\sinh(\phi_H r / R_p)}{\sinh(\phi_H)} \qquad 8)$$

$$\frac{C_i}{C_{i,s}} = 1 + \left(\frac{\phi_i}{\phi_H}\right)^2\left(1 - \frac{C_H}{C_{H,s}}\right) \qquad 9)$$

where

$$\phi_H = R_p\sqrt{\frac{k_H}{D_H}} \qquad 10)$$

$$\phi_i = R_p \sqrt{\frac{k_i}{D_i} \frac{C_{H,s}}{C_{i,s}}} \qquad 11)$$

ϕ_H and ϕ_i are Thiele moduli characterizing reaction-diffusion process of hydrogen and generation-diffusion process of hydrocarbon component i in the catalyst pores, respectively; and, ϕ_i is a measure of the relative scale of reaction and diffusion rates in the catalyst pores. For large ϕ_i, the diffusion rate is smaller than the reaction rate and hence the effect of internal diffusion on the total observed rate is significant, or even controlling. For the same catalyst pellet, the effective diffusivity D_i is calculated using two correlations:

$$D_n = D_0 e^{-0.3n} \qquad 12)$$

and

$$D_n = D_0 n^{-0.6} \qquad 13)$$

where D_0 is a constant and n is the carbon number. Equation (12), which predicts a strong dependence of diffusivity on carbon number was used in reference 2 . However, it has been argued that the dependence is actually much weaker than required by Equation (12) and that the formula shown in Equation (13) should be used (6).

It can be seen from Equation (9) that the relative concentration of component i depends on its Thiele modulus and hydrogen concentration distribution in the catalyst pores. Clearly, the higher the value of ϕ_i, the higher the relative concentration $C_i/C_{i,s}$, and therefore the higher the reversible rate when it is considered. Also it is seen that the surface concentration is important in determining the Thiele modulus and thus pore concentration. When vapor-liquid separation is considered, the surface concentration of each component at the catalyst particle boundary is the

same as its bulk liquid concentration in a CSTR, ignoring external diffusion. The latter can be obtained with model simulation (5).

Reactor Modeling and Simulation

The CSTR modeling and simulation for FT synthesis has been reported in detail elsewhere (5). Briefly, the CSTR is assumed to operate at constant temperature and pressure without catalyst deactivation. Reaction product is separated into liquid and vapor, which are assumed to be in thermodynamic equilibrium following Raoult's law under the reaction conditions. For simplicity of simulation, it is further assumed that hydrocarbon products are linear paraffins from C_1 to C_{100} and that they follow single α ASF distribution. The vapor pressure of each paraffin is calculated using Equation (14), obtained from the literature (7). In this equation, the unit for vapor pressure is atm and the unit for temperature is Kelvin.

$$P_i^s = 176.0452\exp\left(-427.218\left(\frac{1}{T} - 1.029807\times 10^{-3}\right)(i-1)\right) \qquad (14)$$

For this section, CO and H_2O are assumed to be insoluble in the reactor liquid. For a cobalt catalyst, the ratio of H_2/CO in the feed is about 2:1, about the utilization ratio, and this will be the ratio in the reactor. Therefore, we can select either CO or H_2 as dependent variable in the kinetic expression. For the iron catalyst, the water-gas-shift activity provides a source of hydrogen. However, equation (2) is known to be applicable for kinetic description for the iron catalyst. Thus, in this manuscript, hydrogen is selected for the iron catalyst as well. H_2 is considered soluble in hydrocarbon liquid since it is critical in evaluating the product Thiele modulus as reflected in Equation (9). The hydrogen solubility in the reactor liquid is calculated based on the following formula for Henry's law constant (8)

$$H = 2.291 \times 10^{7} \exp\left(-1.2326 + 583 / T\right) \quad (15)$$

in which H is in kPa cm^3/mol and T in Kelvin.

Three conditions are selected to illustrate the hydrocarbon product distribution in catalyst pores. A pressure of 20 atm and CO conversion of 60% are common for the three conditions considered while condition A consists of temperature 230 ^{o}C and an α value 0.85, condition B consists of temperature 270 ^{o}C and an α value 0.65, and condition C consists of temperature 310 ^{o}C and an α value 0.85.

Results And Discussion

Diffusion Limitation. In any heterogeneous catalytic reaction, the so-called rate determining step is the one whose mass transfer capability is the smallest one of the series steps and thus represents the rate of the overall reaction process. When a step becomes the determining step, it means that its mass transfer capability cannot meet the demand of its upstream steps or that required by its downstream steps. This concept applies to a process consisting of a series of steps since the mass transfer reflux is the same for each step under steady state. For Fischer-Tropsch synthesis products, it is true that the heavier the hydrocarbon, the more difficulty its diffusion in catalyst pores because the diffusivity decreases significantly with carbon number. This fact has been extended and is considered to be the major assumption that leads to the conclusion that the higher hydrocarbon product causes severer transport limitation (2-4). The above argument implies that the mass transfer reflux is the same for each hydrocarbon product. This is not the case in FT reactions in which the higher the carbon number, the lower its production rate, and therefore it imposes less demand on the mass transfer capability by diffusion in catalyst pores. According to the correlation in Equation (11), the hydrocarbon diffusivity decreases with carbon number at the rate of $D_{n+1}/D_n = 0.74$. The

magnitude of this rate is comparable with a typical single α value in FT synthesis in which the hydrocarbon production rate decreases by the factor of $r_{n+1}/r_n = \alpha$. Therefore, it is not necessarily more difficult for a heavier component, compared to a lighter one, to be transported out of the catalyst pores. It is true that the rate of diffusion of heavier material is smaller than for lighter material. But in terms of diffusion limitation, it is not necessarily more difficult . For example, while the heavier material has a lower diffusion rate, it also has lower diffusion duty since smaller amounts are generated. More importantly, the heavier material has a higher solubility in the liquid phase, and this contributes to developing a more uniform concentration distribution in the catalyst pores (Figure 4). Therefore, the diffusion limitation of the heavier material may be lower than for the lighter one. It should be recognized that the concentration profile in the catalyst pores, rather than diffusivity, is being used to judge the impact of diffusion limitation. For instance, when the α value is less than 0.74, the concentration gradient required to transfer a hydrocarbon product out of catalyst pores actually decreases with increasing carbon number. In general, the presence of diffusion limitation should be judged using the Thiele modulus, or more precisely, the concentration profile in the catalyst pores, rather than simply looking at the diffusivity even though it is an important component in the definition of Thiele modulus.

Single Phase Product. As shown in Equation (11), the Thiele modulus of a hydrocarbon product depends on its concentration at the catalyst surface, in addition to its generation rate constant and its diffusivity. Due to the complexity of the Fischer-Tropsch reaction, many researchers assume that the products are in a single phase, either vapor or liquid phase, when developing their models. With this assumption, the product concentration at the catalyst surface should also follow a single α distribution under steady state, if the FT reaction follows single α chemistry. Thus, the Thiele modulus of a hydrocarbon product is inversely proportional to the square root of its effective diffusivity and must increase with carbon number. As a result,

internal diffusion limitations always have to occur and, starting from some carbon number, then increase with increasing carbon number, as shown in Figure 1. This appears to be why the two α product distribution was attributed exclusively to the effect of internal diffusion limitation of hydrocarbon products (2).

The assumption of single phase product distribution is an oversimplification of the problem since this ignores the effect of vapor-liquid equilibrium in a typical FT reactor. It has been argued that, in the presence of vapor-liquid equilibrium, the chemical potential of a given species is identical in both liquid and vapor phases and thus the rate of a chemical reaction cannot depend on the identity of the phase and the hydrocarbon solubility in the liquid phase (2, 9). The scope of thermodynamics and kinetics needs to be considered. As a thermodynamic intensive property, chemical potential defines the processing direction and the processing limit, but does not define the processing rate. According to the standard definition, the chemical potential of a species in a phase is the sum of its standard free energy and the contribution of such species in its current mixture, and the later is a function of its composition. The fundamental difference between a vapor only and a vapor/liquid system lies in the fact that the standard free energy of a species in the liquid phase is different from that in the vapor phase; the difference can be quantified as a function of its vapor pressure. For an idea vapor/liquid system in equilibrium, the relationship between vapor and liquid can be described using Raoult's law. The concentration of a species in the liquid phase depends not only on its vapor composition but also its vapor pressure under the process conditions. For two species whose chemical potentials are identical in both vapor and liquid phases, the component having a lower concentration in the vapor phase may have a higher concentration in the liquid phase, simply because it has lower vapor pressure. In a Fischer-Tropsch reactor, due to the effect of vapor liquid separation (when it exists), the hydrocarbon concentration in the liquid phase increases with increasing carbon

number, and is in contrast to the opposite trend in vapor phase (5). As a result, the product concentration profile in the catalyst pores and the trend of its diffusion limitation are totally different in the vapor and vapor/liquid systems.

On the other hand, reaction kinetics, or simply reaction rate, has to be used to evaluate catalyst performance. Without question, the catalyst performance depends on the phase in which the catalyst resides because the reactant concentration varies in the different phases, even though these phases are in equilibrium and the chemical potential of the reactant is identical in each phase. Any impact resulting from the others phases has to go through the phase the catalyst is in contact with and can therefore affect the catalysts performance indirectly. Although an active site on the catalyst surface does not depend on whether the reactant molecule comes from the liquid or vapor phase, it does depend on how many molecules surround it. According to collision theory, the nature of chemical reactions is a measure of effective collisions between reactant molecules. A higher population of reactant molecules will lead to a higher probability for effective collisions and thus higher reaction rates. Very often, the assumption of a vapor phase operation gives rise to incorrect conclusions when there is vapor-liquid separation and the catalyst is in the liquid phase, especially when the reaction rate is of concern.

Light Hydrocarbon Products (C_{20-}). It is a general observation that for light hydrocarbons (C_{20-}), most of the products are removed from the reactor through the vapor phase. This observation has been supported by VLE simulation for a CSTR slurry reactor in which the hydrocarbon product follows a single α distribution in vapor phase (5). Within this range, the ratio of the Thiele moduli of two successive hydrocarbons becomes the competition between their relative volatility and their diffusivity, as shown in the following equation:

$$\left(\frac{\phi_{i+1}}{\phi_i}\right)^2 = \frac{P_{i+1}^s}{P_i^s} \Big/ \frac{D_{i+1}}{D_i} \qquad 16)$$

A magnitude of ϕ_{i+1}/ϕ_i greater than unity indicates that the diffusion limitation increases with increasing carbon number, while a value less than unity points to the opposite direction. Although disagreement remains about the relationship between hydrocarbon diffusivity and carbon number, Equation (12) is used in this work since it shows the strongest dependency on carbon number. Substituting Equations (12) and (14) into Equation (16) shows that ϕ_{i+1}/ϕ_i is greater than unity only when the temperature is higher than 304 ^oC, which approaches the typical high temperature Fischer-Tropsch synthesis with its gas phase operation. At lower temperatures or if diffusivity follows Equation (13), there is no opportunity for ϕ_{i+1}/ϕ_i to be greater than unity.

VLE Effect. In the presence of vapor-liquid separation, the product concentration at the catalyst surface, $C_{i,s}$ as in Equation (11), is the same as the bulk liquid concentration, and can be obtained by VLE simulation since the impact of vapor-liquid separation has to be considered. Figure 2 shows the liquid composition in a CSTR slurry reactor under conditions simulated in this work. Conditions A and C chosen for example calculation represent normal operating conditions under steady state when both vapor and liquid are generated and Condition B represents an unsteady state condition. Under these conditions, the hydrocarbon concentration increases with carbon number to a maximum and then decreases. Condition B is an unsteady state operation in which the liquid product does not accumulate because of the low alpha value. This type of operation will lead to drying out of a CSTR reactor over time due to excessive evaporation of the starting solvent and the inability of the low alpha catalyst to generate the liquid products faster than they are removed in the vapor phase.

Applying the liquid concentration shown in Figure 2 to Equation (11), the Thiele modulus of each hydrocarbon component can be calculated. Figure 3 shows the Thiele modulus of each hydrocarbon component relative to that of C_2 which is selected as reference because it is the lowest boiling molecule of interest. Under Condition C, when the reaction temperature is 310 ^oC, ϕ_i/ϕ_2 increases with increasing carbon number indicating the direction of severer diffusion limitation. Although this temperature is typical of a low α and vapor phase operation, its impact on two α product distribution should not be ruled out, no matter how slowly ϕ_i/ϕ_2 changes with carbon number. When the operating temperature is lower than 300 ^oC , ϕ_i/ϕ_2 decreases with increasing carbon number up to about C_{20}, and then increases. This value becomes higher than unity only when the carbon number is higher than 30. This phenomenum indicates that the hydrocarbon diffusion in catalyst pores does not become more and more difficult as expected with the assumption of a single phase product. In fact, it is just the opposite; it becomes relatively easier with increasing carbon number for the lower carbon number components. When there is no diffusion limitation for C_2, there is also no diffusion limitation for higher hydrocarbons until at least carbon number C_{30}. Even if the removal of C_2 is diffusion limited, it is not necessary for higher hydrocarbons to have diffusion limitation because the effect of internal diffusion become less and less significant with increasing carbon number up to about C_{30}. This eliminates the cornerstone assumption of any model that requires stronger product diffusion limitation with increasing carbon number.

Of course, for carbon numbers higher than 30, there might be diffusion limitation starting with some hydrocarbon component. These heavy hydrocarbons tend to accumulate in catalyst pores until they have enough driving force to transfer the products out of the pores. However, this issue should not affect the total FT product distribution since olefins of these high carbon numbers typically are not produced from the catalyst surface. The accumulation of heavy

hydrocarbons in catalyst pores may lead to internal diffusion limitation of reactants and catalyst deactivation, but does not produce a two α distribution. It therefore can be concluded that, in the presence of VLE, the internal diffusion limitation of products does not necessarily exist and, even if it does exist, should not be responsible for the two alpha product distribution in FT synthesis.

Figure 4 shows the relative concentration profile of several hydrocarbon components in the catalyst pores under Condition A and ϕ_H=1.0 (catalyst efficiency 94%). For carbon numbers lower than 20, the higher the carbon number, the lower its relative concentration in the catalyst pores, indicating that the effect of internal diffusion is less significant with increasing carbon number. This is, in fact, the same result as has been discussed above when the analysis is made in terms of the Thiele modulus.

Figure 5, plotted with the volumetrically average concentration of C_2 vs. the hydrogen Thiele modulus, shows that the effect of internal diffusion of C_2 increases with ϕ_H. When there is no internal diffusion limitation of hydrogen, e.g., ϕ_H <0.2, there is also no internal diffusion limitation of C_2. Of course there is also no diffusion limitation for other hydrocarbons up to about C_{35} as has been discussed previously (Figures 3 and 4). The same conclusion can be drawn simply by examining Equation (9) directly. It also can be seen from Figure 5 that, with the same catalyst efficiency (same ϕ_H), the significance of product diffusion is affected by reaction conditions. When the catalyst efficiency is only 80% (ϕ_H = 2.0), the average concentration of C_2 in the catalyst pores can be less than 1% higher than its surface concentration under Condition B, while it can be 37% higher under Condition A.

Olefin Reincorporation. The major assumption of the above discussion is that all of the products are non-reactive paraffins. This assumption significantly simplifies the development of reaction and mass transfer models. Also, comparison of the concentration profile of

hydrocarbon products in the catalyst pores becomes straightforward. In practice, however, olefins are also produced and these have been confirmed experimentally to be reactive. In other words, the pathway for termination to olefins is reversible. As a supplement to this work, the following sections present the hydrocarbon concentration profile in the catalyst pores when olefin reincorporation is also taken into account.

The chemical potential of a species is its partial molar Gibb's free energy in a mixture. It is the contribution of such species to the total free energy of the mixture. The chemical potential of species i in an ideal gas mixture (μ_i^v) and in an ideal solution (μ_i^L) can be described using Equations (17) and (18), respectively.

$$\mu_i^v = G_i^v + RT\ell n y_i \quad 17)$$

$$\mu_i^L = G_i^L + RT\ell n x_i \quad 18)$$

In these two equations, G_i^v and G_i^L are Gibb's free energies of pure gas and pure liquid of species i at the mixture temperature and pressure, respectively. Y_i and x_i are molar fractions of species i in the gas phase and in the liquid phase, respectively. For a vapor-liquid system in equilibrium, the chemical potential of a species is identical in both phases, i.e., $\mu_i^v = \mu_i^L$. Thus, the following two equations can be derived.

$$RT\ell n\frac{y_i}{x} = G_i^L - G_i^v = RT\ell n\frac{P_i^s}{P} \quad 19)$$

$$y_i P = x_i P_i^s \quad 20)$$

Equation 15 is Raoult's law and the detailed derivation is available, such as the text by Smith and Van Ness (10).

In Fischer-Tropsch synthesis, the reversible reactions of olefins are considered when modeling the product distribution. The absolute reversible rate of an olefin species depends on its concentration (or activity if considering real solution) in the phase where reactions take place. Therefore, it is important to know how the olefin concentration changes with carbon number in different phases, even though these phases are in equilibrium. If the reaction takes place in gas phase, in which the hydrocarbon concentration decreases with increasing carbon number, it is obvious that the reversible reaction rate of olefin has to follow the same trend, assuming that the rate constant does not depend on carbon number. When there is vapor-liquid separation and the reactions take place in the liquid phase, liquid phase composition should be used to characterize the reaction rates. For two components with successive carbon number in the system, we have

$$\frac{x_{i+1}}{x_1} = \frac{y_{i+1}}{y_i}\frac{P_i^s}{P_{i+1}^s} \qquad 21)$$

The dependency of hydrocarbon concentration on carbon number in the liquid phase does not necessarily follow the same trend as that in the vapor phase. In a typical low temperature Fischer-Tropsch reaction, the liquid concentration increases with increasing carbon number in the low carbon number range, because the vapor pressure rapidly decreases with increasing carbon number.

Additional assumptions are required since little quantitative data are available for olefin reactions under Fischer-Tropsch synthesis conditions. It is assumed that chain growth on the catalyst surface follows a single α rule. For each chain growth intermediate, the same olefin fraction is generated among the total hydrocarbons of that carbon number before considering the

reversible reaction of olefins. To simplify, it is further assumed that all of the products are olefins. The olefin reaction kinetics to higher hydrocarbons follows k_rC_i, in which k_r is the rate constant that is independent of carbon number. Finally, it is also assumed that the primary reaction of CO and H_2 are not affected by the olefin reaction.

Any hydrocarbon component i is generated from CO and H_2, from lighter olefins ranging from carbon 2 to carbon i-1, and is decreased by conversion to higher hydrocarbons at a rate of k_rC_i. The material balance of component i in the catalyst pores is shown in Equation (22).

$$D_i \frac{1}{r^2}\frac{d}{dr}\left(r^2 \frac{dC_i}{dr}\right) = -k_i C_H - \sum_{j=2}^{i-1} k_r(1-\alpha)\alpha^{i-j-1}C_j + k_r C_i \qquad 22)$$

The analytical solution to Equation (22) is

$$\frac{C_i}{C_{i,s}} = \left(1 - \sum_{j=1}^{i-1} B_{ij}\right)\left(\frac{R_p}{r}\right)\frac{\sinh(\phi_{ir} r / R_p)}{\sinh(\phi_{ir})} + \sum_{j=1}^{i-1} B_{ij}\left(\frac{C_j}{C_{j,s}}\right) \qquad 23)$$

where

$$B_{ij} = \frac{1-\alpha}{\alpha}\frac{\phi_{jr}^2}{\phi_{ir}^2 - \phi_{jr}^2}\left(\frac{\phi_i^2}{\phi_j^2} - \sum_{k=j+1}^{i-1} B_{ik}\frac{\phi_k^2}{\phi_j^2}\right) \qquad B_{i1} = \frac{\phi_H^2}{\phi_{ir}^2 - \phi_H^2}\left(\frac{\phi_i^2}{\phi_H^2} - \sum_{j=2}^{i-1} B_{ij}\frac{\phi_j^2}{\phi_H^2}\right)$$

$$\phi_i = R_p\sqrt{\frac{k_i}{D_i}\frac{C_{H,s}}{C_{i,s}}} \qquad \phi_{ir} = R_p\sqrt{\frac{k_{ir}}{D_i}} \qquad \phi_H = R_p\sqrt{\frac{k_H}{D_H}}$$

These equations are too complicated to allow visual examination on how pore concentrations change with carbon number. Condition A was used to illustrate the product concentration profile with Thiele modulus of H_2 = 2.0, and k_r/k_H = 0.025. The latter corresponds

to about 10% of the olefins generated in the primary termination step being reincorporated into growing chains. Figure 6 shows the dependence of the volumetrically average concentration of product in the catalyst pores on the carbon number. When considering the reversible olefin reaction, the relative concentration of light products decreases even more rapidly than the situation of non-reactive paraffin products. It is clear that, with or without considering olefin reaction, the relative concentration of light hydrocarbons (C_{20-}) decreases with increasing carbon number in the catalyst pores, indicating decreasing severity of internal diffusion limitation with increasing carbon number.

To distinguish among the models predicting the impact of diffusion on FTS is a demanding task. On the one hand, diffusion effects that arise after the reactant enters the bulk liquid phase can be defined with certainty by adding isotopically tracers. Once the product becomes a part of the bulk liquid-gas phases that are present external to the catalyst particle, the labeled and unlabeled compounds must become identical with respect to the impact of diffusion on secondary reactions. Such studies are being conducted in our lab. To establish the impact of diffusion on the primary and secondary reactions that occur within the catalyst particle prior to equilibrating with the bulk liquid-gas phases is a demanding task. One approach that has been used is to vary the size of the primary catalyst particle and to show that the experimental data match the values predicted from diffusion models. In principle this would be easy to do in the slurry phase; however, it is likely that catalyst particles small enough to cover the required size range agglomerate in the slurry phase.

One approach that has potential is to use the same catalyst particle under conditions where different amounts of liquid phase are present during the synthesis. At least in theory this is possible using supercritical conditions. Using a cobalt catalyst in a fixed-bed reactor, FTS was conducted using identical conditions except that the inert gas was argon in one case and a

mixture of pentane and hexane in the other (11). Thus, space velocity, partial pressure of reactants and temperature remained constant while the density of the inert diluent was varied. With argon dilution the density was low and at, or near, that of a gas whereas the mixture of pentane and hexane provided a liquid-like density (ca. 80% of the density of a liquid). The conditions were adjusted so that a conversion of CO was established at about 40% when the inert gas was a mixture of pentane and hexane. When argon replaced the hydrocarbon mixture the CO conversion gradually declined during seven days, ending at about 20% conversion. During the period of operating with argon, less non-volatile products were collected in the receiver than was calculated, based on the material balance. When the argon was replaced by the hydrocarbon mixture, the CO conversion increased to the 40% level. In addition, the amount of wax collected the first day of operation with the hydrocarbon mixture exceeded the amount calculated from mass balance. During the next eight days of operation with the hydrocarbon mixture the conversion remained constant and the amount of excess wax that was collected declined each day to approach that calculated for mass balance. However, the alpha value for the wax products was essentially the same whether argon or hydrocarbon mixture was added. Thus, while it appears that diffusion within the catalyst particle materially impacted CO conversion, it did not have a measurable impact upon hydrocarbon carbon number.

A key point of this paper is that one should use the Thiele module, rather than simply diffusivity, to justify diffusion limitation. Diffusivity is only one of the parameters contributing to diffusion limitation. Other factors, such as solubility or catalyst surface concentration, also contribute. This work shows that diffusion limitation is due to the competition between relative diffusivity and relative solubility; under most FT conditions, solubility dominates as in equation (16).

Conclusion

Due to the effect of vapor liquid separation in the Fischer-Tropsch reactor under steady state, the relative concentration of a hydrocarbon product in the catalyst pores decreases with increasing carbon number until about C_{20}. This indicates that, in this carbon number range, the heavier the hydrocarbon, the less severe the internal diffusion limitation. The impact of internal diffusion of a product may become significant only when there is internal diffusion limitation of reactants, and this significance decreases with increasing carbon number. It is thus deduced that the two alpha product distribution in Fischer-Tropsch reactions is not due to the effect of product diffusion limitation, even if it exists under some reaction conditions.

The view advanced here is that diffusion limitation should be based on a concentration profile in the catalyst pores, or Thiele Module, not simply diffusivity. For any species, diffusion limitation is based on a comparison of its generation rate (products) or disappearance rate (reactants) with its diffusion rate, and the latter is a function of its surface composition which depends on vapor-liquid separation.

Acknowledgment

This work is supported by U.S. DOE contract number DE-AC22-94PC94055 and the Commonwealth of Kentucky.

Nomenclature

C	molar concentration
D	diffusivity
G	Gibb's free energy
H	vapor liquid equilibrium constant
k	reaction rate constant
$\bar{n}$	average carbon number of hydrocarbon product mixture
P	pressure
P^s	saturated vapor pressure of hydrocarbon
r	reaction or generation rate (with subscription), radial position in a catalyst particle
R	gas constant
R_p	catalyst particle radium
T	temperature
x	liquid phase molar fraction
y	vapor phase molar fraction
α	chain propagation probability on surface, a function of carbon number
ϕ	Thiele Module
μ	chemical potential

<u>subscript</u>

H	hydrogen
HC	hydrocarbon
i	carbon number
r	olefin reaction rate constant
s	surface

References

1. B.C. Gates, J.R. Katzer, and G.C.A. Schmit, “Chemistry of Catalytic processes”, McGraw-Hill Chemical Engineering Series, McGraw-Hill, 1979, p261-263.

2. Iglesia, E., Reyes, S.C., and Soled, S.L; “Reaction-transport selectivity models and the design of Fischer-Tropsch catalysts” in "Computer-Aided Design of Catalysts and Reactors," (E. R. Becker and C. J. Pereira, Eds.), Marcel Dekker, Inc., 1992, pp 199-257.

3. Madon, R.J., and Enrique, Iglesia E., Journal of Molecular Catalysis A: Chemical, 163 (2000) 189-204.

4. Tsubaki N. and Fujimoto K., Fuel Processing Technology, 62 (2000) 173-186.

5. Zhan, X. and Davis, B.H., Petroleum Science and Technology, 18 (2000) 1037-1053.

6. Kuipers, E.W., Vinkenburg, I.H. and Oosterbeek H., J. Catalysis, 152 (1995) 137-146.

7. Caldwell, L. and van Vuuren, D.S., Chem. Eng. Sci., 41 (1986) 89-96.

8. Deckwer, W.D.; “Bubble Column Reactors”, John Wiley and Sons, 1992.

9. Iglesia E., Applied Catalysis A: General, 161 (1997), 59-78.

10. Smith, J. M. and Van Ness, H. C., “Introduction to Chemical Enginering Thermodynamics,” McGraw-Hill, Inc., 1987.

11. Jacobs, G., Chaudhari, K. Sparks, D. Zhang, Y., Shi, B., Spicer, R., Das, T. K., Li, J. and Davis, B. H., submitted.

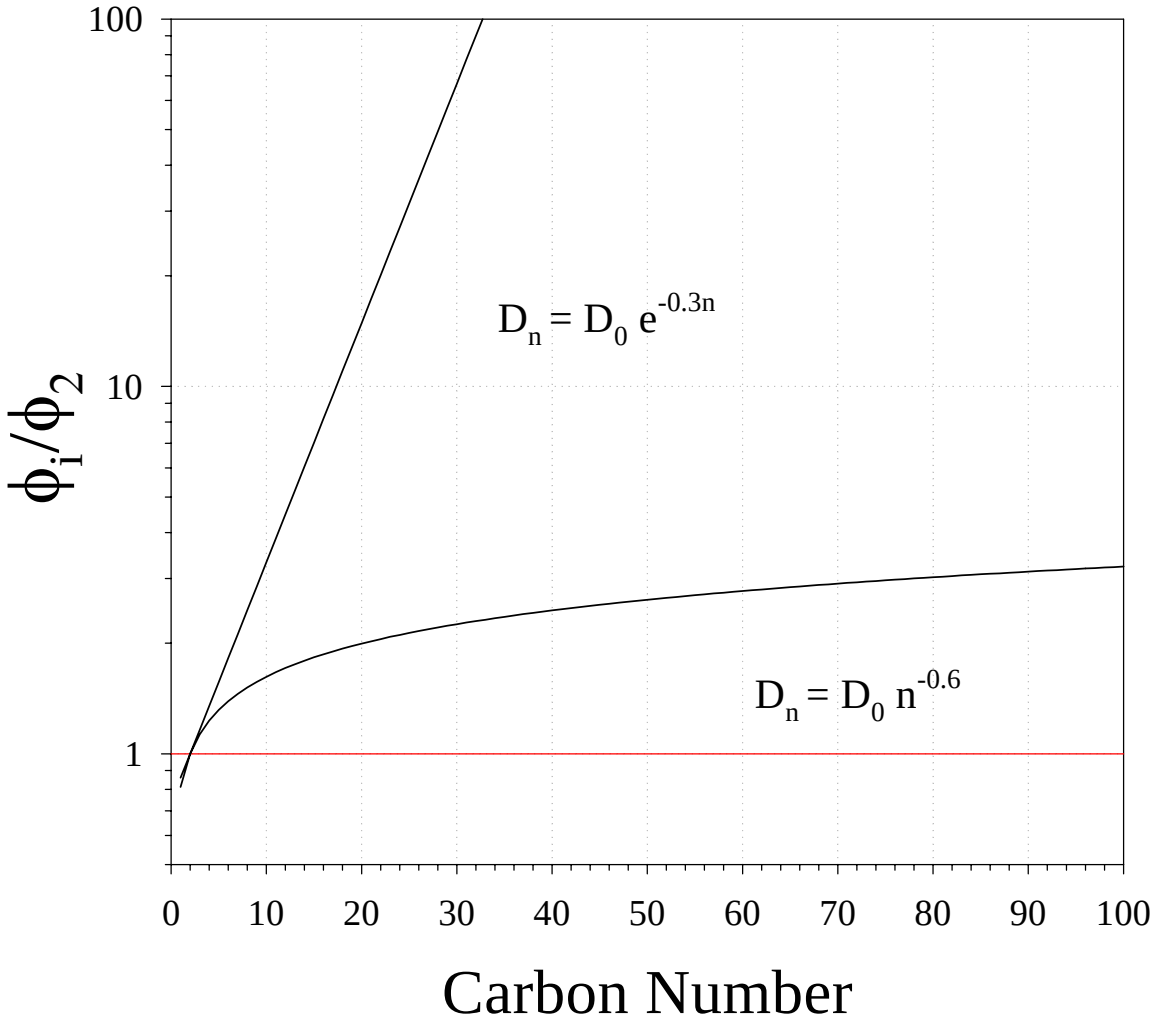

Figure 1 Thiele Modulus of Hydrocarbons with products in single phase

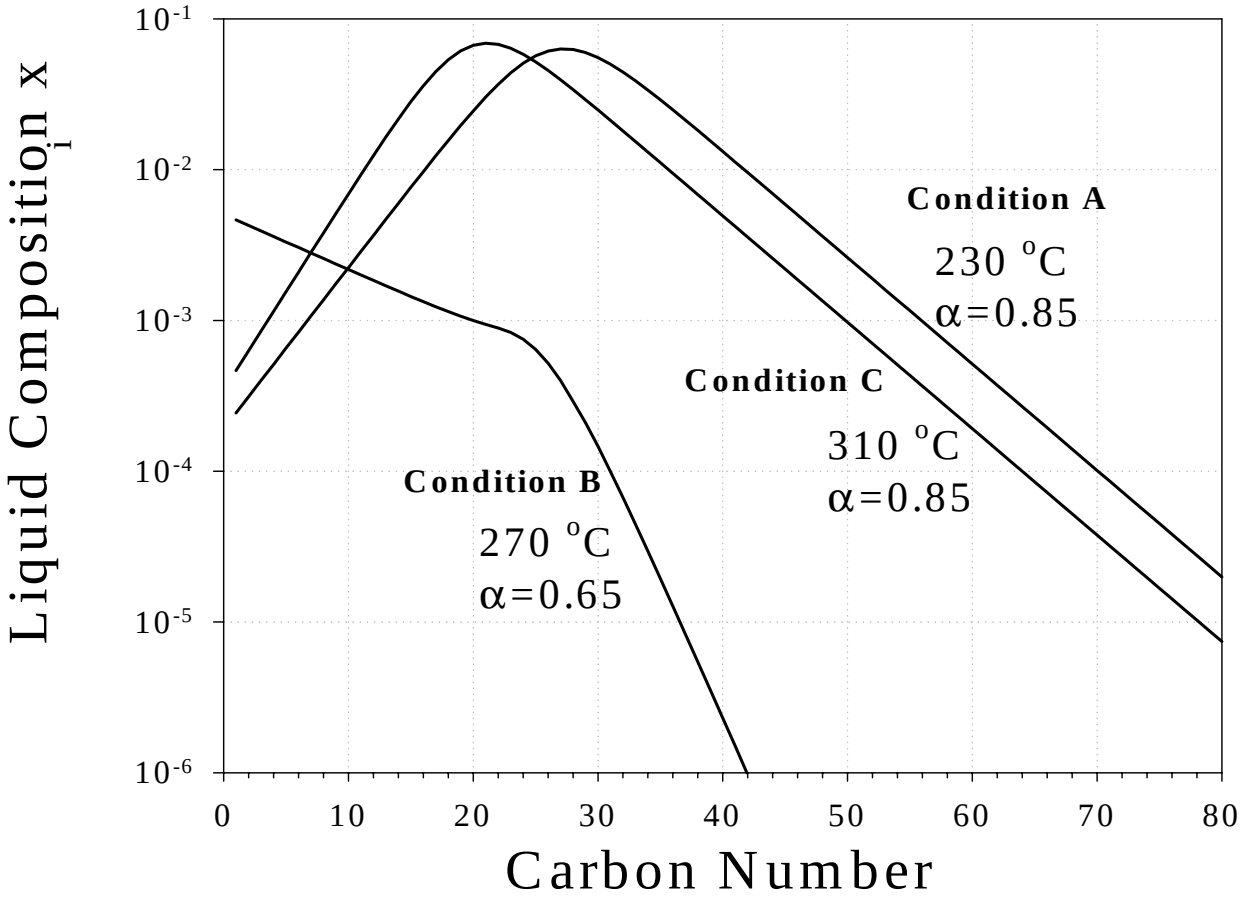

Figure 2 Liquid compositions in CSTR reactor (see reactor modeling and simulation section for definition of conditions of A, B and C).

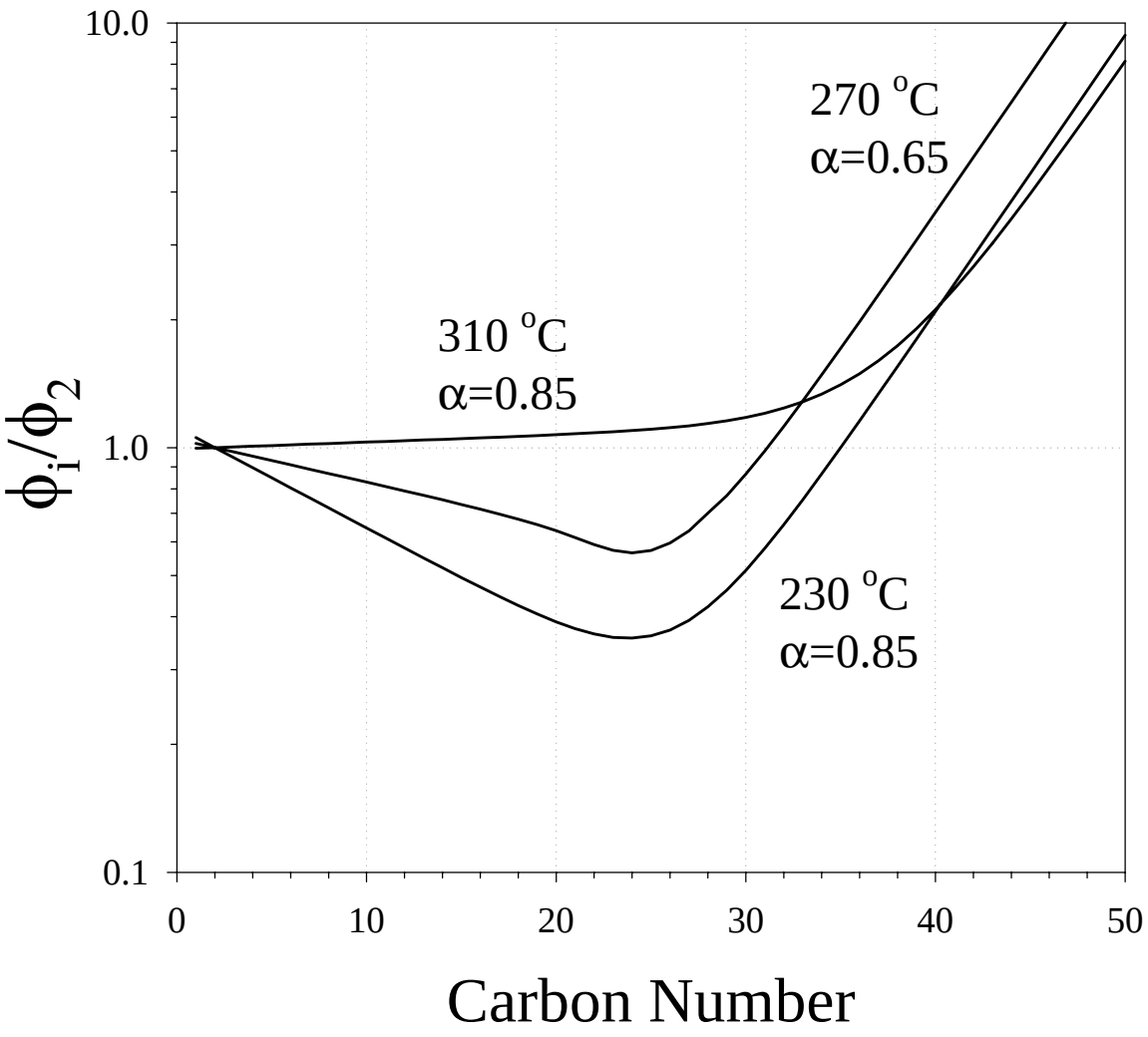

Figure 3 Thiele Modulus of Hydrocarbons with VLE and $D_n=D_0\, e^{-0.3n}$

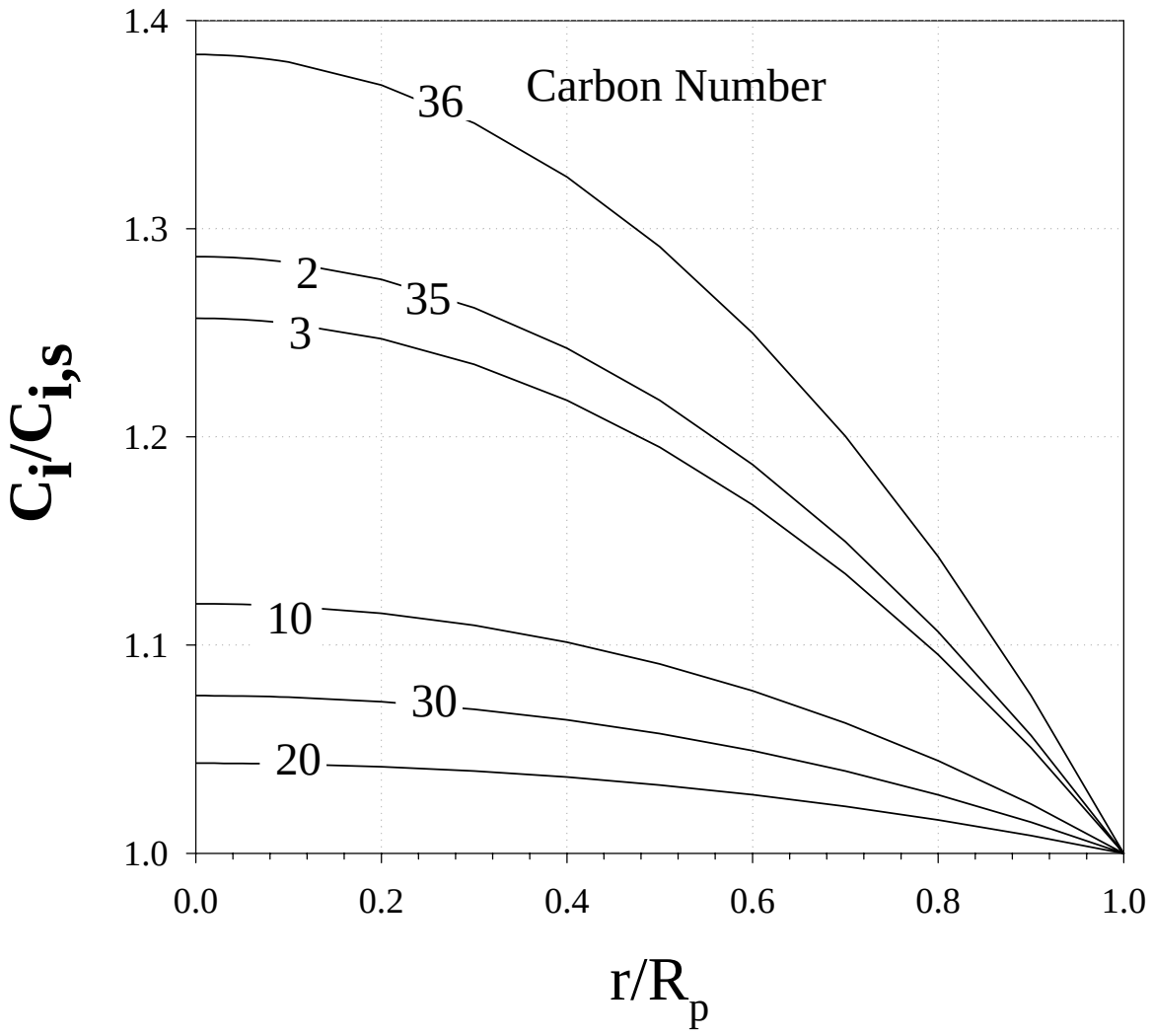

Figure 4 Hydrocarbon Concentration Profile in Catalyst Pores at Condition A with $\phi_H = 1.0$ ($\eta_H = 94\%$)

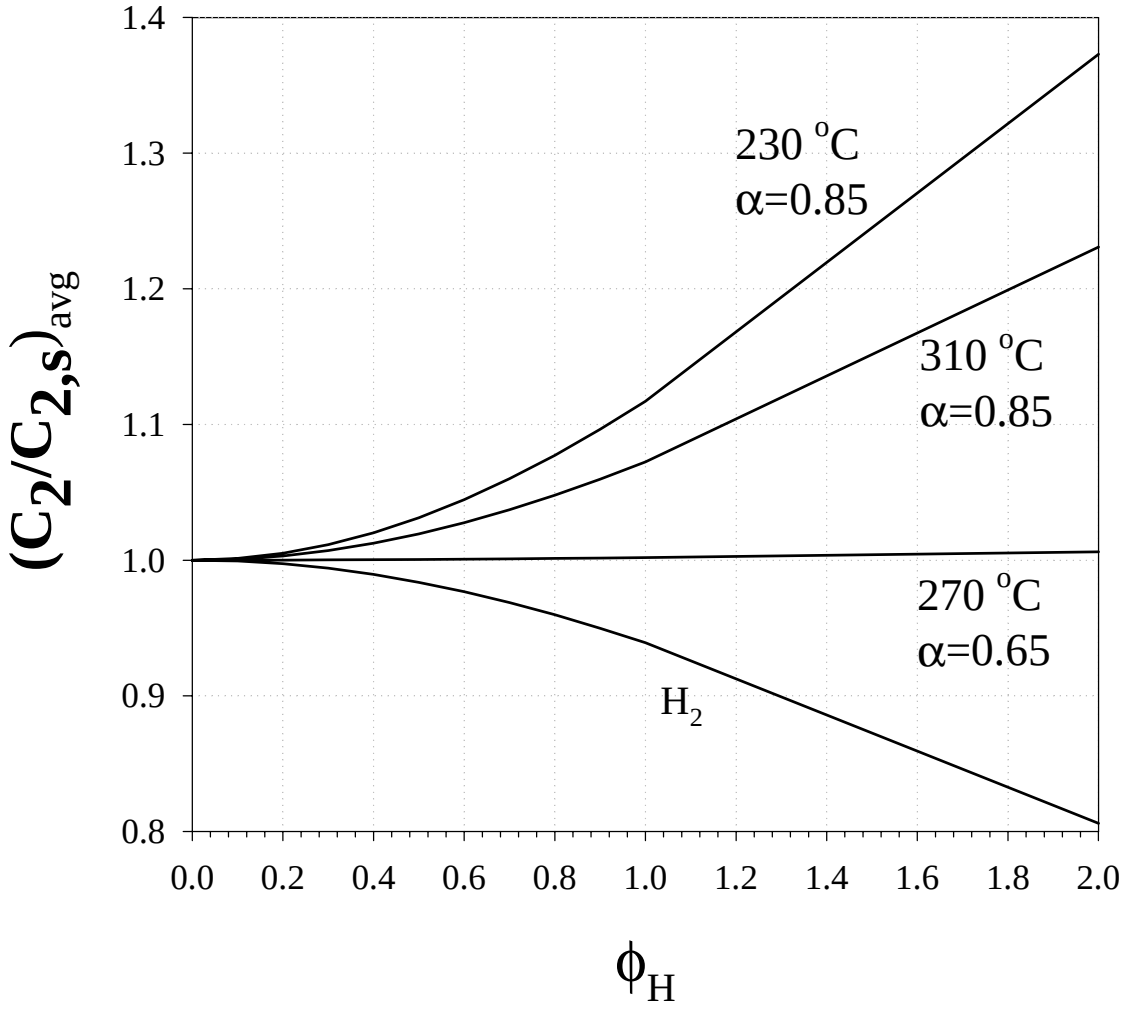

Figure 5 Effect of Hydrogen Thiele Modulus on Average Concentration of C_2 in Catalyst Pores

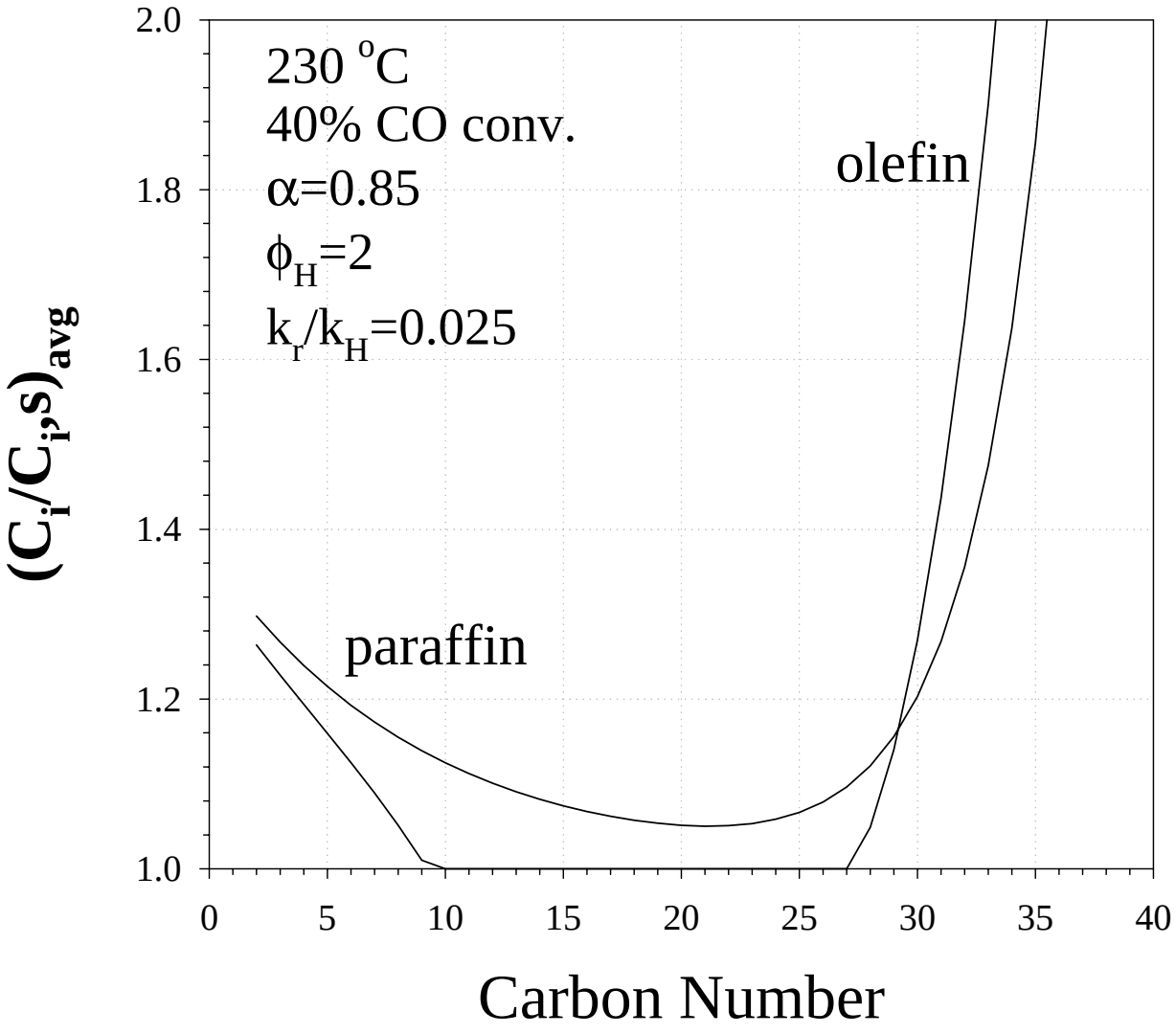

Figure 6 Average Concentration of Hydrocarbon Products in the Catalyst Pores with Olefin Reincorporation

E. Product Distribution of Fischer-Tropsch Synthesis

Abstract

Fischer-Tropsch product distribution models available in the open literature are discussed. It is concluded that the effect of vapor-liquid separation is the most probable reason for the observation of a two alpha product distribution. A mathematical model has been developed to describe the product distribution, based on the recognition that the termination path to olefin products is reversible. The observed product distribution at the reactor outlet consists of the contributions from the intrinsic chain propagation on the catalyst surface and the effect of olefin reactivity. The reaction product does not follow an Anderson-Schulz-Flory single alpha distribution even on the catalyst surface. The effect of olefin "reincorporation" is significant only for the low carbon number range when there is a high fraction of olefins. In the high carbon number range, alpha appears to be constant because there is a small or no olefin reincorporation effect. An excellent fit between the values predicted by the model and experimental data has been demonstrated.

Introduction

Fischer-Tropsch (FT) synthesis can be conducted in either vapor phase or vapor-liquid reactors depending on the product demand and the catalyst performance. Vapor phase reactors feature high temperature operation (>300^{o}C) and low alpha products (e.g., light olefins and gasoline). Alpha is related to the rates of termination and propagation steps, and therefore the average molecular weight of the products. Single alpha product distribution is a common observation with this type of operation. When high alpha products are the goal (e.g., diesel, wax), the synthesis is typically carried out in fixed-bed and slurry bubble column reactors at low temperatures (<250^{o}C). In these reactors, products separate into vapor and liquid phases. A two alpha product distribution has been observed in both laboratory and pilot scale tests (1), in

contrast to the so-called Anderson-Schulz-Flory (ASF) single alpha distribution. Several models have been proposed to explain the two alpha observation, including: two active sites responsible for different chain growth pathways (2-4), diffusion enhanced olefin readsorption in catalyst pores (5-9), and the effect of vapor-liquid-equilibrium (VLE) which causes accumulation of heavier products in the reactor and thus enhances olefin reactivity (10-13). An extensive review in this area has recently been made by Van Der Laan and Beenackers (14).

In most FT reactors, when vapor liquid separation is involved, the sample taken is actually not representative of what is produced during the sampling period, unless an impractically long time is taken for the reactor to reach "steady state". This sampling behavior has been suspected to be responsible for the two alpha product distribution due to VLE of products in the reactor. Recently, we have proved that, without considering the reactivity of olefin products, simple accumulation effect of heavier products by VLE cannot be responsible for the two alpha observation in a slurry reactor under normal operating conditions (15)

It is generally agreed that the reversible olefin termination path is responsible for the two alpha product distribution. Yet, there is still significant uncertainty about how this reversible reaction works. The diffusion enhanced olefin readsorption model attributes the two alpha observation to increasing internal diffusion limitations of the olefin products due to reduced diffusivity with increasing carbon number. However, this model ignores the presence of a liquid phase in which the catalyst resides. Our recent work indicated that the internal diffusion limitation of hydrocarbon products does not necessarily exist in catalyst pores unless there is also an internal diffusion limitation of reactants (16). In addition, due to the effect of vapor-liquid separation of hydrocarbon products in the FT reactor, the severity of diffusion limitation of light hydrocarbons (C_{20-}) actually decreases with increasing carbon number, just opposite to the cornerstone assumption of the diffusion model. Consequently, it was concluded that internal

diffusion limitation of the hydrocarbon products could not be responsible for the two alpha distribution, even though it might alter the observed alpha value (16).

The effect of VLE on the two alpha product distribution has been proposed by a few researchers, although it was also rejected by other researchers (17-18). The basic idea of this model is that the higher olefin carbon number, the longer the residence time in the reactor and therefore the greater the contribution of the reversible olefin reaction. As a result, product distribution appears as a function of carbon number. However, these studies are based on their conclusion of single α chemistry for surface chain growth. The olefin reactions were then treated separately in terms of so-called secondary reactions. In addition, some other common experimental observations were not properly predicted or explained. In this work, we demonstrate conceptually that the two alpha observation could be due to the effect of VLE when considering olefin reactivity. For simplicity of discussion, a continuously stirred tank reactor (CSTR) is used for this modeling study.

Reaction Pathway and Model Development

The Fischer-Tropsch synthesis is a very complicated reaction and the details of reaction mechanism remain to be defined. Over the years it has been recognized that a simple polymerization mechanism should describe the product distribution, with the surface chain growth intermediate being an olefinic (19) or a paraffinic species (20). For the purpose of qualitatively understanding the product distribution, it is unimportant to distinguish the type of surface intermediate because both of them lead to the same dependency on carbon number. In this work, it is assumed that the chain growth follows the pathways shown in Figure 1, ignoring minor side reactions such as alcohol production. It is also assumed that there is only one type of active site on catalyst surface on which any surface process takes place. According to this scheme, the surface intermediate grows by addition of a surface methylene species, and

terminates to paraffin by hydrogenation or to olefin by β-elimination of hydrogen. The termination path to paraffin is irreversible since paraffins are non-reactive under typical FT conditions, while the pathway to olefin is reversible. Surface olefin species can undergo half-hydrogenation reversibly to form a surface chain growth intermediate or desorption as a free olefin molecule within the catalyst pores. The latter can adsorb reversibly on the catalyst surface or diffuse out of the catalyst pore and be removed as a reaction product. This reversible path eliminates the necessity and confusion of inventing terminologies such as readsorption, reinsertion, reinitialization, or reincorporation. These "re-" concepts are sometimes misleading as they give an impression that they are separate processes from the forward dehydrogenation and desorption processes. In fact, inertness of the paraffins and the reversibility of olefin adsorption/ desorption and hydrogenation/dehydrogenation has been well documented (21).

The physical adsorption of olefins on the catalyst surface was taken into account by some researchers when modeling FT product distribution (10, **also chevron group** 22). This factor is not considered in this work since the effect of physical adsorption is virtually the same as that of liquid condensation and wetting. In the presence of vapor-liquid separation, the catalyst pores are filled with liquid which causes the physically adsorbed layer in the vicinity of catalyst surface to vanish. Nevertheless, chemisorption of the olefin may have a significant effect on product distribution. As a rule of thumb, other factors being equal, one may expect that the degree of chemical adsorptivity will increase with increasing molecular weight. However, since very little quantitative data are available for olefin chemisorption and the objective of this work is solely aimed at the effect of VLE, the olefin adsorption and desorption rate constants are assumed to be independent of carbon number.

Figure 2 shows schematically a typical CSTR slurry reactor, in which unconverted reactants and hydrocarbon products are separated into two phases, liquid and vapor. Both liquid

and vapor products are removed continuously to maintain a constant liquid level in the reactor. With the assumption that there is no internal diffusion limitation of reactants, which is essentially true in a slurry reactor with small catalyst particles, the diffusion of hydrocarbon products in the catalyst pores is not considered, as has been proven to be absent (16). Based on the reaction mechanism of Figure 1, the steady state material balance of each surface species of carbon number n is as follows, assuming that the reaction rate constants are independent of carbon number:

Chain growth intermediate, C_n^* : $$k_p S_1 S_{n\text{-}1} + k_o' S_H S_{n=} = (k_p S_1 + k_H S_H + k_o) S_n \quad (1)$$

Surface olefin, $C_{n=}^*$: $$k_o S_n + k_a x_{n,o} = (k_o' S_H + k_d) S_{n=} \quad (2)$$

Olefin, O_n : $$V_R k_d S_{n=} = V_R k_a x_{n,o} + V y_{n,o} + L x_{n,o} \quad (3)$$

Paraffin, P_n : $$V_R k_H S_H S_n = V y_{n,p} + L x_{n,p} \quad (4)$$

From the above material balance equations, the concentration ratios of olefin to paraffin in the liquid phase (f_n) and the chain propagation probability on the catalyst surface (α_n) can be derived as Equations (5) and (6), respectively.

$$f_n = \frac{x_{n,o}}{x_{n,p}} = \frac{k_o k_d}{k_H S_H \left(k_d + k_o' S_H (1 + \tau_n k_a)\right)} \quad (5)$$

$$\alpha_n = \frac{S_n}{S_{n-1}} = \frac{1}{1 + \beta(1 + f_n)} \quad (6)$$

where

$$\tau_n = \frac{V_R}{VH_n + L}; \quad H_n = \frac{y_{n,o}}{x_{n,o}} = \frac{y_{n,p}}{x_{n,p}} = \frac{P_n^s}{P}; \quad \beta = \frac{k_H S_H}{k_p S_1} \tag{7}$$

In Equation (7), τ_n is the average residence time of hydrocarbon product species n in terms of reactor size, H_n is the ideal vapor-liquid equilibrium constant of hydrocarbon product species n, and β is characteristic of surface chain propagation probability at high carbon numbers when olefin production rates approach zero. Under the latter situation, the product propagation probability (α_∞) appears to be independent of carbon number, as shown in Equation (8).

$$\alpha_\infty = \frac{k_p S_1}{k_p S_1 + k_H S_H} = \frac{1}{1+\beta} \tag{8}$$

It is clear from Equation (6) that, due to the effect of vapor liquid separation and olefin reactivity, the surface chain propagation probability does not remain constant as proposed by Anderson (23, 24). Instead, it is a decreasing function of olefin to paraffin ratio or an increasing function of carbon number. Generally, the higher the carbon number, the lower the vapor-liquid equilibrium constant (H_n), the higher the average residence time (τ_n), the lower the olefin to paraffin ratio (f_n), and thus the higher the surface propagation probability (α_n).

In practice, it is impossible to collect hydrocarbon products directly from the catalyst surface. The product distribution is obtained by measuring vapor and liquid products collected at the reactor outlet. The production rate of a hydrocarbon species, n, including both olefin and paraffin in both vapor and liquid phases, is

$$r_n = V(y_{n,p} + y_{n,o}) + L(x_{n,p} + x_{n,o}) = V_R k_H S_H (1 + f_n) S_n \tag{9}$$

and the observed product distribution is thus defined as:

$$\alpha_n' = \frac{r_n}{r_{n-1}} = \frac{1+f_n}{1+f_{n-1}}\frac{S_n}{S_{n-1}} = \frac{1+f_n}{1+f_{n-1}}\frac{1}{1+\beta(1+f_n)} = \lambda_n\alpha_n \qquad (10)$$

Equations (5), (6), and (10) completely describe the observed product distribution of Fischer-Tropsch synthesis in a CSTR reactor. Nonetheless, the same method can be applied to any type of reactor, as long as there is vapor-liquid separation of products. In integral reactors, such as a fixed-bed reactor, the molar flowrates of liquid and gas are local values but this model still holds. In fact, this model is valid for any type of reactor since the molar flowrate will cancel each other as far as the product distribution is of concern.

Model Simulation and Discussion

The observed alpha value, defined in Equation (10), is the one that is widely used to measure FT product distribution. It consists of two parts: the surface chain propagation probability (α_n) and the effect of olefin reactivity (λ_n). Both of these factors increase with increasing carbon number, leading to the observed two alpha distribution. In the high carbon number range, f_n approaches zero and λ_n approaches unity. Thus, α_n' appears as a constant, α_∞. This is the so-called second alpha, as it has been named by many researchers. It should be noted that olefin reactivity affects the product distribution in the low carbon number range rather than that in the high carbon number range. The so-called "second alpha", α_∞ in this work, reflects the "true" product distribution rather than the result of reversible olefin reactions. For instance, for those catalysts having strong hydrogenation ability, f_n could be very small even for low carbon number species. The effect of olefin reactivity is insignificant under this situation since f_n is essentially much smaller than unity. As a result, the product distribution, α_n', appears to follow a single alpha which is α_∞.

Equation (10) indicates that the observed FT product distribution can be quantified simply by using two parameters: olefin to paraffin ratio (f_n) at each carbon number and the β value which can be determined from high carbon number data. These two factors are dependent on the catalyst and reaction conditions. In most cases, even at high conversions, the molar flowrate of liquid product at the reactor outlet is significantly lower than that of gas phase products (hydrocarbon, water, unconverted reactants). Simple flash calculation indicates that this ratio (L/V) is generally less than 0.03 even when CO conversion is 100%. It is even an order of magnitude lower at 50% CO conversion. Therefore, the residence time, τ_n, can be approximated with Equation (11) by ignoring the liquid flow rate.

$$\tau_n = \frac{V_R}{VH_n} = \frac{V_R P}{VP_n^s} \tag{11}$$

At high carbon numbers, H_n becomes so small that the magnitude of VH_n could be comparable with that of L. However, ignoring L has negligible effect on α_n' since the magnitude of VH_n is very small and f_n is close to zero. The saturated vapor pressure of hydrocarbons in Equation (11) can be calculated using Antoine's equation (25) or an empirical correlation for FT products (26).

For simplicity of simulation, it is further assumed that olefin adsorption/desorption ($C_{n=}$ / $C_{n=}^*$) and hydrogen elimination of chain growth intermediate/half hydrogenation of surface olefin($C_n^*/C_{n=}^*$) steps are in equilibrium (Figure 1). This is particularly true at high conversions when the total flow rate at the reactor outlet is lower. With these assumptions, the product removal is slow ($1/\tau_n << k_o, k_o', k_a, k_d$) and Equation (5) reduces to Equation (12), suggesting that the olefin to paraffin ratio is simply proportional to the reciprocal of the average residence time τ_n. In other words, f_n decreases exponentially with carbon number as it is related to the saturated vapor pressure.

$$f_n = \frac{x_{n,o}}{x_{n,p}} = \frac{K_E}{k_H S_H^2 K_{ad} \tau_n} \qquad (12)$$

If the above mentioned equilibria are not valid, the dependency of f_n on carbon number will be weaker than exponentially for low carbon numbers, as can be seen from Equation (5). The higher the carbon number, the more τ_n dominates the denominator of Equation (5), and therefore the closer the dependency of f_n on carbon number to the exponential rule.

The model described with Equations (10)-(12) were tested using data obtained from the literature (7) and generated in our laboratory. The reaction conditions and major results are summarized in Table 1. The model simulation was performed with experimental data of temperature, α_∞, and f_3. As shown in Figures 3 and 4, there is a tight fit between model prediction and experimental data for both olefin to paraffin ratio (Figure 3) and product distribution (Figure 4) at CO conversions higher than 50%.

A common experimental observation of FT product distribution is that higher temperature, higher H_2/CO ratio, and/or lower pressure give lower alpha values. Table 2 shows that these general features can be qualitatively predicted using the model developed in this work. Another common experimental observation is that the deviation from a single α plot occurs in the range of carbon number 8 to14 (1). This phenomenon has not been properly explained with any of the existing models. The only related work is the two active sites model by Donnelly and Satterfield (4), in which the break point was calculated from experimental data since this parameter was required in their model. Nevertheless, a potentially reliable model also should be able to predict, not only to explain, this feature of the product distribution. According to the model developed in this work, the product distribution deviates from single alpha rule for light

hydrocarbon products due to the effect of vapor-liquid separation of hydrocarbon products. The deviation becomes weaker and weaker with increasing carbon number. Starting at some carbon number and thereafter, the alpha value appears to be constant (α_∞) when the olefin to paraffin ratio approaches zero. The general feature is that the α value increases with increasing carbon number and then levels off at α_∞. The deviation point is thus defined as the carbon number at the intersection of the α_∞ line and the linear regression line of the data for the first three carbon numbers (C_4-C_6), as shown in Figure 5. The physical meaning of the deviation point is the carbon number above which the effect of olefin reactivity on product distribution becomes insignificant.

The observed product distribution, as described above, depends on the value of β (or α_∞) and the olefin to paraffin ratio (f_n) at each carbon number. With some assumptions described above, f_n can be simplified to be directly proportional to the vapor pressure. Consequently, with information of reaction temperature, α_∞, and f_3 (depending on reaction condition and catalyst), the dependency of α_n' on carbon number can be simulated and the deviation point can be determined. Table 3 summarizes the effect of temperature and f_3 on the deviation point with α_∞=0.9 and 0.8. The effect of α_∞ is insignificant except at high f_3 and high temperatures. At 300^{o}C and f_3 = 10 with α_∞=0.8, the deviation point is 15.1, which is only 1.5 higher than that with α_∞=0.9. The temperature and f_3 value used in Table 3 pretty much represent the conditions and results of a typical FT reaction. Therefore, the current VLE model predicts the deviation point to be within carbon number 8-14 which is in agreement with generally experimental observations.

In this work, it is assumed that the vapor and liquid are in equilibrium following Raoult's law. One may argue that in practice, non-ideal vapor/liquid system should be considered since hydrocarbons of different molecular weight deviate from ideal behavior differently. For instance, the activity coefficient may increases exponentially with increasing carbon number,

which retards the dependency of olefin to paraffin ratio on carbon number (12-14). However, it should be noted that the non-ideal behavior of a hydrocarbon affects not only its vapor-liquid equilibrium constant (partition coefficient), but also its chemical reactivity in the liquid phase. If the vapor liquid system is taken as non-ideal, the reaction rate of a chemical species in the liquid phase also should be taken as proportional to its activity instead of its concentration. If not, the reaction rate constants of olefins cannot be assumed to be independent of carbon number. As a result, the non-ideal effect (activity coefficient) on olefin to paraffin ratio and product distribution cancels out when ignoring other minor factors, such as the impact of pressure on liquid (Poynting factor), although the average residence time of each hydrocarbon species, as defined in this work, deviates from that of ideal system. Therefore, when modeling the effect of VLE on product distribution, it is essentially unnecessary to account for the thermodynamic deviation of hydrocarbon products from ideal system.

Some researchers attribute the two-α distribution to physisorption of hydrocarbons on catalyst surface in the presumed gas-solid reactions, although the reactions were actually carried out at temperatures lower than the dew point of products. Typically, when the alpha value is higher than about 0.7 (actually depending on reaction temperature, pressure, conversion), there is inevitable formation of liquid phase on catalyst surface. Under these circumstances, the FT reaction actually takes place in the liquid phase. Physisorption should be taken into account only when the reaction is in gas phase, which typically involves high temperature operations. However, high temperature operation in turn does not favor the existence of a physisorption layer. If the products are entirely in the vapor phase, it is not difficult to prove that, without accounting for the effect of physisorption or diffusion, the product should follow a single alpha distribution, even when the olefin reactivity is taken into account. Since the effect of

physisorption, if it exists, on the FT product distribution is essentially the same as that of vapor-liquid separation, no further discussion is attempted here.

From the above discussion, it is clear that the 2-α distribution could be attributed to the effect of vapor-liquid separation of hydrocarbon products in the reactor. In addition, ideal gas and ideal solution assumptions are adequate to approximate the thermodynamic behavior of this system because non-ideal factors, such as activity coefficients, tend to cancel out with each other when evaluating olefin to paraffin ratio.

It has been argued that, in the presence of vapor-liquid equilibrium, the chemical potential of a given species is identical in both liquid and vapor phases and thus the rate of a chemical reaction cannot depend on the identity of the phase and the hydrocarbon solubility in the liquid phase (17, 18). This concept is incorrect unless the impacts of thermodynamics and kinetics are clearly defined. As a thermodynamic intensive property, the chemical potential tells us the processing direction and the processing limit. It does not tell us the processing rate which is the scope of kinetics. According to the standard definition, the chemical potential of a species in a phase is the sum of its standard free energy and the contribution of such species in its current mixture, and the later is a function of its composition. The fundamental difference between vapor and vapor/liquid systems lies in the fact that the standard free energy of a species in the liquid phase is different from that in the vapor phase; the difference can be quantified as a function of its vapor pressure. For an ideal vapor/liquid system in equilibrium, the relationship between vapor and liquid can be described using Raoult's law. Therefore, the concentration of a species in the liquid phase depends not only on its vapor composition but also its vapor pressure under the processing conditions. For two species whose chemical potentials are identical in both vapor and liquid phases, the component having a lower concentration in the vapor phase may have a higher concentration in the liquid phase, simply because it has lower vapor pressure. In a

Fischer-Tropsch reactor, due to the effect of vapor-liquid separation (if it exists), the hydrocarbon concentration in the liquid phase increases with increasing carbon number in the lower carbon number ranges (say C_{20-}), in contrast to the opposite trend in the vapor phase (15). As a result, product concentration profiles in the catalyst pores are totally different in these two systems; that is, a gas phase system and a gas-liquid phase system.

In a multi-phase reactor, the rate of chemical reaction definitely depends on the phase in which the catalyst resides. The chemical reaction is only affected by the changes in the phase which the catalyst is directly in contact with. Any impact resulting from the others phases has to go through this phase and affects the chemical reaction indirectly. If the catalyst is in the liquid phase, a gas reactant has to dissolve in liquid phase before it can participate in reactions. The so-called residence time must be the one in the liquid phase rather than in the gas phase because there is no reaction taking place in the gas phase. In a typical Fischer-Tropsch reaction, although most of the light hydrocarbons (C_{20-}) are removed from gas phase, it does not change the fact that the catalyst can only sense the amount of molecules in the liquid phase rather than those in the vapor phase. An active site on the catalyst surface does not know where the reactant molecule comes from -- liquid or vapor phase; however, it does know how many molecules are in the phase in contact with the catalyst. According to the collision theory, the nature of a chemical reaction is nothing more than the effective collisions between reactant molecules. It is obvious that a higher population will lead to a higher probability of effective collisions and, thus, higher reaction rates. Generally, the assumption of vapor phase operation should not be made when there is vapor-liquid separation and the catalyst is in liquid phase, especially when the reaction rate is of concern.

Conclusion

A mathematical model has been developed to describe the product distribution of Fischer-Tropsch synthesis, based on the recognition that the termination path to olefin is reversible. The observed product distribution at the reactor outlet consists of the contribution from intrinsic chain propagation on the catalyst surface and the effect of olefin reactivity. The 2-alpha distribution can be attributed to the effect of vapor-liquid separation of hydrocarbon products. The reaction product does not follow a ASF single alpha distribution even on the catalyst surface. A tight fit between model prediction and experimental data has been demonstrated. Also, the deviation point of product distribution is predicted to be within carbon number 8-14 under typical FT conditions.

Acknowledgment

This work is supported by U.S. DOE contract number DE-AC22-94PC94055 and the Commonwealth of Kentucky.

Nomenclature

f	olefin to paraffin ratio
H	vapor liquid equilibrium constant
k_a	olefin adsorption rate constant
k_d	olefin desorption rate constant
k_o	hydrogen abstraction rate constant of chain growth intermediate
k_o'	olefin half hydrogenation rate constant
k_p	propagation rate constant of chain growth intermediate
k_H	hydrogenation rate constant of chain growth intermediate
K_E	reaction equilibrium constant of olefin half hydrogenation ($K_E = k_o/k_o'$)
K_{ad}	adsorption equilibrium constant ($K_{ad} = k_a/k_d$)
L	liquid molar flow rate at reactor outlet
P	total operating pressure
P^s	saturated vapor pressure of hydrocarbon
r	reaction rate
R	gas constant
S	concentration of surface species
T	temperature
V	vapor molar flow rate at reactor outlet
V_R	reactor size (catalyst volume, catalyst weight)
x	molar fraction in liquid phase
y	molar fraction in vapor phase
α	chain propagation probability on surface, a function of carbon number
α'	observed product distribution, a function of carbon number

α_∞ chain propagation probability on surface at high carbon numbers, a constant

λ factor of olefin reactivity ($\lambda_n = (1+f_n)/(1+f_{n-1})$)

τ average residence time of hydrocarbon species in the reactor

subscript

= olefin

H hydrogen

n paraffin, olefin, or chain growth intermediate of carbon number n

o olefin

p paraffin

References

1. R. B. Anderson, in "Catalysis," (P. H. Emmett, Ed.) Reinhold Pub. Co., New York, 1956, pp 208, 209.

2. L.-M. Tau, H. Dabbagh, S. Bao and B. H. Davis, Fischer-Tropsch Synthesis: Evidence for two chain growth mechanisms, Catal. Letters, 7 127 (1990).

3. L. Konig, and J. Gaube, "The influence of water and of alkali promoter on the carbon number distribution of FT products formed over iron catalysts", Ber. Bunsenges. Phys. Chem. 91 (l987) l16.

4. T. J. Donnelly, I. C. Yates and C. N. Satterfield, "Analysis and prediction of product distributions of the Fischer-Tropsch synthesis", Energy Fuels, 2, 734-739 (1988).

5. E. Iglesia, S. C. Reyes and R. J. Madon; "Transport-enhanced alpha-olefin readsorption pathways in Ru catalyzed hydrocarbon synthesis", J. Catal., 129 (1991) 238-256.

6. R. J. Madon, E. Iglesia and S. C. Reyes; "Non-Flory product distributions in Fischer-Tropsch synthesis catalyzed by ruthenium, cobalt and iron", ACS Symp. Series, 517 (1993) 383-396.

7. E. Iglesia, S. C. Reyes and S. L. Soled; "Reaction-transport selectivity models and the design of Fischer-Tropsch catalysts" in "Computer-Aided Design of Catalysts and Reactors", (E. R. Becker and C. J. Pereira, Eds.), Marcel Dekker, Inc., 1992.

8. K. Fujimoto, L. Fan and K. Yoshii; New controlling method for product distribution in Fischer-Tropsch synthesis reaction; Topics in Catal., 2, 259-266 (1995).

9. S.-R. Yan, L. Fan, Z.-X. Zhang, J.-L. Zhou and K. Fujimoto; Effect of 1-olefin addition on supercritical phase Fischer-Tropsch synthesis over Co/SiO_2 catalyst; 14th Ann. Int. Pittsburgh Coal Conf., Proc., 1997.

10. E.W. Kuipers, I.H. Vinkenburg, and H. Oosterbeek; "Chain length dependence of α-olefin readsorption in Fischer-Tropsch synthesis", J. Catalysis, 152 (1995) 137-146.

11. A. P. Raje and B. H. Davis, "Effect of vapor-liquid equilibrium on Fischer-Tropsch hydrocarbon selectivity for a deactivating catalyst in a slurry reactor", Energy & Fuels, 10, 552 (1996).

12. H. Schulz and M. Claeys, "Reactions of α-olefins of different chain length added during Fischer-Tropsch synthesis on a cobalt catalyst in a slurry reactor", Applied Catalysis A: General, 186 (1999), 71-90.

13. H. Schulz and M. Claeys, "Kinetic modelling of Fischer-Tropsch product distributions", Applied Catalysis A: General, 186 (1999), 91-107.

14. G. Van Der Laan and A.A.C.M. Beenackers, “Kinetics and selectivity of the Fischer-Tropsch synthesis: A literature review”, Catal. Rev. - Sci. Eng., 41(3&4), (1999) 255.

15. X. Zhan, and B.H. Davis, “Two-alpha Fischer-Tropsch product distribution. A role for vapor-liquid-equilibrium ?”, Petroleum Science and Technology, 18(9&10) (2000) 1037-1053.

16. X. Zhan, and B.H. Davis, “Concentration profile of Fischer-Tropsch products in catalyst pores”, ACS Petroleum Chemistry Preprint, 45(2), 214-217, 2000.

17. E. Iglesia, “Design, synthesis, and use of cobalt-based Fischer-Tropsch synthesis catalysts”, Applied Catalysis A: General, 161 (1997), 59-78.

18. R.J. Madon, and E. Iglesia, “Catalytic reaction rates in thermodynamically non-ideal systems”, Journal of Molecular Catalysis A: Chem., 163(1-2) 2000 189-204.

19. M.E. Dry, “The Fischer-Tropsch Synthesis”, in “Catalysis-Science and Technology” Vol 1 (J.R. Anderson and M. Boudart Eds), Springer-Verlag, 1981.

20. A.T. Bell, “Catalytic Synthesis of Hydrocarbons over Group VIII Metals. A discussion of the reaction mechanism”, Catal. Rev. - Sci. Eng., 23(1&2), 1981, 203-232.

21. B. Shi, R. J. O’Brien, S. Bao and B. H. Davis, “Mechanism of the isomerization of 1-alkene during iron-catalyzed Fischer-Tropsch synthesis,” J. Catal., 199, 202 (2001).

22. T. Komaya, and A.T. Bell, “Estimates of rate coefficients for elementary processes occurring during Fischer-Tropsch synthesis over Ru/TiO_2", J. Catalysis, 146 (1994) 237-248.

23. R. B. Anderson, H. Friedel and H. H. Scorch, “Fischer-Tropsch reaction mechanism involving stepwise growth of carbon chain”, J. Chem. Phys., **19**, 313-319 (1951).

24. R. A. Friedel and R. B. Anderson, J. Am. Chem. Soc., **72**, 1212, 2307 (1950).

25. Thermodynamic Research Center, Texas A&M University; “Selected values of hydrocarbons and Related compounds”, API Project 44, 1983.

26. L. Caldwell and D.S. van Vuuren; On the formation and composition of the liquid phase in Fischer-Tropsch reactors; Chem. Eng. Sci., 41 (1986) 89-96.

Table 1

Reaction Conditions and Results from Literature and In-house

	Reaction 1	Reaction 2
Source	Exxon (7)	CAER
Catalyst	Co/TiO_2	$Co\text{-}Pt/Al_2O_3$
Temperature, ^oC	200	210
Pressure, kPa	2000	2000
CO Conversion, %	72	53
α_∞	0.92	0.85
f_3 (olefin/paraffin of C_3)	2.15	1.84
f_4 (olefin/paraffin of C_4)	1.3	0.98

Table 2 Model Prediction on the Effect of Reaction Conditions on Product Distribution		
Condition	Effect on α_∞	Effect on α_n
T $\uparrow$	$(S_H{}^{\downarrow} + S_1{}^{\downarrow\downarrow}) \Rightarrow \beta^{\uparrow} \Rightarrow \alpha_\infty{}^{\downarrow}$	$(P_n{}^{s\uparrow} + S_H{}^{\downarrow}) \Rightarrow f_n{}^{\uparrow} \Rightarrow \alpha_n{}^{\downarrow}$
P $\uparrow$	$(S_H{}^{\uparrow} + S_1{}^{\uparrow\uparrow}) \Rightarrow \beta^{\downarrow} \Rightarrow \alpha_\infty{}^{\uparrow}$	$(f_n{}^{\downarrow} + S_H{}^{\uparrow}) \Rightarrow \alpha_n{}^{\uparrow}$
H_2/CO $\uparrow$	$S_H{}^{\uparrow} \Rightarrow \beta^{\uparrow} \Rightarrow \alpha_\infty{}^{\downarrow}$	$V^{\uparrow} \Rightarrow f_n{}^{\uparrow} \Rightarrow \alpha_n{}^{\downarrow}$

Table 3 Deviation Point of Alpha Value at α_∞=0.9 (α_∞=0.8)			
f_3 / T, °C	1	5	10
200	8.4 (8.3)	10.6 (10.4)	11.6 (12.0)
250	9.1 (9.0)	11.4 (11.4)	12.5 (13.4)
300	10.0 (9.8)	12.4 (12.6)	13.6 (15.1)

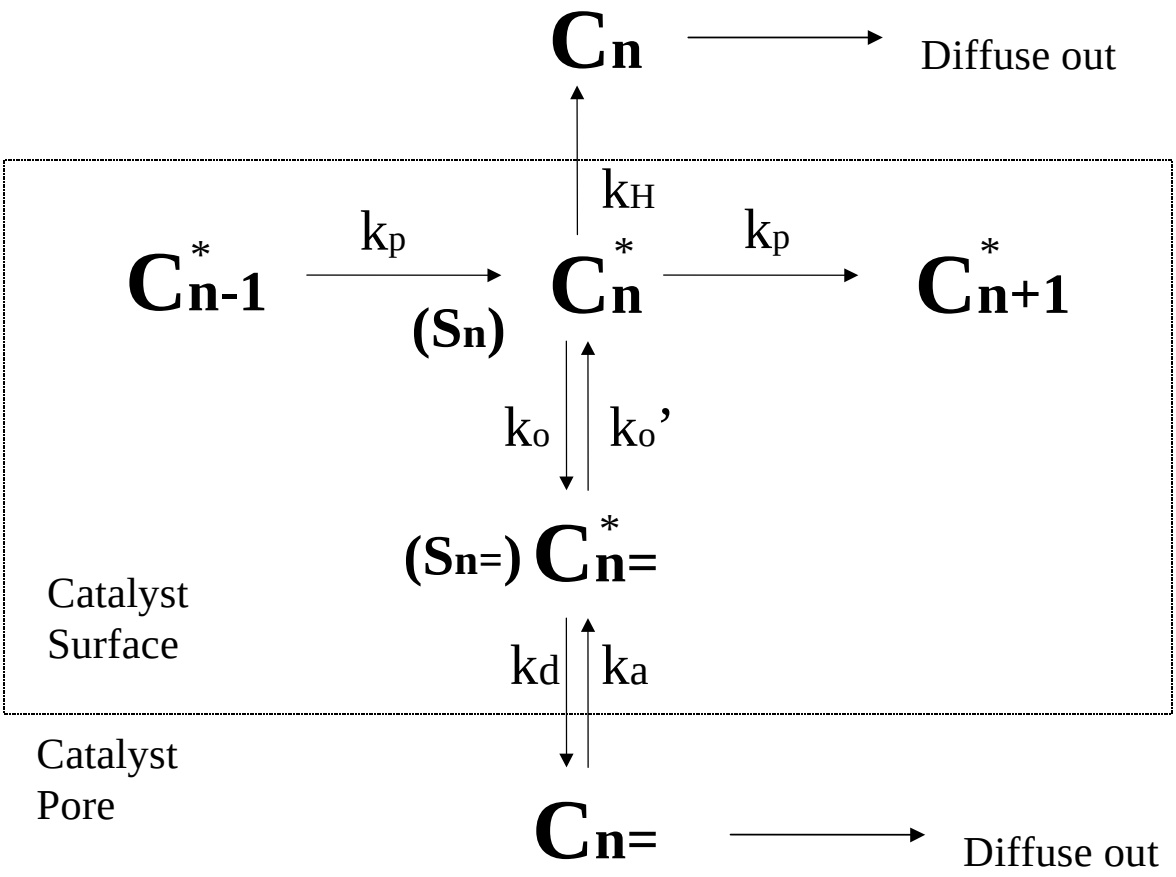

Figure 1 Reaction pathway of Fischer-Tropsch synthesis

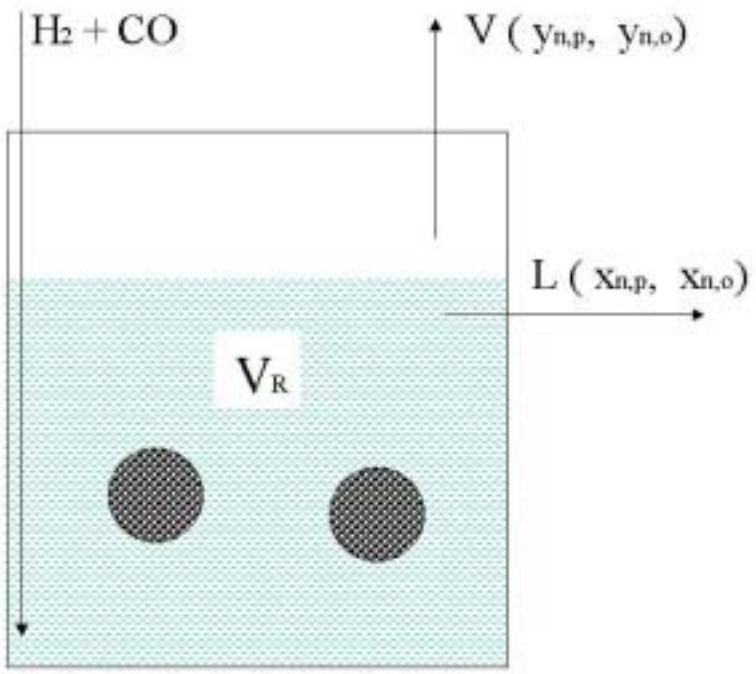

Figure 2 Schematic diagram of a CSTR reactor